Amund Soland

Sea ice conditions in relation to offshore wind development in the Southern Baltic Sea

Master's thesis

NTNU
Norwegian University of Science and Technology
Faculty of Natural Sciences
Department of Physics

◻ NTNU
Norwegian University of
Science and Technology

Amund Soland

Sea ice conditions in relation to offshore wind development in the Southern Baltic Sea

Master's thesis in Applied Physics and Mathematics
Supervisor: Jon Andreas Støvneng & Sigurd Henrik Teigen
June 2023

Norwegian University of Science and Technology
Faculty of Natural Sciences
Department of Physics

NTNU
Norwegian University of
Science and Technology

Abstract

The European Commission projects up to 450 GW of installed offshore wind capacity in the European Union with a potential 85 GW in the Baltic Sea. The construction and maintenance of marine structures in sub-arctic climates where sea ice may occur require a detailed understanding of the local sea ice conditions. The extra cost of sea ice mitigation measures against severe ice loads (e.g. ice breaking cones in the waterline, jacket vs. monopile foundation design) can make or break the business case for projects. This study aims to implement common methods used for understanding the local sea ice conditions and compare the results with benchmarks and local observations.

This study evaluates the use of Freezing Degree Day models to estimate level ice thickness development. A statistical relation between sea ice exposure and sea ice strength coefficients is evaluated against well observed conditions at Norströmsgrund Lighthouse. Furthermore a statistical relation between the level ice and sea ice ridge thickness and frequency is evaluated. A comparison is made between various data sources of sea ice parameters and models of these parameters. The sea ice conditions at the Baltyk I, II and III licences are described and compared to conditions elsewhere in the Baltic Sea. Based on the local sea ice conditions, level ice draft distributions throughout the freezing season is determined. 100 000 freezing seasons are simulated based on level ice distributions. From these simulations and the probability of sea ice presence the extreme values for level ice thickness, and sea ice ridge thickness and frequency is calculated.

Freezing Degree Day models are solutions to Stefan's law relating the energy balance between heat loss and ice growth. Various models and assumptions are compared with observations. The validity of the statistical relations between sea ice parameters is questioned. Climate data from various sources is analysed and compared to model estimates.

Methodology to evaluate sea ice conditions is reviewed and results are analysed. The sea ice conditions in the Baltic Sea is examined to more accurately inform sea ice mitigation designs to the local conditions. The study describes the local sea ice distribution for the various basins in the Baltic Sea, infers sea ice strength and sea ice ridge statistics.

The sea ice conditions in the southern Baltic Sea is significantly less severe than in the northern Baltic Sea. The ice strength coefficient at 50 years return period at Norströmsgrund lighthouse is found to be 1.8 MPa in accordance with detailed observations. The sea ice exposure is 2 orders of magnitude lower at the Baltyk I, II and III licences resulting in significantly lower sea ice strength coefficients. The level ice thickness at 50 years return period is estimated to be 106 cm at the highest in the northern Baltic Sea, and typically less than 40 cm in the southern Baltic Sea.

The statistical and empirical relations between level ice and sea ice ridge statistics are examined as well as the relations between sea ice exposure and the sea ice strength coefficient. Furthermore, these should be adjusted to the location specific conditions that vary between basins in the Baltic Sea.

Sammendrag

Dette arbeidet presenterer en analyse av isforholdene i Østersjøen. Den viktigste parameteren for å beskrive de lokale isforholdene er flatistykkelsen. Fra denne størrelsen kan andre isparamtre estimeres. Havisens termiske vekst estimeres gjennom Freezing Degree Day modeller med og uten termisk isollasjon fra snøfall. Starten på frysesesongen bestemmes av den lokale lufttemperaturen, og slutten av frysesesongen bestemmes av iskonsentrasjon fra fjernmålinger med satellitt. Havisens styrkekoeffisient estimeres basert på iskonsentrasjon og isdrift. Denne metoden er videre anvendt i forskjellige basseng i Østersjøen. Estimert havisstyke er noe høyere enn referanseverdien gitt av den internasjonale standarden ISO19006:2019 for Norströmsgrund fyr i den nordlige Østersjøen. Resultatene for mildere strøk i den sørlige Østersjøen gir iseksponering som er flere størrelsesordner lavere enn i den nordlige Østersjøen og dermed også vesentlig lavere havisstyrke enn i nord. Det er store variasjoner i havisforhold innad i Østersjøen i tid og i rom.

Statistiske forhold etablert for skrugardtykkelse og frekvens basert på flatisens kjøldybde i Beauforthavet er brukt for å estimere skrugardenes tykkelse og frekvens i Østersjøen. Forholdene i Østersjøen er mildere og tilgangen på presise data for havistykkelse er dårligere sammenlignet med forholdene i Beauforthavet. Til tross for ulike forhold i de to bassengene og mangel på høyoppløste tidsserier for istykkelse i Østersjøen samsvarer estimert skrugard tykkelse med publikasjoner som beskriver skrugardtykkelse i den nordlige Østersjøen. Imidleritid er den estimerte skrugardfrekvensen vesentlig lavere enn publiserte observasjoner i den nordlige Østersjøen.

Denne forskningen analyserer isforhold i Østersjøen basert på et bredt utvalg av datakilder. Hovedkildene er ERA5 reanalyse for atmosfæriske data, og iskonsentrasjon basert på fjernmålinger med passive mikrobølger fra NSIDC og BASIS iskartarkiv for informasjon om sjøisutrbredelse. Disse resultatene blir sammenlignet med andre kilder som iskart fra det det svenske meteorologiske og hydrologiske instituttet (SMHI) og finske meteorologiske instituttet (FMI), og andre modeller som Copernicus Marine Service (CMS) globale og lokale produkter for isforhold. I tillegg nevnes andre publikasjoner som har forsøkt å analysere isforholdene via data fra CryoSat-2.

Freezing Degree Day modellene gir tidsserier for havistykkelse som brukes til å definere fordelinger for havistykkelse gjennom frysesesongene. Basert på disse fordelingene simuleres 100 000 frysesesonger for å beskrive ekstremhendelser.

Denne tilnærmingen kartlegger ulike metoder og datakilder og har implikasjoner for utviklingen av havvindinfrastruktur, og informerer bedre design og planlegging av dette. Avhandlingen skisserer også potensielle veier for videre forskning, og argumenterer for mer detaljerte, stedsbestemte analyser for å bedre ta hensyn til de lokale forholdene.

Preface

This thesis is the final work in a degree for a Master of Science in Applied Physics at the Norwegian University of Science and Technology. The work concerns sea ice growth and sea ice ridging in the Baltic Sea, and is a collaboration with Equinor. The title of this thesis, "Sea ice conditions in relation to offshore wind development in the southern Baltic Sea" is a testament to the broad and dynamic nature of the research undertaken. At the heart of this work lies the issue of understanding the local sea ice conditions. The goal of the research is to understand and describe the local sea ice conditions in the Baltic Sea, particularly as they pertain to potential areas for offshore wind farm development in the region.

It is with sincere and profound gratitude that I wish to acknowledge all those who have been supporting me throughout this project and my degree. First to my primary supervisor Dr. Sigurd Henrik Teigen and to Equinor. I am deeply grateful for the opportunity you have given me to continue my internships as thesis work and for your continuous support throughout the project, encouragement and opportunities to grow by challenging myself both whilst in Norway and in Korea. For an excellent bridge from university to industry, I thank you.

A special acknowledgement goes to Professor Knut Vilhelm Høyland at the department of civil and environmental engineering at the Norwegian University of Science and Technology for a very fruitful discussion on the subject of sea ice growth. Your council has given direction to this research.

Additionally I would like to thank my co-supervisor Associate Professor Jon Andreas Støvneng and the Norwegian University of Science and Technology for having challenged me, having kept me curious and for the opportunities to supplement my education with an academic and cultural enrichment abroad. Accordingly, to the professors and to my fellow students at Korea Advanced Institute of Science and Technology I am thankful for a welcoming and rich experience both academically and culturally.

My deepest appreciation goes to my family and my culture. To my parents who taught me to love, to my sisters who taught me to share and to the society I grew up in that allowed me to continue my studies and focus on myself even amidst adversities.

In closing, to the unsung heroes. To all those who have given without expecting anything in return. To the teachers who have sparked and kindled my love for learning and understanding the world around me. You have my deepest respect.

Thank you for illuminating my path and for aiding in shaping who I am today.

Trondheim, June 2023
Amund Soland

List of Figures

List of Tables

Table of Contents

Abbreviations

FDD	=	Freezing Degree Days
CFDD	=	Cumulative Freezing Degree Days
FMI	=	Finnish Meteorological Institute
SMHI	=	Swedish Meteorological and Hydrological Institute
BASIS	=	Data Bank of Baltic Sea Ice and Surface Temperatures
CMS	=	Copernicus Marine Service
SIT_{10}	=	Number of days with sea ice thickness greater than 10 cm
MSIT	=	Maximum sea ice thickness
SIC_{60}	=	Number of days with sea ice concentration greater than 60 %
MSIC	=	Maximum sea ice concentration

Chapter 1

Introduction

1.1 Motivation and Context for the Research

Offshore wind energy is experiencing significant growth that is expected to accelerate, a trend underscored by the installed offshore wind capacity in the EU-27 countries and the United Kingdom of 12 GW and 9.7 GW respectively as of 2020 (Com-2020-741, 2020). The European Commission projects a potential of 450 GW of installed capacity by 2050. Notably, the Baltic Sea had an installed capacity of 2 GW in 2019 and is predicted by WindEurope to contribute 85 GW by 2050 equivalent to approximately 6000 turbines each of 14 MW capacity (Hammer et al., 2023; WindEurope, 2019). Such a scenario indicates more than a 20 fold increase in European waters and a bold 42.5-fold increase in the Baltic Sea within just three decades. In order to meet these projections a deeper understanding of sea ice conditions in the Baltic Sea is necessary, given the direct influence these conditions may have on safe operation and cost of offshore wind development in this area (Høyland et al., 2023).

The unique geographical and climatic characteristics of the Southern Baltic Sea present certain challenges in understanding sea ice conditions. Specifically, this region does not consistently experience severely cold winters capable of producing significant sea ice (Vihma and Haapala, 2009). This irregular occurrence of severe sea ice conditions leads to a limited statistical foundation, reinforcing the need for extended sea ice condition reporting through modeling for sustainable offshore wind power development.

1.2 Identification of the Research Questions

Given the context and challenges described, the primary research question that arises is: How can we understand the historic sea ice conditions and establish design values for sea ice conditions in the Baltic Sea?

In pursuit of the primary research question, several sub-questions will be explored throughout this thesis. These include: How can we calibrate the sea ice strength coefficient

to reflect local conditions accurately? How can we employ fundamental sea ice parameters to develop a deeper understanding of sea ice ridging and extrapolate extreme values from simulations based on historic conditions? What methodologies can we use to approximate sea ice parameters when they are not directly reported? Answers to these sub-questions provide the necessary framework to answer the primary research question, collectively contributing to a comprehensive understanding of sea ice conditions in the Baltic Sea.

To answer these questions this study employs a multifaceted approach that combines FDD models, sea ice strength calculations, and Monte Carlo simulations. These methodologies are supported by data from a variety of sources, including ERA5, Copernicus Marine Service, NSIDC, CryoSat-2, BASIS Archive, FMI, and SMHI. Significant improvements and modifications have been made to existing models, particularly the FDD model, by incorporating factors such as snowfall insulation and adjustments for the start and end of the freezing season.

1.3   The Baltic Sea

The Baltic Sea, as illustrated in Figure 1.1, stretches from its opening into the Atlantic in Kattegat to its innermost gulfs in the Bay of Bothnia and the Gulf of Finland. Different sea ice conditions are observed in the southern Baltic Sea than the conditions observed in the northern gulf (Gulf of Bothnia, Gulf of Finland and Gulf of Riga). This study focuses on the understanding and modeling of these diverse sea ice conditions, utilizing key concepts and methodologies from various fields of research.

Leppäranta and Myrberg (2009) recognises a series of major and minor sub-basins in the Baltic Sea, and connections between them. Notably, for the purpose of this thesis the minor sub-basins have been combined with neighbouring ones due to lack of data especially in the southern sub-basins. The various Danish sub-basins have been grouped into one referred to as Danish waters, the Bay of Gdansk has joined the Eastern Gotland Basin, and the Åland Sea and Archipelago Sea have both joined the Sea of Bothnia. Figure 1.1 shows a manual classification of grid cells and their respective sub-bassin based on the sub-basin recognised by Leppäranta and Myrberg (2009).

Basins of the Baltic Sea
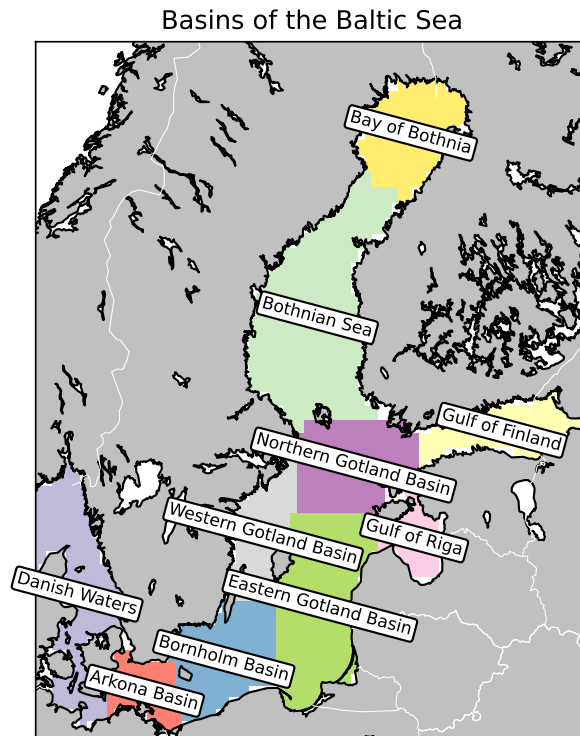
Figure 1.1: The sub-basins of the Baltic Sea recognized in this thesis.

The Baltic Sea has a varied sea ice climate and internal variation between basins in the north and the south is significant. To evaluate the results for locations in this thesis benchmarks at Norströmsgrund lighthouse in the northern Baltic Sea and at Kriegers Flak in the Southern Baltic Sea were used. Additionally, the three licences Bałtyk I, II and III in Polish waters are mentioned in this thesis and their locations are marked in Figure 1.2.
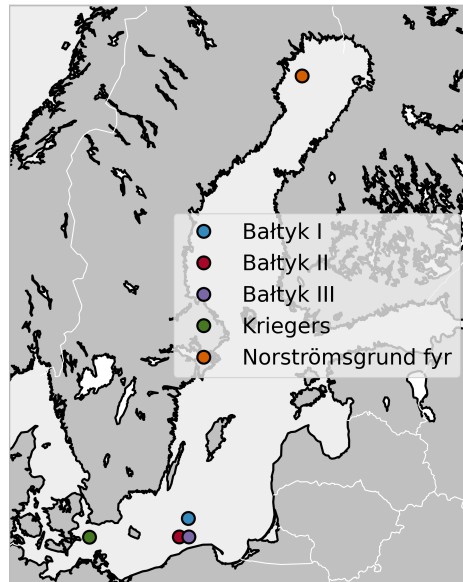
Figure 1.2: Benchmark locations at Norströmsgrund Lighthouse in the northern Baltic Sea, the wind farm Kriegers Flak in the Arkona basin and the Bałtyk I, II and III in the Bornholm basin.

1.4   Local sea ice conditions

This study is concerned with describing sea ice conditions in the Baltic Sea by describing key sea ice parameters. The most fundamental sea ice parameters are the sea ice thickness, sea ice concentration and the sea ice drift velocity. Sea ice development is generally classified as either first-year ice or multiyear ice. There are many differences in the properties between these types of ice, however since the ice-cover in the Baltic Sea completely melts each season there is only first-year ice. Sea ice typically develops every winter in the north and only for extreme winters does the ice develop outside the sheltered and shallow lagoons of the south. The Baltic Sea ice Brackish which yields lower salinity and porosity in the sea ice (Ice Struct JIP). This thesis implements a pure thermal model, which is assumed valid to describe the overall thickness development of first-year level ice (Vihma and Haapala, 2009; Leppäranta, 2005; Leppäranta and Myrberg, 2009).

Sea ice concentration is significantly easier than sea ice thickness as it is only a question about distinguishing between open ocean and frozen ice. These are surfaces with different properties and is classifiable from satellite mounted instruments. There are difficulties in measurements, especially in the melting season where puddles may form on top of sea ice structures, however this problem is outside the scope of this thesis.

Sea ice thickness is more difficult to directly measure thus models are often implemented to estimate this parameter. This thesis implements a freezing degree day model to estimate the thermal growth of sea ice vertically. The sea ice thickness is allusive and whilst this thesis describes the thermal growth of sea ice, stopping here would not be describing the full range of sea ice thickness even when assuming first year ice. This is due to

the sea ice ridge thickness extremes, being due to mechanical growth which can be an order of magnitude thicker than the local level ice. Estimating the sea ice ridge thickness and sea ice ridge spatial frequency is complicated, especially in areas like the southern Baltic Sea, where the occurrence is infrequent and actual measurements are scarce to come by. To this end, statistical relations used in the literature, relating the sea ice ridge parameters and the local level ice thickness is implemented. The local level ice thickness is a function of the cumulative freezing degree days in a freezing season, which correlates with the severity of a freezing season, thus the ridge parameter relations are also indirectly a function of this freezing season severity measure.

To calibrate load calculations to local conditions a sea ice strength coefficient, C_R, is used. The methods of determining this coefficient and its application in offshore wind is a developing research area. This thesis does not correct for the velocity effect although the empirical correction is presented.

1.5 Structure of the Thesis

The thesis is structured as follows: Chapter 2 describes the data sources and data parameters, the models related to level ice development, relations between level ice and ridging, relations between sea ice exposure and the sea ice strength coefficients and relevant numerical techniques for synthesising time series data. Chapter 3 presents the research findings, highlighting significant insights related to sea ice conditions in the Baltic Sea. Chapter 4 offers a deeper analysis of these results, discussing their implications for offshore wind energy development. Finally, Chapter 5 summarises the key findings and provides suggestions for future research in this area.

This thesis is a continuation of a project thesis which formed a basis for this thesis to build upon and in order for this thesis to be self contained, the introduction in this chapter 1, the data and method sections about data sources and parameters 2.2-2.4.6, 2.5.1-2.5.2, 2.6, the results concerning sea ice strength coefficients and the sea ice parameters described in chapter 3.1-3.3 and the discussion in chapters 4.1-4.3 will be based on the previous project thesis.

Chapter 2

Data and Method

2.1 Key Concepts and Literature

In the pursuit of comprehending the nature of sea ice conditions in the Baltic Sea a variety of data sources and models of sea ice conditions have been analysed. This research is grounded in numerous key concepts and theories building upon and combining methods derived from prior research. The major themes evaluated herein include Freezing Degree Day (FDD) models, sea ice strength coefficients, and Monte Carlo simulations of parameters describing sea ice ridging.

Freezing Degree Day (FDD) models, as discussed in seminal papers such as (Leppäranta, 2015), are instrumental in predicting sea ice growth - a crucial aspect of determining sea ice conditions. The FDD models implemented in this research are variations of the FDD models presented by Tikanmäki and Heinonen (2022), building upon a thorough review by M. Lappäranta (Leppäranta, 1993, 1983) based on the original derivation of the by Stefan (1891).

Sea ice strength calculations, as explored by Kärnä et al. (2006), provide insight into the potential impact of sea ice on offshore infrastructure. The definition and use of sea ice strength coefficients for offshore wind is a developing topic.

Monte Carlo simulations serve as a critical tool for assessing the variability and uncertainty inherent in sea ice conditions. They allow for the prediction of a wide range of potential outcomes based on statistical distributions, which can be used to significantly enhance our understanding of sea ice dynamics when data is poor.

A probabilistic methodology to determine sea ice strength coefficients based on exposure relative to a known benchmark is explored by Thijssen and Fuglem (2015). The methods presented expands upon global and local load calculations based on recommendations from the international standard (ISO 19906:2019), and previous work from Kärnä and Masterson (2011).

Empirical relations for the determination of ice ridge parameters from the level ice draft was derived by Samardžija and Høyland (2023) based on sonar profiling data of sea ice drafts in the Beaufort Sea.

A recent study by van der Stap et al. (2023) has evaluated the feasibility of monopile foundations for offshore wind in the Baltic Sea and concluded that the Bay of Bothnia and the northern Bothnian Sea are infeasible whiteout ice mitigation measures. The study did not conclude on the southern Bothnian Sea and the Gulf of Finland. The remaining sub-basins were deemed feasible.

Descriptions of sea ice and sea ice conditions in the Baltic Sea build upon the work of Leppäranta (2005); Leppäranta and Myrberg (2009); Wadhams (2000).

2.2 Sea ice characteristics

This section is based on the international standard for arctic offshore structures chapter A.8.2.4.3 (ISO 19906:2019) and the IceStruct JIP chapter 3: Sea ice characteristics (Ice Struct JIP).

Sea ice is generally classified as either first-year ice or multi-year ice depending on if the ice melts completely between freezing seasons. These categories are described be significantly different parameters for sea ice strength and thus loads will also differ. This study is concerned with sea ice loads in subarctic regions where sea ice never remains between freezing seasons.

Sea ice can develop mechanically and thermally. Thermal ice development leads to regular sea ice shaped as sea ice sheets through thermal growth in freezing seasons and melting between freezing periods. Mechanical ice growth is the formation of new sea ice structures through the breaking up and re-consolidation of individual sea ice floes.

For the purpose of this study the salinity of the sea ice is not directly considered. The calibration of sea ice strength to data from Norströmsgrund Lighthouse scales the sea ice strength to the conditions at this reference location, thus all unaddressed parameters that influence the sea ice exposure at Norströmsgrund Lighthouse are indirectly addressed in the sea ice strength scaling.

Sea ice loads on vertical monopile structures are estimated based on extreme value analysis of nominal local and global pressures. The nominal local sea ice loads on offshore structures will vary significantly based on the sea ice floe size, drift velocity, internal structure, sea ice strength and external geometry. The parameters considered in this analysis is the sea ice thickness (SIT), sea ice concentration (SIC) and the sea ice drift velocity.

Sea ice drift velocity is difficult to model accurately without a complicated climate model. This study explores an estimation based on the local wind conditions and compares its results with the Copernicus Marine Service reanalysis product (Hornnes et al., 2022).

2.3 Characteristic parameters

The important parameters to estimate C_R for sea ice load calculations is the local sea ice concentration and sea ice drift velocity. From these sea ice condition parameters estimates of the annually average length of sea ice drifting past the location can be estimated and C_R can be calibrated accordingly.

Sea ice thickness observations are recorded by various local meteorological institutes since understanding the local sea ice conditions is of vital importance for shipping and

trade. However, computer readable maps over the entire Baltic Sea are only publicly available since 2018 from the Finnish Meteorological Institute (Karvonen et al., 2022). It should be noted that an effort was made in 1981 to create a complete computer readable map of the Baltic Sea for the years 1960 to 1979, called the Data Bank of Baltic Sea Ice and Surface Temperatures (BASIS).

For other years not covered by these records the sea ice thickness has to be estimated. The current standard for sea ice thickness estimations is the use of freezing degree day models presented in the international standard for arctic offshore structures (ISO 19906:2019) and joint industry projects (Ice Struct JIP). A recent study by Tikanmäki and Heinonen (2022) uses an insulating variation of this freezing degree day model for select locations in the southern Baltic Sea. This model is one of many modifications of the freezing degree day model published by Leppäranta (2015). The insulating and non-insulating freezing degree day models presented by Leppäranta M. are implemented and their results are compared with sea ice thickness observations and reanalyses for benchmark locations in the Baltic Sea.

Sea ice drift velocity has been reported in a reanalysis product by Copernicus Marine Services in the period from 1993 to 2020. Free drift is an alternative assumption for a simple method used to estimate the sea ice drift velocity. The method relates the ice drift velocity to the local wind velocity through drag coefficients.

In this study a sub map of the Baltic Sea defined by their South-Western corner at [9.41°E, 53.76°N] and the North-Western corner [29.66°E, 66.26°N] respectively has been used for the following data sources when the dataset is provided for areas outside the Baltic Sea as well.

Source	Time horizon	Grid resolution	Temporal resolution	SIC	SIT
CMS_G	1993-2020	5'	Daily	Reanalysis	Reanalysis
BASIS	1960-1979	15' × 30'	2 days / week	Observed	Observed
NSIDC	1978-2022	25 km	Daily	Observed	N/A
ERA5	1959-2022	31 km	Hourly	N/A	FDD model
CMS_B	1993-2020	5'	Daily	Discarded	Discarded
FMI	2018-2022	1 km	Daily	Observed	Observed

Table 2.1: Data source specification summary and how each source provides sea ice thickness (SIT) and sea ice area fraction, commonly known as sea ice concentration (SIC). CMS_G is the GLOBAL_MULTIYEAR_PHY_001_030 Copernicus Marine Service product. CMS_B is the BALTIC_SEA_REANALYSIS_PHY_003_011 Copernicus Marine Service product (Hornnes et al., 2022). CMS_B was discarded due to unphysical sea ice thicknesses along the polish coast. NSIDC refers to the NSIDC-0051 version 2 product (DiGirolamo et al., 2022) which reports sea ice concentration in both hemispheres. ERA5 refers to the ECMWF reanalysis of global climate and weather (Hersbach et al., 2022). ERA5 also provides 10 meter wind data from which the sea ice drift velocity is estimated. FMI refers to the digital ice charts provided by the Finnish Meteorological Institute (Karvonen et al., 2022).

2.4   Data sources
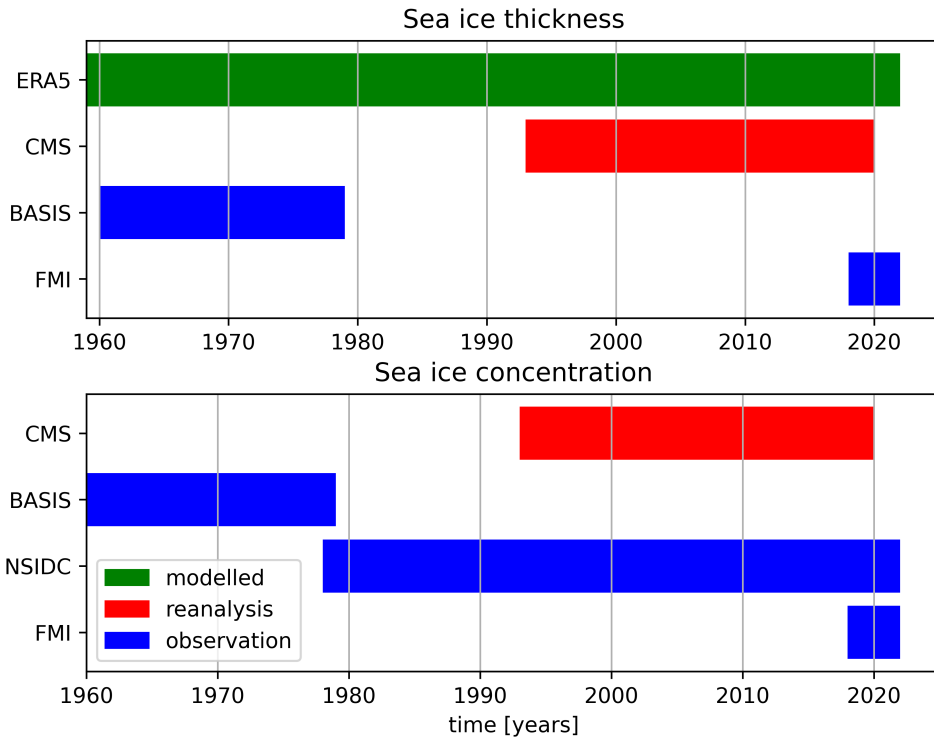
Figure 2.1: Timelines over data availability for the two primary sea ice parameters sea ice thickness and sea ice concentration. The parameters that were directly observed and recorded are marked in blue, those parameters that are based on reanalyses are marked in red, whilst parameters that are modelled based on other climate parameters are marked in green.

2.4.1   ERA5

The ERA5 reanalysis products is a family of hourly datasets on a 31 km by 31 km grid produced by coupled land, wave and atmospheric climate models. The reanalysis was downloaded from 01.01.1959 to 30.06.2022, however it is updated to 5 days before real time and presents a large number of climate parameters hourly (Hersbach et al., 2022). The parameters used in this study are the two meter temperature (T2M), total precipitation (TP) and longitudinal and latitudinal components of the wind.

Two meter temperature is the atmospheric temperature at two meters above the terrain. Over oceans this corresponds to two meter above sea level.

Total precipitation is reported in meters of water equivalent. From this parameter snowfall depth can be determined based on the relative mass densities of water and snow.

2.4.2   Copernicus Marine Service

Copernicus Marine Service (CMS) provides a global physical reanalysis of ocean conditions under the name GLOBAL_MULTIYEAR_PHY_001_030. This reanalysis product will be referenced as CMS_G. Additionally Copernicus Marine Service provides a reanalysis of the Baltic sea called BALTICSEA_REANALYSIS_PHY_003_011. This reanalysis product will be referenced as CMS_B.

The global CMS_G is based on GLORYS12V1 oceanic model, whilst CMS_B is based on the Ice-Ocean NEMO-Nordic model.

These reanalyses provide the sea ice area fraction (SIC), the sea ice thickness (SIT) and the sea ice drift velocity. Both products are daily and cover the period 01.01.1993-31.05.2020.

2.4.3   National Snow and Ice Data Centre

The National Snow and Ice Data Center (NSIDC) has provided the NSIDC-0051 version 2 dataset. This sea ice concentration dataset is based on the bootstrap algorithm interpretation of satellite microwave intensity recordings. The product contains data from 26.10.1978-22.05.2022 and it is provided on a polar stereographic grid.

2.4.4   CryoSat-2

Cryosat-2 records altimetric data. A recent paper has used deep learning to interpret these altimetric data as sea ice thickness (Landy et al., 2022). The interpretation of data is provided from 2010-2022. This data is primarily made for arctic regions, however the Baltic Sea is contained within the dataset thus the interpreted CryoSat-2 data will be compared to other sea ice thickness observations.

2.4.5   The Basis Archive

The Data Bank of Baltic Sea Ice and Sea Surface Temperatures (BASIS) is a cooperative project between the Finnish Meteorological Institute and the Swedish Meteorological and Hydrological Institute. The effort to digitize hand drawn ice charts on to punch cards was carried out in 1981 and was reproduced and distributed in the Network Common Data Format (netCDF) by the U. Löptien and H. Dietze from the GEOMAR Helmholtz centre for Ocean Research in 2014 (Löptien and Dietze, 2014).

The data preserves the original data structure and reports sea ice concentration, sea ice type and sea ice thickness from 23.11.1960 to 03.06.1979.

2.4.6   Finnish Meteorological Institute

The Finnish Meteorological Institute (FMI) provides digitally recorded ice charts since 01.01.2018 to 30.05.2022. These observations are based on expert observation and analysis and Synthetic-Aperture-Radar (SAR) image from either Sentinel 1 (A or B) or Radarsat-2 (Karvonen et al., 2022). The digital FMI ice charts provide sea ice concentration and

sea ice thickness data on a 1 km by 1 km grid over the Baltic Sea with a daily temporal frequency.

2.4.7 Swedish Meteorological and Hydrological Institute

The Swedish Meteorological and Hydrological Institute (SMHI) is the Swedish state bureau tasked with monitoring weather, wind and water. The institute produces drawn ice charts of the entire Baltic Sea. During the winter season the sea ice charts have been published daily since 2003 and twice weekly with ocean surface temperature in the period 1979-2017.

2.5 Freezing Degree Day models

Freezing Degree Day (FDD) models are pure thermal growth models considering the vertical growth of level ice based on the severity of a freezing season as measured by the number of degrees below freezing integrated through time.

A naive FDD model starts on the first freezing degree day and lasts until the last one. The international standard of Petroleum and natural gas industries - Arctic offshore structures (ISO 19906:2019) recommends the use of a 30 day running temperature average of temperatures below 0 °C as a threshold for determining the start of the freezing season. This mitigates the overestimation of the number of freezing degree days that actually contribute to sea ice development.

The international standard and a joint industry project (ISO 19906:2019; Ice Struct JIP) recommends the use of freezing degree day models as an estimate of the level ice thickness at the end of the freezing season and cautions against using the instantaneous number of freezing degree days for high accuracy level ice thickness estimates throughout the freezing season. This thesis does not aim to use the FDD results through the season as estimates of the instantaneous level ice thickness, however the use of a sea ice concentration cutoff was still used to determine the end of the freezing season.

2.5.1 Sea ice growth models

The framework for sea ice growth models presented was published as a review article. The following derivation of the analytical solution for an idealised case of bare ice growth is based on the work by Stefan (1891) and reviewed by Leppäranta (1993).

The basic assumption for Stefan's law is a classical heat conduction problem,

$$\frac{\partial}{\partial t}(\rho_i c_i T) = \nabla \cdot (\kappa_i \nabla T) + q, \tag{2.1}$$

where t is time, ρ_i is the mass density of ice, c_i is the specific heat of ice, T is the ice temperature, κ_i is the heat conductivity of ice, and q is heating from other external sources penetrating the ice surface.

Sea ice is assumed isotropic and infinite in the horizontal plane. These assumptions lead to no horizontal temperature gradient and thus also no internal horizontal heat flux, and the thermodynamic problem reduces to

$$\frac{\partial}{\partial t}(\rho_i c_i T) = \frac{\partial}{\partial z}(\kappa_i \frac{\partial}{\partial z} T) + q, \tag{2.2}$$

Due to conservation of heat flux the heat flux across the ice-air boundary must be equal, and due to the constant temperature surface in freezing liquids the vertical boundary conditions for the problem becomes.

$$\begin{cases} \text{top:} & \kappa_i \frac{\partial}{\partial z} T = Q_T \\ \text{bottom:} & T = T_f \end{cases}. \tag{2.3}$$

where T_f is the freezing temperature of the sea water, and Q_T is the vertical heat flux along the ice-air boundary.

Ice grows by water freezing, thus ice thickness normally grows on the bottom boundary of the ice assuming the ice top surface does not submerge. Ice will be assumed to not submerge in this thesis, a justification is added in appendix A.

These boundary conditions and assumptions allows the reformulation of the thermodynamic problem in terms of the sea ice thickness as

$$\rho_i L \frac{d}{dt} h_i = \kappa_i \frac{\partial}{\partial z} T|_{bottom} - Q_w, \tag{2.4}$$

where h_i is the thickness of the sea ice , Q_w is the horizontal heat flux at the ice-water boundary and L is the latent heat of freezing sea water.

2.5.2 Stefan's law

The most basic sea ice growth model is Stefan's Law. Stefan's law is a simple solution to (2.4) based on the following assumptions originally presented by Stefan (1891).

1. There is no thermal inertia.

2. There is no internal heat source.

3. The temperature at the top ice-air interface $T = T(t)$ is a known function of time.

4. There is no heat flux between the water and the ice.

The assumptions 1 and 2 imply a constant temperature gradient along the horizontal direction,

$$\frac{\partial}{\partial z} T = constant. \tag{2.5}$$

Assumption 3 simplifies ice-air heat flux boundary condition to

$$T = T(t). \tag{2.6}$$

Applying these results with the final assumption 4 the thermodynamic problem (2.4) reduces to

$$L\rho_i \frac{d}{dt}h_i = \frac{\kappa_i(T_f - T_i)}{h_i}. \tag{2.7}$$

The degree day model for ice growth is based on this solution to Stefan's Equation (2.7).
(Tikanmäki and Heinonen, 2022; Leppäranta, 2015)

$$\frac{d}{dt}h_i = \frac{\kappa_i}{\rho_i L_f}\frac{T_f - T_i(t)}{h_i}, \tag{2.8}$$

where h_i is the sea ice thickness, κ_i is the sea ice thermal conductivity, ρ_i is the mass density of sea ice, L_f is the latent heat of fusion for sea water, T_f is the freezing temperature of sea water, $T_i = T_i(t)$ is the temperature of the sea ice upper surface through time t. $\kappa_i = 2.2\ \mathrm{W\ m^{-1}K^{-1}}$, $\rho_i = 917\ \mathrm{kg\ m^{-3}}$, L_f and T_f are assumed to be a constants whilst

$$FDD(\tau) = \int_0^\tau d\tau \frac{dt}{d\tau}\max[0, T_f - T_i(t)] \tag{2.9}$$

are the cumulative freezing degree days such that solutions to (2.8) can be written in the form

$$h(\tau) = \sqrt{h_0 + a^2 FDD(\tau)}, \tag{2.10}$$

where $a = \sqrt{\frac{2\kappa_i}{\rho_i L_f}}$. Here units of time is converted from units of seconds t to units of days τ, For first year ice the integration starts before the freezing season, thus $h_0 = 0$ such that (2.8) simplifies to

$$h(\tau) = a\sqrt{FDD(\tau)}. \tag{2.11}$$

The international standard for arctic offshore structures (ISO 19906:2019) provides a model of the same mathematical form for sea ice thickness based on sea water crystallization

$$E[h] = a\sqrt{E[FDD]}, \tag{2.12}$$

where $E[h]$ is the expected end of freezing season sea ice thickness, $E[FDD]$ is the expected end of freezing season cumulative freezing degree days and empirically defined constants $a = 2.6 \times 10^{-2}$.

This model can be expanded upon to account for insulation due to snowfall and (2.8) is rewritten as:

$$\frac{dh_i}{dt} = \frac{T_f - T_i(t)}{\rho_i L_f(\frac{h_i}{\kappa_i} + \frac{h_s}{\kappa_s})} \tag{2.13}$$

where κ_s is the thermal conductivity of the snow layer, h_s is the thickness of the snow layer and all other coefficients are the same as in (2.8) (Tikanmäki and Heinonen, 2022; Leppäranta, 2015, 1993; Stefan, 1891).

2.5.3 Thermal insulation from snow

Snow accumulating on the ice makes the system a two component system with boundaries water-ice, ice-snow and snow-air.

Introducing heat conduction through the snow into the ice requires the equality

$$\frac{\partial}{\partial t}(\rho_s c_s T) = \frac{\partial}{\partial z}(\kappa_s \frac{\partial}{\partial z} T) + q, \qquad (2.14)$$

where ρ_s is the mass density of snow, c_s is the specific heat of snow and κ_s is the thermal conductivity of snow.

The new boundary conditions are given by the continuity of heat flux, across the snow-air boundary as

$$\kappa_s \frac{\partial}{\partial z} T = Q_T \qquad (2.15)$$

and across the snow-ice boundary as,

$$\kappa_i \frac{\partial}{\partial z}|_{ice} T = \kappa_s \frac{\partial}{\partial z}|_{snow} T. \qquad (2.16)$$

Thermal conductivity of snow is highly sensitive to its mass density (Langham, 1981; Leppäranta, 1983). Additionally, the mass density of snow typically increases from 0.1 g cm^{-3} to 0.3 g cm^{-3} within the first week of snowfall (Leppäranta, 1993, 1983).

Additional problems related to snow in this thermodynamic problem are presented when the boundary between snow and ice blends together and forms a partially smelted and refrozen snow-ice layer. This would invalidate the two-phase system assumption and ice growth is shown to be sensitive to the properties of snowfall for all growth models presented by Leppäranta (1983). This thesis assumes no formation of snow-ice as hypothesised in appendix A and the complications to the thermodynamic problem (2.14) due to snow properties will not be considered further.

It is important to realize that considering insulation due to snow makes the problem no longer analytically solvable as alluded to in appendix B.

Through time series of snow fall or precipitation and the start of the freezing season it is trivial to calculate the cumulative snow fall. Additionally a positive degree day model i applied to the melting of snow with a value of -0.35 cm K^{-1} day^{-1} (Braithwaite, 2017; Holloway, 2023). Snow melting is another parameter to which the snow model is sensitive (Leppäranta, 1983; Langham, 1981).

2.5.4 Determining the start of the freezing season

Ice growth due to the analytical ice growth models discussed above start accumulating sea ice from the first moment the air temperature goes below the freezing temperature of the sea water. Due to diurnal temperature fluctuations and temporary cold periods the air temperature can go below freezing much earlier in season than the start of the actual ice growth. Even when ice forms due to early cold periods the ice is likely to melt again if the temperature goes above the freezing temperature of the sea water when the ice is thin. To more accurately determine level ice thickness and ice growth through the freezing season a running average air temperature threshold is suggested (ISO 19906:2019). The threshold

suggested in the international standard is a 30 day running average of air temperature below 0 °C.

2.5.5 Determining the end of the freezing season

To determine the length of the freezing season a method for determining the end of the freezing season is needed in addition to the start of the freezing season as presented above. Given the ease of access to sea ice concentration compared to sea ice thickness it is much easier to determine if there is ice than how thick that ice is. This informed a choice of sea ice concentration thresholds. When sea ice concentration goes below a cutoff threshold SIC^* the sea ice growth can be terminated and the end of freezing season sea ice thickness can be determined.

2.6 Sea ice strength loads

The international standard for petroleum and natural gas industries - Arctic offshore structures (ISO 19906:2019) refers to ice loads due to crushing as

$$F_G = whp_G, \tag{2.17}$$

where F_G is the peak global load due to crushing, w and h are width and height parameters defining the area normal to the crushing direction. Here

$$p_G = C_R \left[\left(\frac{h}{h^*} \right)^n \left(\frac{w}{h} \right)^m + f_{AR} \right], \tag{2.18}$$

is the global pressure defined with sea ice strength coefficient C_R, h^* a reference height of 1 m for unit consistency,

$$n = \begin{cases} -0.5 + 0.2h & \text{if } h < 1\text{m} \\ -0.3 & \text{if } h \geq 1\text{m} \end{cases}. \tag{2.19}$$

$m = -0.16$, and

$$f_{AR} = e^{\frac{-w}{3h}} \sqrt{1 + 5\frac{h}{w}} \tag{2.20}$$

is an empirical term calibrating for the geometry of the interaction.

2.6.1 Sea ice exposure

This chapter is based on derivations by Thijssen and Fuglem (2015). The sea ice strength coefficient is calibrated for local variations through the sea ice exposure E_h in (2.29). The choice of sea ice exposure term in this study is the average annual length of sea ice drifting passed a given location defined as

$$E_h = \frac{\sum_{y=1}^{Y} E_{h,y}}{Y}. \tag{2.21}$$

Here y is the index for each year being averaged over until the final year index Y and

$$E_{h,y} = \int dt[\Lambda \cdot u].$$
(2.22)

where t is time, Λ is the sea ice area fraction or sea ice concentration (SIC), u is the sea ice velocity field.

Ice actions vary significantly based on sea ice parameters and empirically the sea ice concentration has been shown to be an important parameter in this regard. Thus to account for lesser loads occurring with lower sea ice concentrations Λ, a calibration of (2.22) is made based on a paper by Thijssen and Fuglem (2015). The authors propose to calibrate the sea ice strength coefficient C_R by using an effective sea ice concentration

$$\Lambda^* = \Lambda \cdot C(\Lambda),$$
(2.23)

where

$$C(\Lambda) = \begin{cases} 0.6, & \text{if } \Lambda \geq 60\% \\ 0.01, & \text{if } \Lambda < 60\% \end{cases}.$$
(2.24)

The adjusted sea ice exposure term called the sea ice concentration adjusted annual sea ice drift length is

$$E_{h,y}^* = \int dt[\Lambda^* \cdot u].$$
(2.25)

2.6.2 Nansen factor for sea ice drift velocity

Sea ice drift velocity is an important parameter to the analysis herein, however it remains difficult accurately assess without a far more involved climate model.

The sea ice drift velocity u is expressed as

$$u = Na \cdot v,$$
(2.26)

where v is the local 10 m wind velocity and Na is the Nansen number defined as:

$$Na = \sqrt{\frac{\rho_a C_a}{\rho_w C_w}},$$
(2.27)

where ρ_a is the density of air, ρ_w is the density of water, C_a is the sea ice drag coefficient in air and C_w is the sea ice drag coefficient in water. For typical conditions in the Baltic Sea, this fraction is approximately 0.025 (Hornnes et al., 2022; Leppäranta and Omstedt, 1990).

2.6.3 Sea ice strength coefficients C_R

The sea ice strength coefficient C_R is modelled by Kärnä and Qu through an empirically fitted Gumble extreme value distribution with a cumulative probability function (Thijssen and Fuglem, 2015; Kärnä et al., 2006)

$$F_p(p) = \exp(-\exp(-\frac{p - \mu - \alpha \cdot \ln N}{\alpha})), \tag{2.28}$$

where $\mu = 0.7057\,\text{MPa}$, $\alpha = 0.1092\,\text{MPa}$, p is the globally averaged pressure determining the ice strength coefficient in mega pascals through the cumulative probability $F_p(p)$. The term

$$N = N_0 \cdot \frac{E_h}{E_0} \tag{2.29}$$

is an adjustment to the reference strength parameter N_0 based the sea ice strength relative to this reference. Here E_h is a measure of the local sea ice exposure compared to a reference measure E_0 corresponding to the value of E_h at the location where N_0 is determined.

Høyland et al. (2023) brings light to further calibrations to the sea ice strength coefficient C_R for crushing mode effects like the "velocity effect", "compliance effect" and "dynamic augmentation" that make the crushing loads valid for low far-field velocities. A suggested empirical factor of 1.4 is used by Kärnä and Masterson (2011) to account for this.

The research herein has not applied this suggested empirical factor.

2.7 Sea ice ridge statistics

Sea ice ridge frequency and ridge keel draft thickness have been related to level ice draft through statistical relations based on data from an ice profiling sonar experiment in the Beaufort Sea (Samardžija and Høyland, 2023). This research was motivated by two difficulties for accurate probabilistic simulations of ice ridge loads identified by Samardžija et al. (2018).

1. How to quantify the correlation between the level ice thickness and the ridge keel draft.

2. How to adequately quantify the correlation between the level ice thickness and the ridge keel draft.

Weekly deepest keel draft is related to level ice draft as

$$h_{KD} = h_{iD}a_1 + b_1, \tag{2.30}$$

where h_{KD} is the weekly deepest keel draft, h_{iD} is the level ice draft and, $a_1 = 8.63$ and $b_1 = 3.99$ m are least-square approximation constants to the linear relation.

Weekly mean keel draft is related to level ice draft as

$$h_{KD}^* = h_{iD}a_2 + b_2, \tag{2.31}$$

where h_{KD}^* is the weekly mean ridge keel draft, h_{iD} is the level ice draft and, $a_2 = 6.03$ and $b_2 = 0.51$ m are least-square approximation constants to a linear fit.

The number of ridges observed per week is similarly fitted to the exponential,

$$N_R = h_{iD}^{b_3} a_3, \tag{2.32}$$

where N_R is the number of ridges per week, h_{iD} is the level ice draft and, $a_3 = 84.69$ m and $b_3 = 1.318$. For the sake of unit parity take the level ice draft h_{iD} should be divided by a reference value 1 m to make the core of the exponential dimensionless.

Spatial ridge frequency is approximated to be related as,

$$\omega_{NR} = N_R/a_4, \tag{2.33}$$

where ω_{NR} is the spatial ridge frequency and $a_4 = 61.8$ km/week. Thus we can relate the spatial ridge frequency ω_{NR} to the level ice draft h_{iD} as

$$\omega_{NR} = h_{iD}^{b_3} \frac{a_3}{a_4}. \tag{2.34}$$

2.8 Monte Carlo simulation and extreme values

The thermal growth of sea ice is well described by the freezing degree day model, however sea ice ridges where the sea ice thickness extremes are found in first year ice are a mechanical growth phenomenon. The sea ice ridge parameters are described by statistical relations with the thermally grown level ice thickness. To synthesize time series of sea ice ridge parameters based on freezing season conditions the freezing degree day modelled level ice thickness results is grouped by basin to reflect the variations between the various sub basins. These basin groups are further grouped into monthly buckets allowing the formation of level ice thickness distributions for each month and sub basin. Along with the probability for ice in a given month-basin, defined as the number of data points in the sub basin with FDD predicted sea ice relative to the total population of datapoints in the month-basin. The distributions of level ice thickness are transformed to level ice draft thickness and logarithmic normal distributions are fitted to the data according similar to the distributions identified by Samardžija and Høyland (2023) for the level ice draft in the Beaufort Sea.

To synthesize sea ice ridge parameter distributions for each sub basin random samples are drawn from the population of month-basin distributions according to their respective probability of ice throughout the freezing season and the sea ice ridge draft thickness and sea ice ridge spatial frequency distributions for each sub basin is defined according to the Samardžija and Høyland (2023) empirical relations.

Chapter 3

Results

This chapter presents the results of the modeling and data analysis devised to better understand the sea ice conditions in the Baltic Sea. The results are classified into four sections.

The first section presents the freezing season start and end boundaries as well as the sea ice thickness results of a Freezing Degree Day (FDD) model. The model has been applied to ERA5 surface temperature time series data. Variations of the FDD model with and without taking the insulating effects of snow into consideration are evaluated at the Norströmsgrund Lighthouse. The results of this experiment is then compared to a series of other data sources reporting the sea ice thickness directly. Furthermore the sea ice concentration conditions presented in those same data sources are presented. The data sources and their parameters are shown in table 2.1.

The second section presents the sea ice strength coefficient based on two different models. The first model is a free drift model applied to ERA5 wind speed time series data joined with NSIDC sea ice concentration data. The second model is the CMS_G reanalysis.

The third section takes the results of the FDD model with the defined freezing season start and end, and forms distributions for the chance of sea ice and subsequently the magnitude of the level ice thickness for every month for every basin recognised in Figure 1.1. From these distributions, the weekly deepest sea ice ridge draft and sea ice ridge spatial frequency distributions are simulated with a Monte Carlo approach.

In the last section the results of an analog study of typical freezing seasons in Polish coastal waters is carried out. The sea ice charts published by SMHI are compared with the results from the implemented FDD model.

3.1 Sea ice concentration

The sea ice concentration threshold used for determining the end of the freezing season is the NSIDC sea ice concentration. This research has used the nsidc-0051 version 2 product introduced earlier. In addition to determining the end of the freezing season this sea ice concentration data is used to adjust sea ice exposure for the estimation of sea ice strength coefficients in later sections.

The maximum sea ice concentration per NSIDC grid cell and the number of days with sea ice concentration above 60 % are shown in Figure 3.1. This shows that in the period 1978 to 2022 the NSIDC does record ice throughout the Baltic Sea with a maximum of 100 % sea ice concentration covering the Bay of Bothnia, the Bothnian Sea, the Gulf of Finland, the Gulf of Riga, and the shelterd sections of the Danish Waters. The figure also shows that the southern basins Arkona, Bornholm, and the Eastern, Western and Northern Gotland have all experienced sea ice everywhere, but it remains below 100 % for significant parts of the basins. There is a general tendency for lower maximum sea ice concentration (MSIC) further away from the coast and closer to the mouth of the Baltic Sea. These tendencies are also present in Figure 3.1b, additionally here the tendency for less ice the further south is more visible. The number of days per year with sea ice concentration above 60 % shows that the Bay of Bothnia, the inner Gulf of Finland and the Gulf of Riga, the Bothnian Sea and the most sheltered sections of the Danish Waters are most commonly experiencing significant sea ice according to NSIDC.

(a) The maximum sea ice concentrations per grid cell registered in NSIDC.

(b) Average number of days with sea ice thickness greater than 60 % per year from NSIDC. The average includes seasons without sea ice.
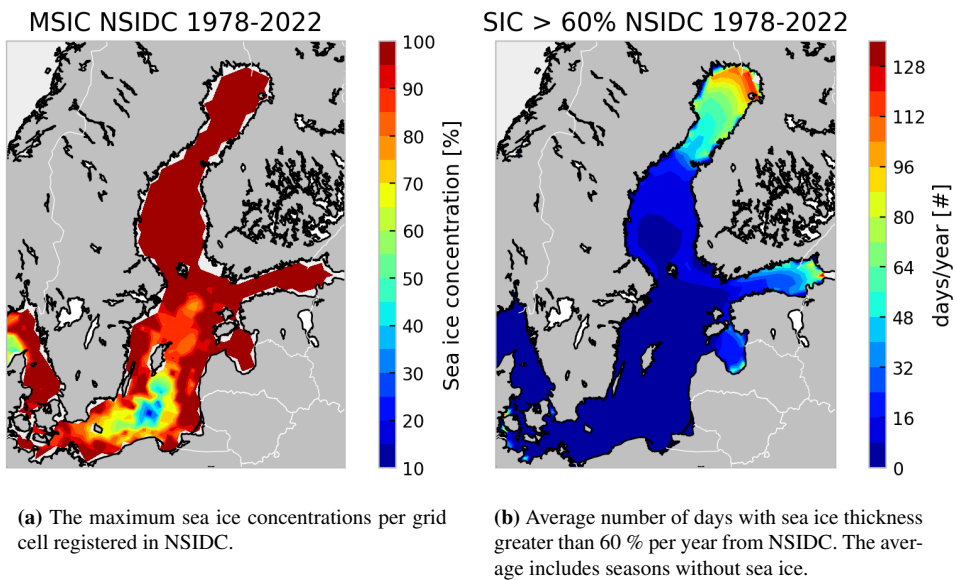
Figure 3.1: Sea ice concentration from the National Snow and Ice Data Center (NSIDC) spanning 1978-2022.

3.2 Sea ice thickness derived from freezing degree day models

The implemented FDD model is purely considering vertical sea ice thickness growth and does not take melting into consideration. Melting is primarily occurring at the end of the freezing season, thus defining the temporal boundaries of the freezing season will partially account for this oversight in the naive FDD model. The start of the freezing season is

determined as running average of the local surface temperature. The end of the freezing season is determined with a sea ice concentration threshold.

3.2.1 Defining the temporal boundary conditions of the FDD model

The starting boundary condition of the FDD model defined by the time when the 30 days running average daily mean air temperature drops below zero. (Figure 3.2) shows that the freezing season starts first in the northern Bay of Bothnia. Then it expands to the rest of the Bay of Bothnia as the freezing season starts in the inner Gulf of Finland. From these two locations the freezing season generally follows the tendency of first freeze along the coast, then expand southward and toward the opening of the Baltic Sea as the open waters freeze. Notably the sheltered Danish Waters generally freeze over earlier than the Arkona and Bornholm Basin. The southern basins does not cross the starting boundary condition defining a freezing season every winter. This is accounted for in the average by disregarding the seasons that does not qualify according to this condition. Note that these are the typical macroscopic sea ice development scenarios. Regional sea ice development scenarios, especially in the southern basins have tendency to develop both towards the opening of the Baltic Sea and inwards. This will be explored through an example in Polish coastal waters later.

Figure 3.2: Average date for the start of the freezing season using a 30 day running average, below 0 °C two meter temperature threshold. By definition, the average excludes freezing seasons that never start.
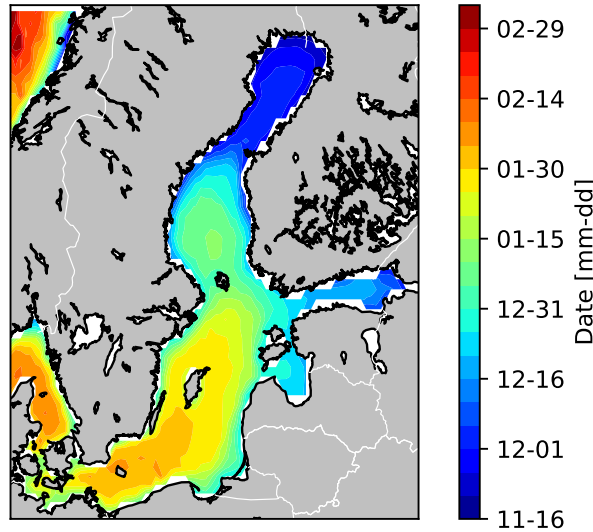
The end of the freezing season is not well defined for the FDD model considered herein. The model does not consider ice melting thus the freezing season has to end by other means. The choice of sea ice concentration data as a cutoff was made. The average end date of the freezing season is not significantly sensitive to the change in NSIDC cutoff sea ice concentration threshold as shown in Figure 3.3, however sea ice concentration data is of easier access than sea ice thickness data thus the choice of this parameter to end the freezing season was made.
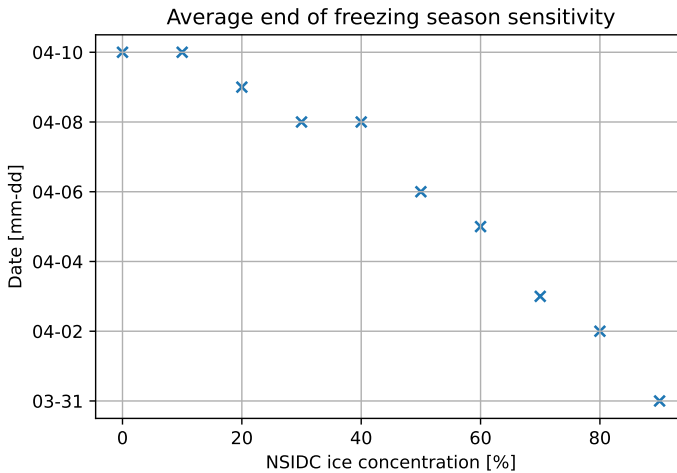
Figure 3.3: Sensitivity of the average end of the freezing season, over the entire Baltic Sea, to the NSIDC cutoff sea ice concentration. The average excludes freezing seasons without ice.

The choice of a 10 % NSIDC sea ice concentration threshold for the freezing season cutoff was made. The resulting average end of the freezing season is shown in Figure 3.4. The freezing season is shown to end first in the south of the Baltic Sea and end later the further into the Baltic. On average the season ends in late February to early March in the southern basins increasing to May in the Bay of Bothnia and the Gulf of Finland. Notably the northern basins identified in Figure 1.1 seem to be dominated by separate modes, meaning there is a stark change in end of the freezing season as one moves from one basin to another whilst there is relatively less change inside the basins. Notably the Åland Sea and the Archipelago Sea are defined by a common mode distinct from the mode defining the Bothnian Sea into which they were joined in this study. The north-eastern Bay of Bothnia freezes over earlier than the rest of the Bay of Bothnia. The same effect is present to a lesser degree in the Gulf of Finland and even less in the Gulf of Riga. Where the average end of the freezing season is later further in and in the more sheltered waters. Furthermore an open ocean section of the southern Baltic Sea south of Gotland overlapping with the region of the Baltic Sea where the MSIC was the lowest in Figure 3.1a, has a significantly earlier average end of the freezing season than the surrounding waters.
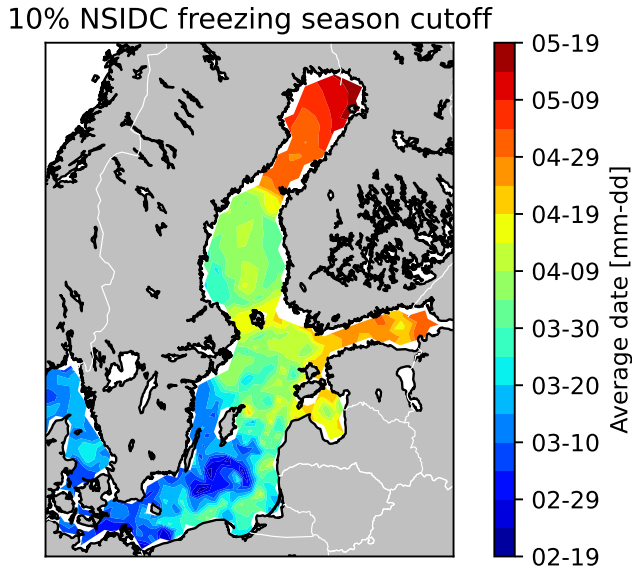
Figure 3.4: Average date for the end of freezing season using a 10% NSIDC sea ice concentration cutoff. The average excludes freezing seasons without ice.

The average start and end of the freezing season as determined by these methods are shown in Table 3.1. There is a clear distinction between the southern and northern basins. The first six basins in this table, the southern and central basins, have an average start of the freezing season in late January. In the Gulf of Riga and the Bothnian Sea the average start of the freezing season is in early January. The Gulf of Finland starts freezing in late December and in the Bay of Bothnia the freezing typically starts in early December. The different modes defining the start of the freezing season defined by the surface temperature is correlated with the distance into the Baltic Sea, the latitude and the distance from the coast.

The average date for the end of freezing season as defined by a 10 % NSIDC sea ice concentration cutoff is more significantly defined by separate modes for each sub basin of the Baltic Sea as shown in Figure 3.4 and Table 3.1 and introduced above.

Basin	mean start date	mean end date	$\sim$ mean duration [days]
Danish Waters	24. Jan	11. Mar	46
Arkona Basin	24. Jan	06. Mar	41
Bornholm Basin	28. Jan	13. Mar	44
Western Gotland Basin	22. Jan	17. Mar	54
Eastern Gotland Basin	22. Jan	28. Mar	65
Northern Gotland Basin	18. Jan	09. Apr	81
Gulf of Riga	5. Jan	17. Apr	102
Gulf of Finland	23. Dec	26. Apr	124
Bothnian Sea	2. Jan	08. Apr	96
Bay of Bothnia	07. Dec	06. May	150

Table 3.1: The average date for the start and end of the freezing season by basin using the FDD model. The end date of a freezing season without ice is not well defined thus the means for the end of the freezing season are excluding the freezing seasons without NSIDC ice.

3.2.2 FDD ice thickness results with ERA5 and NSIDC

Applying the start and end of the freezing season constraints in Chapter 3.2.1, to define the freezing season boundaries for the FDD model yields a results with temporal bounds. The maximum level ice thickness is shown in Figure 3.5. A similar pattern to earlier is shown where severity of the freezing season and in this case the maximum sea ice thickness per grid cell is decreasing from its maxima in the northwestern Bay of Bothnia and the Gulf of Finland as one approaches the mouth of the Baltic Sea. In maximum level ice thickness there is a difference of between 10 cm and 15 cm between large parts of the western and eastern shores of the Bothnian Sea. The Bay of Bothnia has a similar difference between the south and the north. The pattern of thicker ice in the north, along the coast and farthest from the opening of the Baltic Sea is also found in this data both when considering locations in the same sub basin and between sub basins.
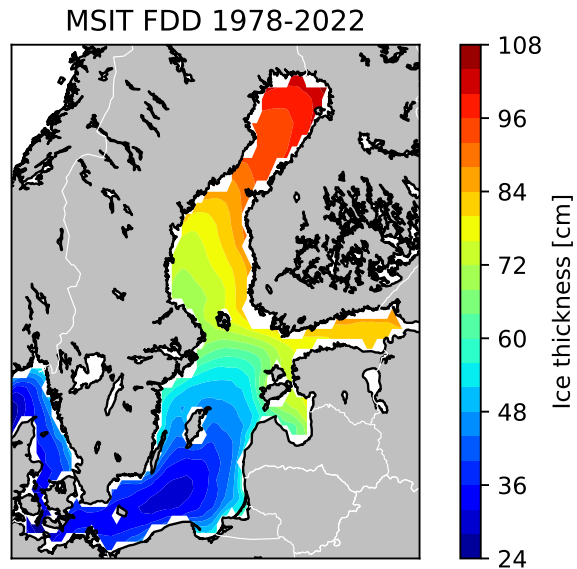
Figure 3.5: Maximum Sea Ice Thickness (MSIT) FDD results with freezing season adjustment for the entire Baltic Sea.

3.2.3 The insulating effect of snowfall

Two types of freezing degree day models were considered in this thesis. The FDD models with and without insulation from a snowfall layer. All these models are sensitive to parameter choices as defined in 2.5 and as recognised by Leppäranta (1983) in the sea ice growth models review.

The insulating effect of snow can have a significant impact on the level ice thickness growth. Figure 3.6 shows results from two FDD models for the Norströmsgrund location. In red a FDD model without snow insulation and in blue a model with snow insulation.
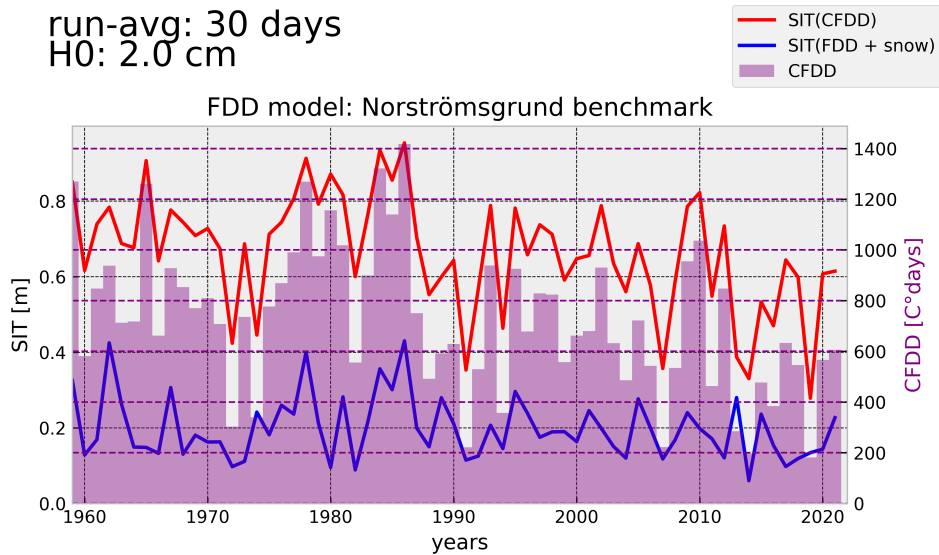
Figure 3.6: Sea ice thickness estimates for Norströmsgrund lighthouse in the Bothnian Bay using a freezing degree day (FDD) model that takes insulation effects due to snow fall into account in blue and a FDD model that does not take insulation due to snow fall into account in red. The cumulative freezing degree days (CFDD) for each year is shown as a bar plot in pink corresponding to the rightmost vertical axis. A running average condition of 30 days below zero degrees Celsius was imposed on the two meter air temperature before the start of each freezing season. Snow fall was ignored with sea ice thicknesses (H0) below 2 cm.

The non-insulating model uses the empirically defined coefficient a from equation (2.12). Equivalently the insulating model uses values for k_i, ρ_i and L_f as if $a = \sqrt{\frac{2\kappa_i}{\rho_i L_f}} = 2.6 \times 10^{-2}$, the empirically defined constant suggested in the international standard (ISO 19906:2019). This choice of parameters yields the maximum sea ice thickness presented in Figure 3.7. For this choice of effective parameters the sea ice thicknesses are typically reduced by less than 25% of the non insulating value and the maximum sea ice thickness shown in the figure is typically reduced by less than 20%. In some interesting cases there is almost no reduction, see for example the northern Gulf of Riga and the eastern Bothnian Sea. Note in the extremes we rely only on the most extreme winters, and if there was little precipitation that winter then the effect of a single event has large impact on the results.

An alternate choice of parameters as shown by Tikanmäki and Heinonen (2022) and presented in 2.8 results in a more severe effective reduction. Tikanmäki and Heinonen reports an effective reduction of between 2 cm and 7 cm for their Bornholm data or typically less than 25% of the non insulating value. A similar implementation, and additionally using the adjusted freezing season start and end as defined above typically reduces the level ice thickness by between 50 % and 75 %. The stark difference in effective reduction might be due to the difference in snow fall. This model considers all precipitation falling when the air temperature is below freezing to fall as snow. Furthermore the total precipitation is transformed from units of meters of water equivalent to units of meters of snow according

to the relative ratio of the mass density of snow and the mass density of water. These assumptions likely do not hold on the floe in the ocean due to spray from waves facilitating the formation of snow-ice, wind blowing snow away, the density of snow changing through time, solar radiation and other sources inducing change in the snow layer.

The precipitation data is the "Total Precipitation" product from the ERA5 dataset (Hersbach et al., 2022).

For further considerations in this thesis the non insulating model is used as it is more conservative and relies on less variables. The parameters in the insulating model are shown to have a significant impact on the effective reduction in the level ice thickness in agreement with Leppäranta (1993, 1983).
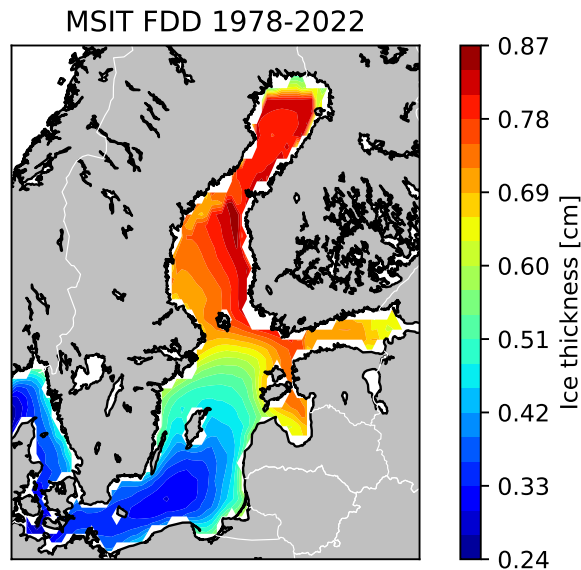
Figure 3.7: Maximum Sea Ice Thickness (MSIT) FDD results with freezing season adjustment and insulation due to snow for the entire Baltic Sea.

3.2.4 Ice thickness from the BASIS archive

Maximum sea ice thickness and sea ice concentration as well as an estimate for freezing season duration were extracted from the BASIS digitized archive of historical ice charts in the Baltic Sea and displayed in Figure 3.8 and 3.9. The BASIS maximum reported sea ice thicknesses are as thick in sections of Danish Waters, Western Gotland Basin, the Gulf of Finland and the Bothnian Sea as in the Bay of Bothnia. The northern Bay of Bothnia has a significantly longer reported freezing season than the rest of the Baltic Sea both in terms of the 60% sea ice concentration threshold and the 10 cm sea ice thickness threshold. Note

that the Archipelago Sea is significantly different than the surrounding sub basins in terms of sea ice thickness but not as starkly in terms of sea ice concentration. The open ocean in the Southern Baltic Sea is clear in the BASIS dataset. Several of these gridpoints have no recorded sea ice and many have very few recordings, and those they have are of low severity.

(a) Maximum Sea Ice Thickness registered per grid cell in the BASIS archive.

(b) Average number of days per year with sea ice thickness greater than 10 cm in BASIS. The average is over all years and does not exclude freezing seasons without ice.
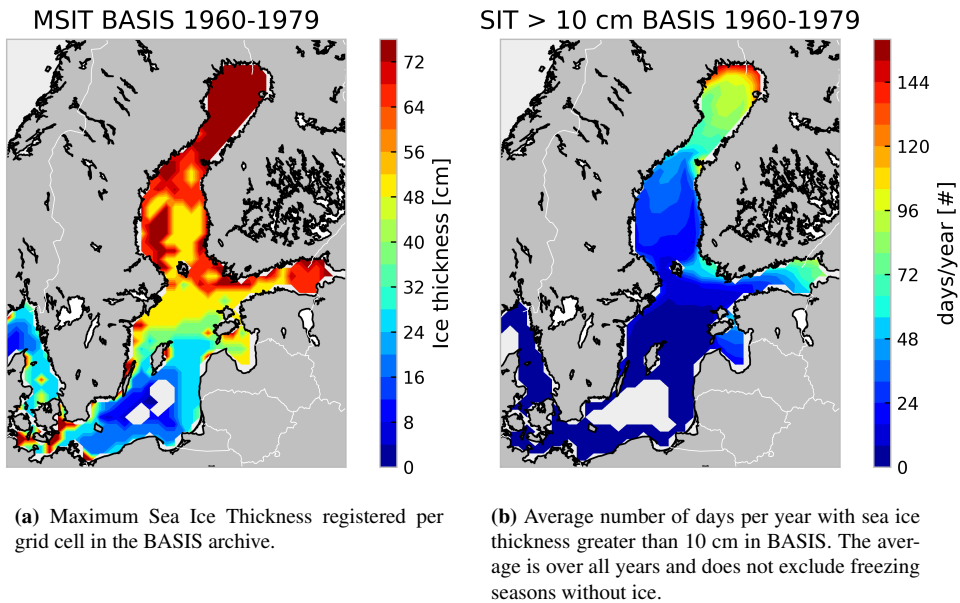
Figure 3.8: Sea ice thickness from the Data Bank of Baltic Sea Ice and Surface Temperatures (BASIS) spanning 1960 to 1979.

(a) Maximum Sea Ice Concentration registered per grid cell in BASIS.

(b) Average number of days per year with sea ice concentration greater than 60 % in BASIS. The average is over all years and does not exclude freezing seasons without ice.
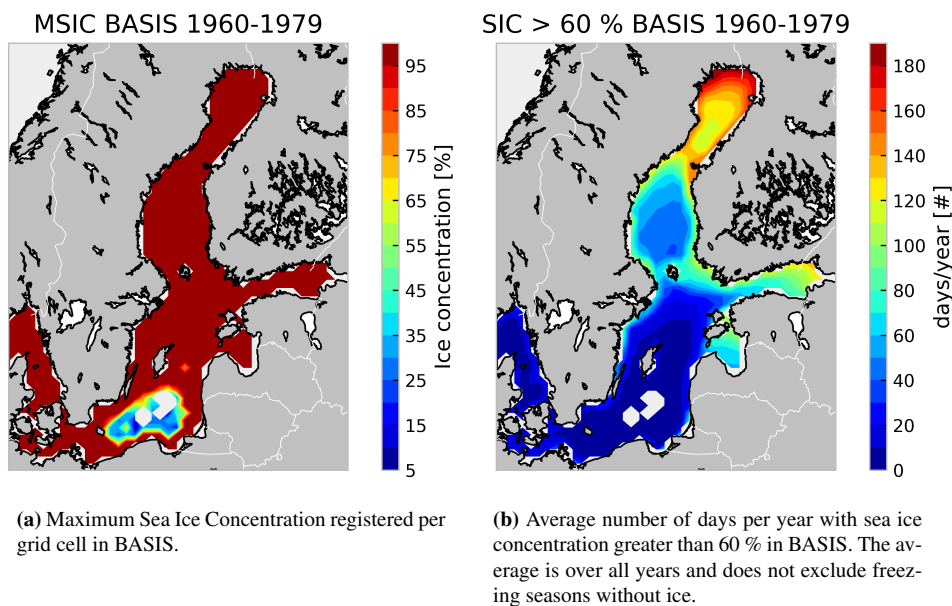
Figure 3.9: Sea ice concentration from the Data Bank of Baltic Sea Ice and Surface Temperatures (BASIS) spanning 1960 to 1979.

3.2.5   Finnish Meteorological Institute sea ice conditions

The sea ice thickness and sea ice concentration in the FMI dataset is of very high spatial resolution. Some minor islands are visible as masked Not A Number values in the figures 3.10 and 3.11. Despite their high spatial resolution the data is only distributed on an easily computer readable format starting with data from 2018. The charts show similar magnitude in the maximum sea ice thickness, however their contours are significantly different. The FMI data also shows that the most severe sea ice conditions are along the coast in the northern Bay of Bothnia, however with a significant peak in sea ice thickness in the central parts of the Bay of Bothnia. The duration of the freezing season by both the 60% sea ice concentration threshold and the 10 cm sea ice thickness threshold are between 20 and 30 days for most areas with recorded ice.

(a) Maximum Sea Ice Thickness per grid cell in FMI.

(b) Average number of days with sea ice thickness greater than 10 cm per year from FMI. The average is over all years and does not exclude freezing seasons without ice.
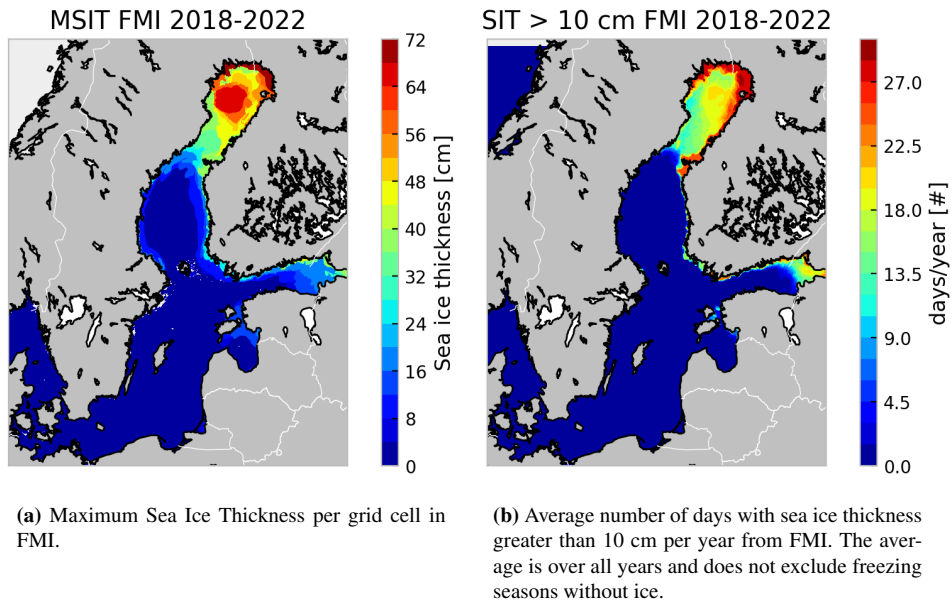
Figure 3.10: Sea ice thickness from the Finnish Meteorological Institute (FMI). The data spans 2018 to 2022.

(a) Maximum Sea Ice Concentration per grid cell in FMI.

(b) Average number of days with sea ice concentration greater than 60 % per year from FMI. The average is over all years and does not exclude freezing seasons without ice.

Figure 3.11: Sea ice concentration from the Finnish Meteorological Institute (FMI). The data spans 2018 to 2022.

3.2.6 Copernicus Marine Service sea ice conditions

The CMS$_B$ dataset was discarded due to unphysical sea ice thicknesses of several meters in Polish waters. In the following the CMS dataset refers to the CMS$_G$ dataset introduced in 2.4.2. The sea ice data from the CMS dataset are sho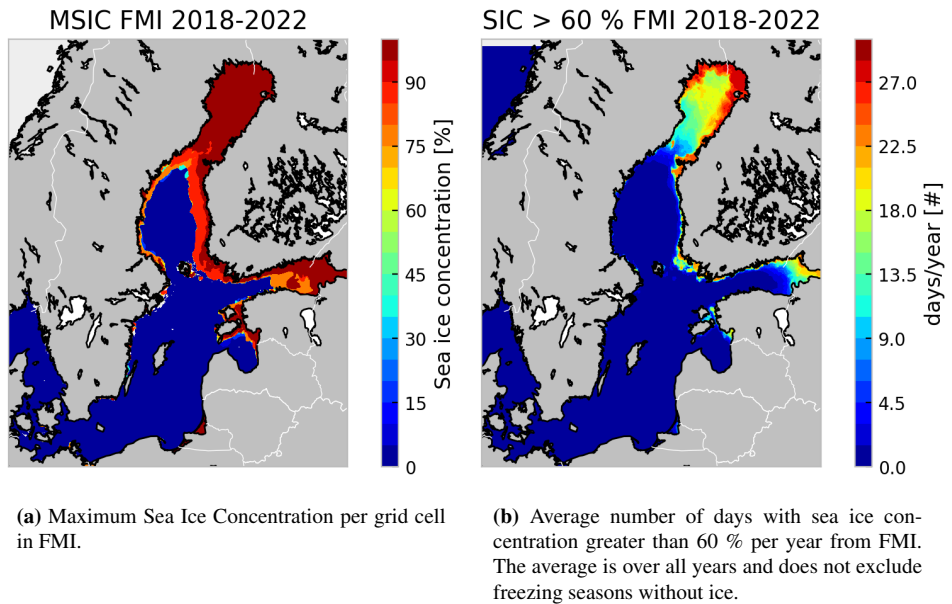wn in the Figures 3.12, 3.13 and 3.15. Notably the sea ice thickness data from CMS dataset is less than 10 cm in the exposed parts of the Danish waters and some of the non coastal parts of the Arkona and Bornholm basins. The sea ice thickness is also thicker in the Åland Sea than Archipelago sea. The thickness in the Quark, the border region between the Bothnian Sea and the Bay of Bothnia has notably thinner sea ice than the parts of the sub basins surrounding it. The sea ice thickness data is speckled with peaks significantly higher than the surrounding sea ice. One such peak in the south-eastern Bay of Bothnia records a sea ice thickness of 2.7 m and stands out clearly in the contour 3.12a. In general the there is more ice the further north, closer to the shore and the furthest into the Baltic Sea. Note that the eastern parts of the Bothnian Sea have significantly more sea ice than western parts of the same basin.

The sea ice concentration is very low in the southern basins. Note that CMS estimates very little sea ice along the polish coast and in the Arkona and Bornholm basins as well as the area around Gotland.

The sea ice exposure is close to zero in the immediate vicinity of a coastline. The exposure then forms maxima further out at sea when compared to the highest sea ice thickness and sea ice concentration. The highest exposure is found in the Quark along the Finnish Coast, however the most consistent exposure, i.e. the area with the most days with sea ice exposure is in the northern Bay of Bothnia.

(a) Maximum Sea ice Thickness per grid cell registered in CMS.

(b) Average number of days with sea ice thickness per grid cell greater than 10 cm per season. The average is over all years and does not exclude freezing seasons without ice.
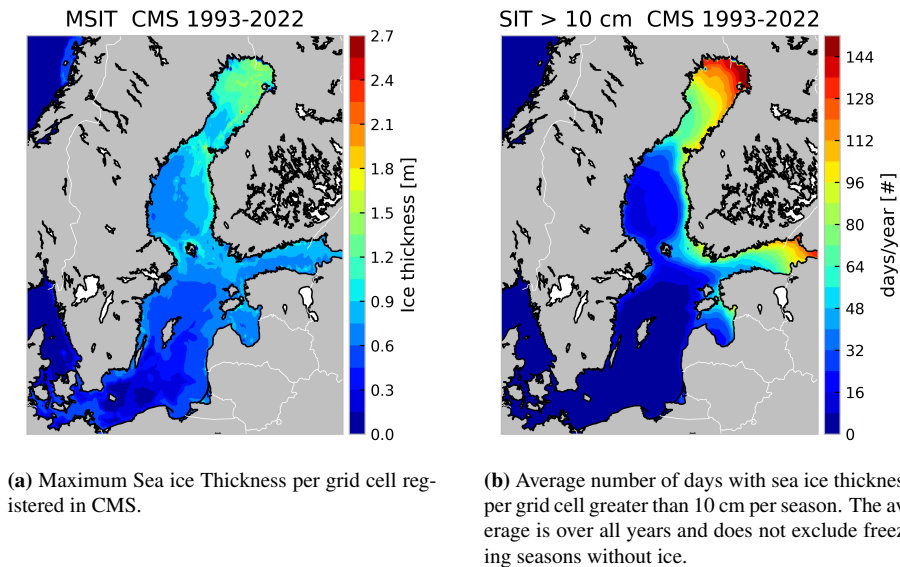
Figure 3.12: Sea ice thickness from the Copernicus Marine Service (CMS) GLOBAL_MULTIYEAR_PHY_001_030 reanalyses.

(a) Maximum Sea Ice Concentration per grid cell registered in CMS.

(b) Average number of days with sea ice concentration per grid cell greater than 60 % per year in CMS_G. The average is over all years and does not exclude freezing seasons without ice.
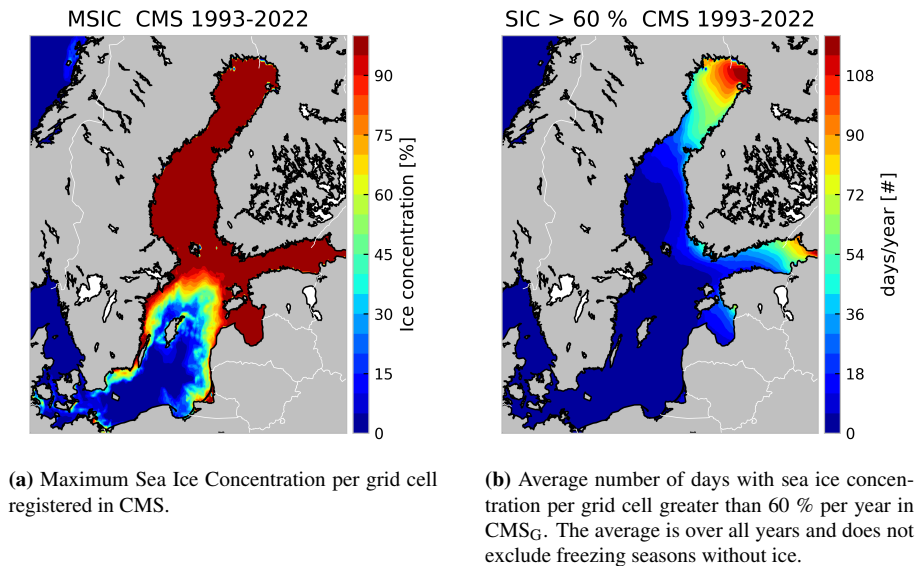
Figure 3.13: Sea ice concentration from the Copernicus Marine Service (CMS) GLOBAL_MULTIYEAR_PHY_001_030 reanalyses.

3.2.7 Data comparison

The various data sources have been briefly introduced and the characteristics defining certain aspects of each data source was highlighted. In the following the data will be given more context and presented in comparison with other locations and basins. Note the locations of interest discussed are key benchmark locations, Norströmsgrund lighthouse in the north and the Kriegers Flak offshore wind farm in the south. Furthermore, the Baltyk I, II and III locations are presented. All these locations are marked in figure 1.2. The basins referred to are shown in figure 1.1.

Firstly, the CMS data estimate significantly thicker sea ice in the northern basins than all the other sources and significantly less sea ice concentration in the southern basins. FMI is based on few seasons, furthermore these seasons were not particularly severe either. These seasons show little sea ice in the southern basins. The BASIS archive typically reports less severe sea ice conditions than the other sources.

The non insulating FDD model is generally conservative and estimates sea ice thicknesses similar to or higher than the other sources for all locations except CMS in the Bay of Bothnia.

The duration of the freezing season in the FDD model as defined by a running average temperature threshold for the start and sea ice concentration threshold for the end describes similar behavior for the duration of the freezing season as is estimated by the various estimates for freezing season duration through the number of days per year with ≥ 10 cm sea ice thickness or the ≥ 60 % sea ice concentration for the different data sources.

Statistics on sea ice thickness and concentration is presented in Table 3.2. Note that whilst SIT_{10} is well behaved for the ERA5 based FDD model it is not reported here due to

a caution raised by the international standard (ISO 19906:2019) to not use FDD estimated sea ice thickness as instantaneous measurements throughout the season. However, the standard encourages the use of FDD models to estimate the end of season sea ice thickness.

Table 3.2: Sea ice parameter records for key areas of interest in the Baltic Sea. MSIT is the Maximum Sea Ice Thickness and MSIC is the Maximum Sea Ice Concentration. SIT_{10} is the average number of days per year with a sea ice thickness greater than 10 cm and SIC_{60} is the average number of days per year with a sea ice concentration above 60 %. Norströmsgrund refers to Norströmsgrund Lighthouse in the Bothnian Bay. See 1.2 for location placements. * The BASIS archive records two datapoints per week, thus these calculations assume that all days between two closest datapoints that satisfy a condition will also satisfy that condition. SIT_{10} is not reported for the ERA5 FDD model as presented above.

Area	MSIT [cm]				MSIC [%]			
	ERA5	CMS	BASIS	FMI	CMS	BASIS	NSIDC	FMI
Norströmsgrund	95	122	73	65	100	100	100	100
Kriegers Flak	34	27	26	0	4	100	100	0
Bałtyk I	31	17	17	0	< 1	0	39.6	0
Bałtyk II	34	2	17	0	< 1	25	65.2	0
Bałtyk III	35	7	0	0	< 1	100	74.8	0

Area	MSIT [cm]				MSIC [%]			
	ERA5	CMS	BASIS	FMI	CMS	BASIS	NSIDC	FMI
Danish Waters	55	19	32	< 1	5	100	96	< 1
Arkona Basin	41	43	38	< 1	21	100	99.9	3
Bornholm Basin	47	27	18	< 1	13	72	91	< 1
W. Gotland Basin	69	56	39	< 1	53	98	99.9	4
E. Gotland Basin	64	47	24	< 1	30	84	99.9	4
N. Gotland Basin	82	66	51	< 1	77	100	100	8
Gulf of Riga	77	72	48	6	99	100	100	38
Gulf of Finland	88	77	63	6	99	100	100	72
Bothnian Sea	95	79	62	10	99	100	100	45
Bay of Bothnia	106	111	72	54	99	100	100	99

Area	SIT_{10} $[\frac{days}{year}]$				SIC_{60} $[\frac{days}{year}]$			
	ERA5	CMS	BASIS*	FMI	CMS	BASIS*	NSIDC	FMI
Norströmsgrund	-	98	85	16	70	130	64	17
Kriegers Flak	-	< 1	2	0	0	7	1	0
Bałtyk I	-	< 1	0	0	0	0	0	0
Bałtyk II	-	0	< 1	0	0	< 1	< 1	0
Bałtyk III	-	0	< 1	0	0	2	< 1	0

| Area	SIT_{10} $[\frac{days}{year}]$				SIC_{60} $[\frac{days}{year}]$			
	ERA5	CMS	BASIS*	FMI	CMS	BASIS*	NSIDC	FMI
Danish Waters	-	< 1	2	< 1	< 1	11	3	< 1
Arkona Basin	-	1	1	< 1	< 1	12	4	< 1
Bornholm Basin	-	< 1	< 1	< 1	< 1	7	2	< 1
W. Gotland Basin	-	7	5	< 1	< 1	24	8	< 1
E. Gotland Basin	-	3	1	< 1	< 1	12	11	< 1
N. Gotland Basin	-	22	16	< 1	6	38	31	< 1
Gulf of Riga	-	42	32	4	20	77	74	2
Gulf of Finland	-	80	53	8	44	95	101	6
Bothnian Sea	-	30	30	6	9	69	39	3
Bay of Bothnia	-	98	89	25	65	142	114	20

Table 3.3: Freezing degree day statistics from the ERA5 based freezing degree day model at areas of interest in the Baltic Sea. $CFDD_{avg}$ is the average cumulative freezing degree days per year. $CFDD_{max}$ is the maximum cumulative freezing degree days estimated by this model in the years 1978-2022.

| Area	$CFDD_{avg}$ [°C · Day]	$CFDD_{max}$ [°C · Day]
Norströmsgrund	715	1413
Kriegers Flak	40	227
Bałtyk I	59	225
Bałtyk II	50	210
Bałtyk III	41	180
Area	$CFDD_{avg}$ [°C · Day]	$CFDD_{max}$ [°C · Day]
Danish Waters	67	874
Arkona Basin	55	452
Bornholm Basin	52	403
W. Gotland Basin	102	734
E. Gotland Basin	96	669
N. Gotland Basin	173	1066
Gulf of Riga	271	961
Gulf of Finland	452	1216
Bothnian Sea	333	1401
Bay of Bothnia	805	1823

3.3 Sea ice strength coefficients C_R

The second experiment presented in this thesis is the determination of the sea ice strength coefficient C_R. The sea ice strength coefficient depends on ice exposure estimated from sea ice concentration and sea ice drift velocity. The strength coefficient was calculated with two different sets of data sources. First a combination of ERA5 wind speeds to form a free drift sea ice model combined with NSIDC sea ice concentration, and second a CMS based approach.

The ERA5-NSIDC based sea ice strength coefficients are presented in figure 3.14a-3.14c. The exposure that defines the different coefficients is shown in figure 3.14d. The exposure with the ERA5-NSIDC approach is significantly higher than the CMS exposure in figure 3.15. Notably the contours are also different as the ERA5-NSIDC approach yields sea ice drift in the immediate vicinity of the coast which is not found in the CMS approach. Interestingly the strength coefficients in the CMS approach have similar results to the ERA5-NSIDC coefficients in the northern Baltic Sea, including the Gulf of Riga, the Gulf of Finland, the Bothnian Sea and the Bay of Bothnia. The stark difference between the two are in the south where the CMS dataset estimates no ice for most of the open ocean area and and a significant part of the coastline of those southern basins, see Figure 3.15.
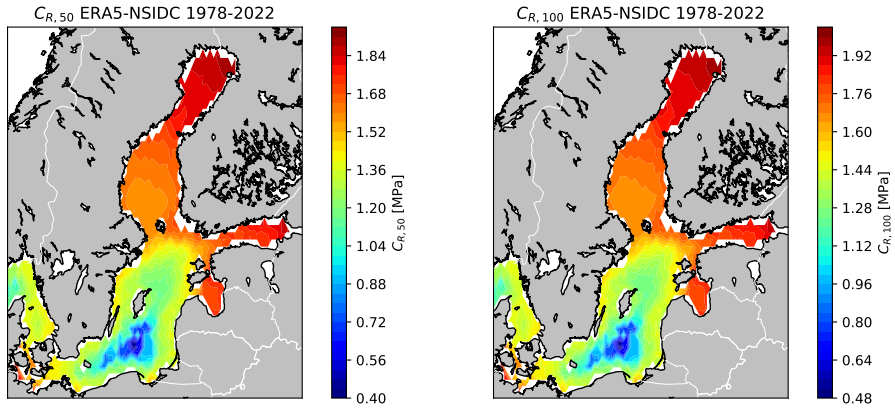
(a) The sea ice strength coefficient for a 50 year return period.

(b) The sea ice strength coefficient for a 100 year return period.
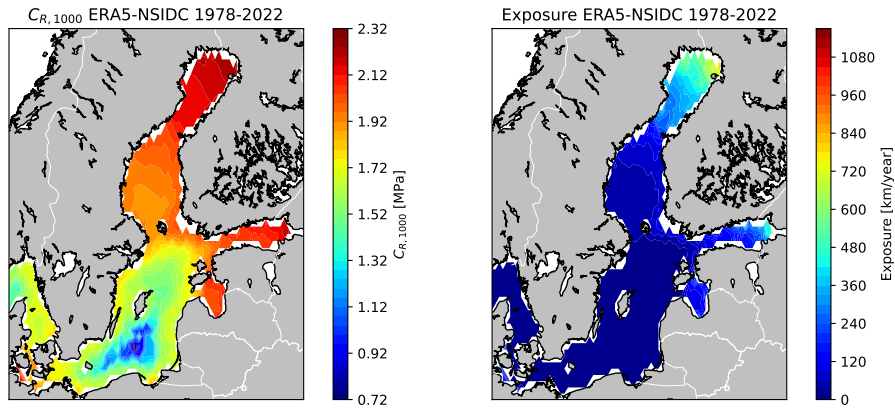
(c) The sea ice strength coefficient for a 1000 year return period.

(d) Sea ice exposure based on ERA5 wind speeds and NSIDC sea ice concentration.

Figure 3.14: The sea ice strength coefficient calculated for various return periods with wind velocity data from ERA5 and sea ice concentration data from NSIDC.

Exposure CMS 1993-2022

Exposure > 1km CMS 1993-2022
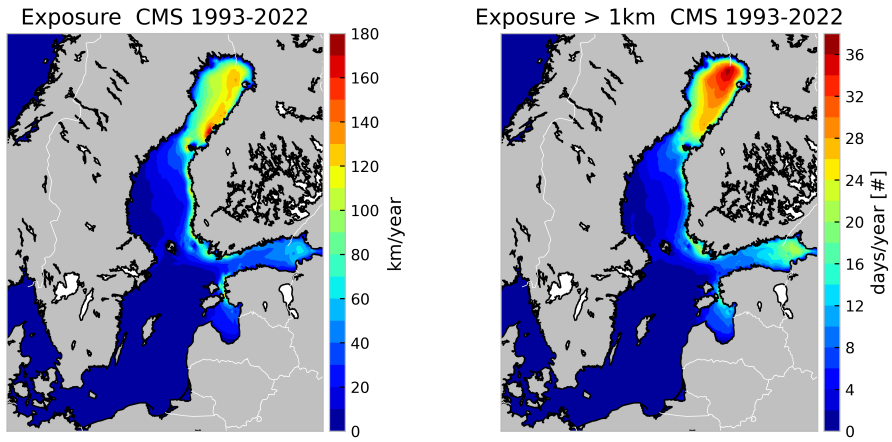
(a) Sea ice exposure per grid cell measured in km of sea ice drifting past each year. The sea ice exposure is adjusted for sea ice concentration according to formula 2.25.

(b) The yearly average number of days per grid cell with sea ice exposure above 1 km per day.

Figure 3.15: Sea ice exposure from the Copernicus Marine Service GLOBAL_MULTIYEAR_PHY_001_030 (CMS$_G$) reanalysis.

Table 3.4: Load coefficients calculated based on NSIDC adjusted sea ice concentration and an ERA5 based sea ice free drift model. The load coefficients $C_{R,Y}$ are the sea ice strength coefficients C_R calculated for return periods of Y years. Exposure is the annual average exposure calculated from 1978-2022, the duration of NSIDC sea ice concentration records. Norströmsgrund refers to Norströmsgrund Lighthouse. See Figure 1.2 for location placements.

Area	Exposure $[\frac{km}{year}]$	$C_{R,50}$ $[MPa]$	$C_{R,100}$ $[MPa]$
Norströmsgrund	378	1.83	1.91
Kriegers Flak	7.4	1.40	1.48
Bałtyk I	1×10^{-2}	0.74	0.81
Bałtyk II	7×10^{-1}	1.14	1.22
Bałtyk III	2.0	1.26	1.34
Area	Exposure $[\frac{km}{year}]$	$C_{R,50}$ $[MPa]$	$C_{R,100}$ $[MPa]$
Danish Waters	19	1.38	1.46
Arkona Basin	7	1.38	1.45
Bornholm Basin	1	1.10	1.18
W. Gotland Basin	5	1.34	1.42
E. Gotland Basin	3	1.19	1.27
N. Gotland Basin	24	1.45	1.53
Gulf of Riga	119	1.69	1.76
Gulf of Finland	240	1.76	1.84
Bothnian Sea	91	1.65	1.73
Bay of Bothnia	465	1.85	1.93

Note that CMS based sea ice strength coefficients in the southern basins are based on data that is very sparse and inconsistent with the other sources. The sea ice strength coefficients based on very low exposures in general such as the specific grid points of the Bałtyk licences instead of the basins they are in yield coefficients based on a much lower number of datapoints.

Note that due to the logarithmic nature of the statistical distribution of the strength coefficients from Equation (2.28) parameterised by the adjusted sea ice exposure even large changes in sea ice exposure have only a small effect on the coefficient.

3.4 Ridge parameters derived from sea ice draft distributions

3.4.1 Baltic sea vs. Beaufort sea

The sea ice ridge parameters sea ice ridge draft thickness and spatial frequency are drawn from distributions of the level ice draft thickness. These statistical relations were based on level ice draft and sea ice ridge parameters by Samardžija and Høyland (2023) from the Beaufort Sea.

The Beaufort Sea has more severe freezing seasons and does contain multiyear ice as well as first year ice. The relations were based on level ice draft distributions from the Beaufort Sea with the majority of data points between 0 m and 2.5 m. The FDD data for

the Baltic Sea are mostly between 0 m and 1 m even for the most severe month-basins in the Baltic sea.

In the following subchapters, the month-basin distributions for level ice draft is presented for the Bornholm Basin containing the Baltyk I, II and III licences in the southern Baltic Sea and the Bay of Bothnia in the northern Baltic Sea. The other basin-month distributions and subsequent level ice draft thickness, sea ice ridge draft thickness and sea ice ridge spatial frequency distributions are added in Appendix C.

3.4.2 Determining the level ice draft thickness

Level ice draft is the submerged section of the level ice. The draft is calculated from the level ice thickness based on the relative mass densities of ice and water from Chapter 2.5.2. The monthl distributions for the level ice draft in the Bornholm Basin is displayed for December through March in Figure 3.16. The April and May distributions have very few data points and thus also a very low probability of ice and little influence on the final sea ice parameter distributions. The level ice draft grows through the season and reaches a maximum a little under 1 m in the end of the season.
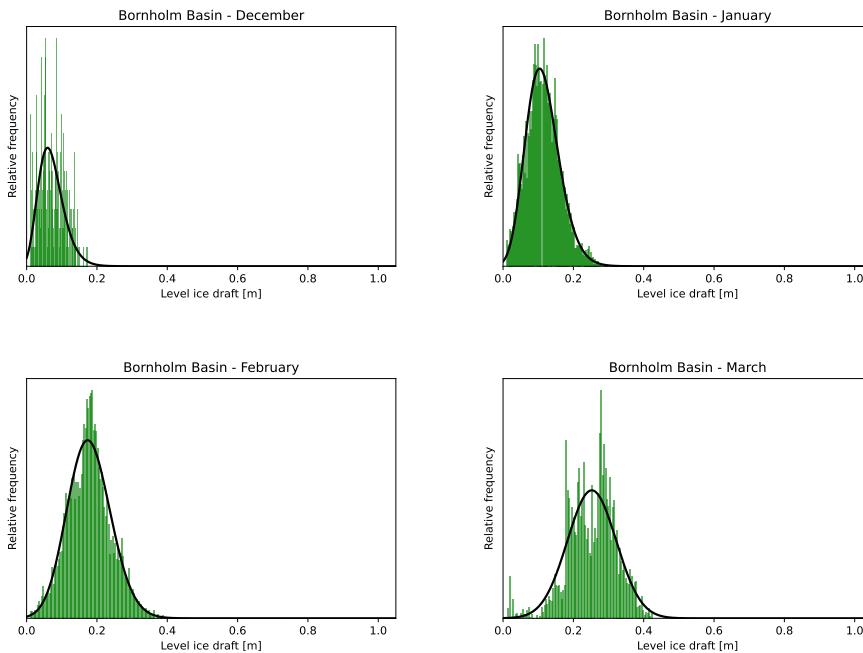

Figure 3.16: Bornholm Basin monthly level ice distributions.

The monthly distributions for the level ice draft in the Bay of Bothnia is displayed for December through March in Figure 3.17. The level ice draft grows through the season and reaches a maximum a little under 1 m in the end of the season. Note that the level ice

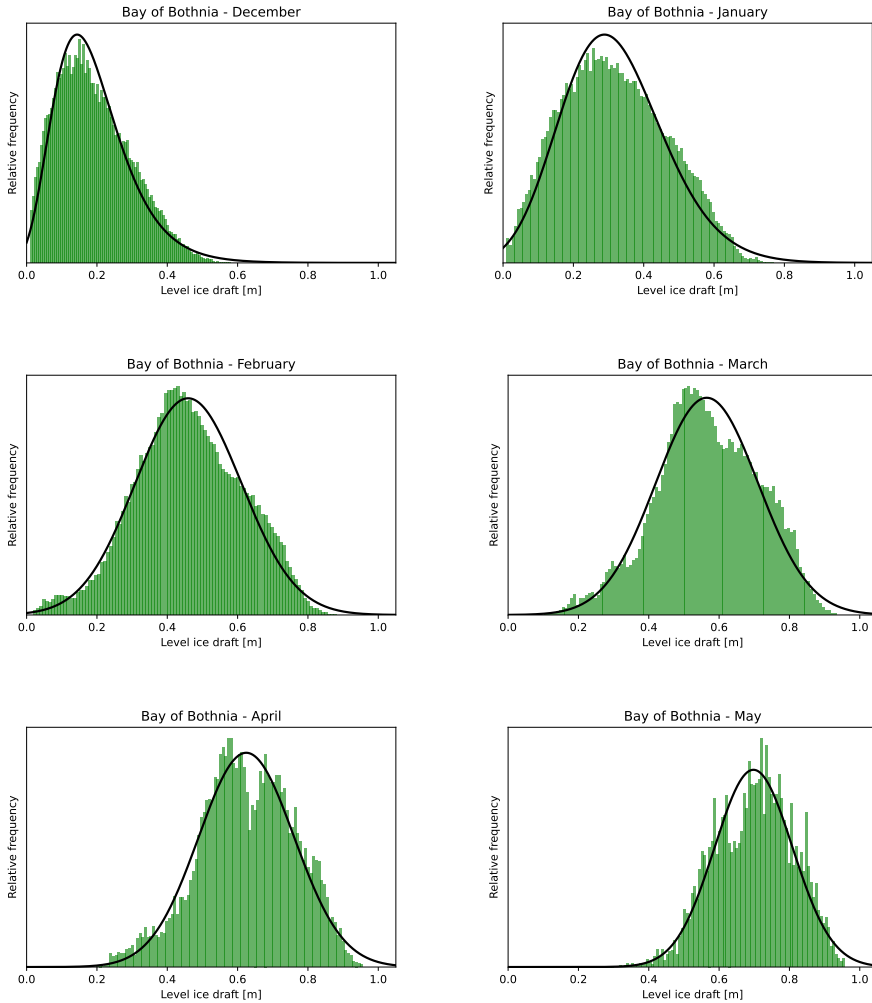draft in this thesis, defined by the assumed ice and water densities, is 90% of the level ice thickness.

Figure 3.17: Level ice draft distributions through the freezing season.

3.4.3 Simulated distributions

Distributions of the level ice thickness, the weekly deepest keel and ridge spatial frequency in the Bornholm Basin are well behaved and show that 90% of the level ice in the Bornholm Basin is estimated to be distributed between 0.07 m and 0.37 m with a mean level ice thickness at 0.20 m, 90% of the weekly deepest keels are distributed between 8.88 m and 9.96 m, and 90% of the spatial frequency datapoints are distributed between 0.04 ridges
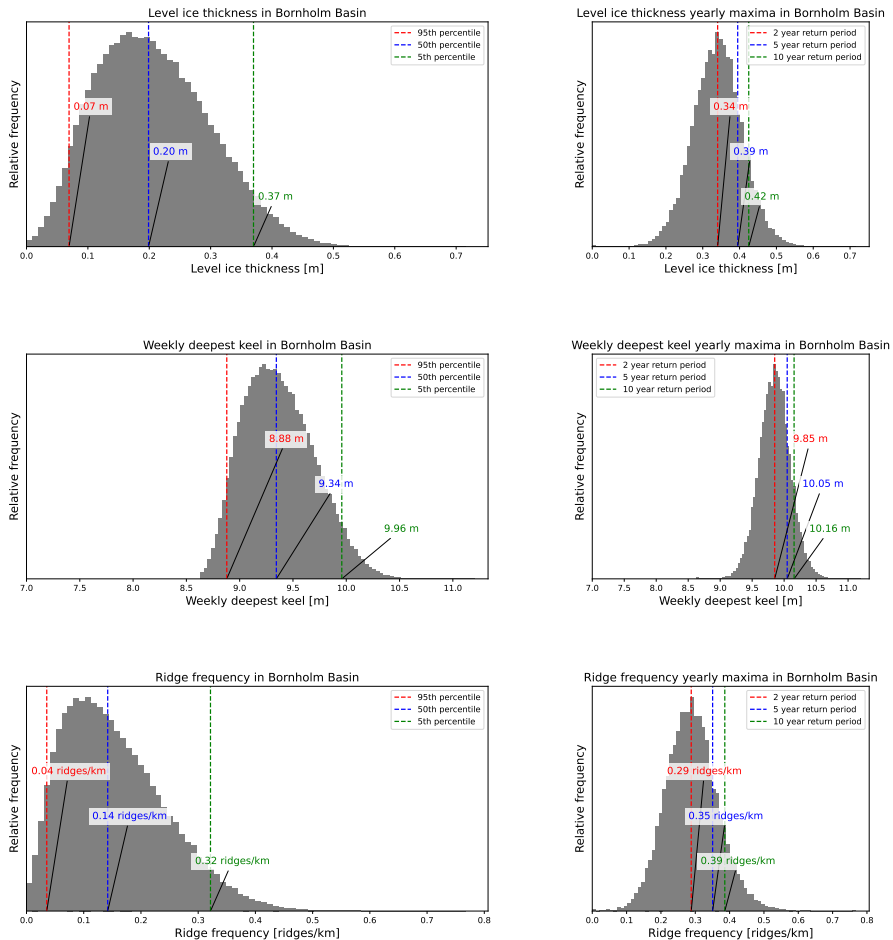
per km and 0.32 ridges per km.

Figure 3.18: Simulated level ice thickness, sea ice ridge keel and sea ice ridge spatial frequency distributions in the Bornholm Basin.

Distributions of the level ice thickness, the weekly deepest keel and ridge spatial frequency in the Bornholm Basin are distributed with two separate modes and show that 90% of the level ice in the Bay of Bothnia is estimated to be distributed between 0.12 m and 0.88 m with a mean level ice thickness at 0.54 m, 90% of the weekly deepest keels are distributed between 9.04 m and 11.81 m, and 90% of the spatial frequency datapoints are distributed between 0.07 ridges per km and 1.01 ridges per km.

The two-mode level ice draft distribution corresponds with the early freezing season month-basin distributions with mean around 0.2 m and the later season month-basin distributions with means around 0.7 m.
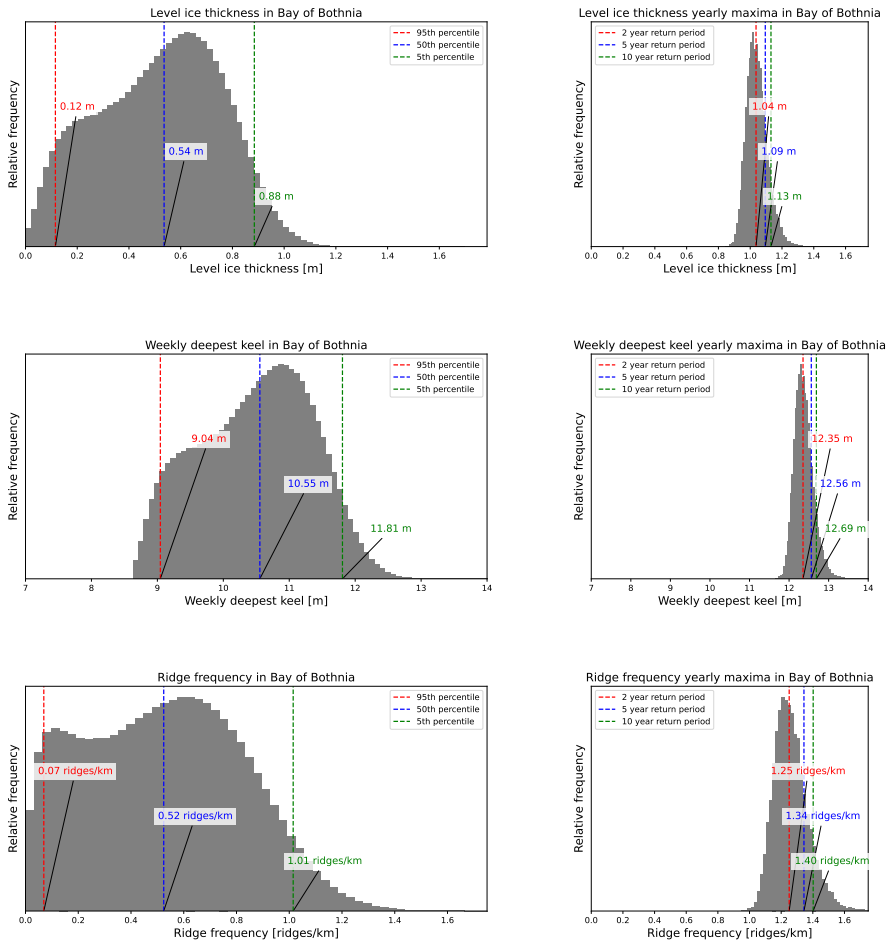
Figure 3.19: Simulated level ice thickness, sea ice ridge keel and sea ice ridge spatial frequency distributions in the Bay of Bothnia.

3.5 Freezing season development case studies

A case study of ice charts from the Swedish Meteorological and Hydrological Institute was also made. The study was prompted by the significant differences between the previously studied sources of sea ice conditions.

3.5.1 Polish coastal ice development

A comparison between the NSIDC and the SMHI sea ice charts at given locations was made manually. The SMHI ice charts used were the "twice weekly winter season 1979-

2017" ice and sea surface temperature charts. A list of dates with sea ice presence in NSIDC at the Baltyk I, II and III locations was compared with a list of ice charts from SMHI. For each of the selected NSIDC dates the closest, in time, SMHI ice chart was identified. Several NSIDC ice charts point to the same SMHI ice chart due to their higher temporal resolution. The SMHI ice charts flagged with this approach were evaluated manually and the highest SMHI ice concentration in Polish coastal waters east of Darlowo and west Wladyslawowo was recorded.

NSIDC sea ice presence at Baltyk I in the period 1979 to 2017 count 21 NSIDC datapoints. These 21 NSIDC datapoints point to 16 separate SMHI ice charts. In the following each SMHI ice chart is only counted once. Of the 16 SMHI ice charts with NSIDC sea ice presence at Baltyk I 10 recorded sea ice in the region of Polish coastal waters described above.

For Baltyk II, 159 NSIDC datapoints record sea ice in this timeperiod. These 159 NSIDC datapoints refer to 76 separate SMHI ice charts of which 23 record sea ice presence in the specified region of Polish coastal waters.

For Baltyk III, 225 NSIDC datapoints record sea ice. Of the corresponding 112 SMHI separate ice charts 22 record sea ice in the specified region of Polish coastal waters.

The overlap of the NSIDC and SMHI where largely between 1979 and 1988 with a small number of ice chart overlaps in 1989, 1996 and 2011.

Polish coastal ice development

For the majority of the polish coastline sea ice typically develops from west to east starting in the Bay of Pomerania in the southwestern Baltic Sea between Poland and Germany. In the far eastern regions of the Polish coast the ice typically develops from the Puck Bay into the Gdansk Bay and outwards.

The freezing season in 1985 in Polish Waters as reflected in the SMHI ice charts is shown in figures 3.21-3.28. For convenience the SMHI ice chart legend is shown in Figure 3.20. The legend depicts different stages of ice coverage from new ice to fast ice. The legend also depicts ice characteristics such as level ice, rafted ice and ridged ice.
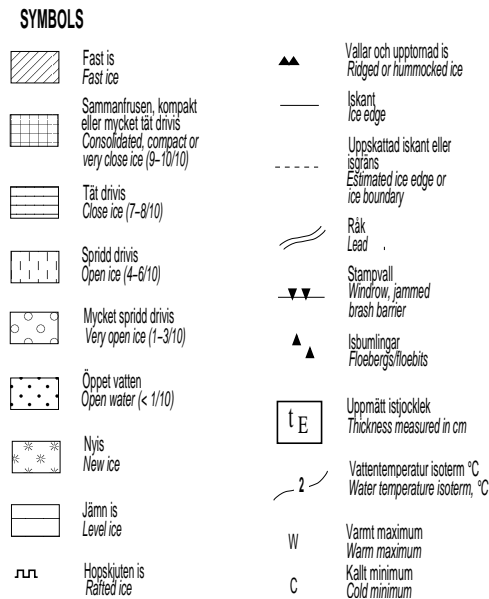
SYMBOLS

▨	Fast is *Fast ice*	▲▲	Vallar och upptornad is *Ridged or hummocked ice*
▦	Sammanfrusen, kompakt eller mycket tät drivis *Consolidated, compact or* *very close ice (9–10/10)*	——	Iskant *Ice edge*
▤	Tät drivis *Close ice (7–8/10)*	- - - -	Uppskattad iskant eller isgräns *Estimated ice edge or* *ice boundary*
▥	Spridd drivis *Open ice (4–6/10)*	⌇	Råk *Lead*
⊡	Mycket spridd drivis *Very open ice (1–3/10)*	▼▼	Stampvall *Windrow, jammed* *brash barrier*
⫶	Öppet vatten *Open water (< 1/10)*	▲	Isbumlingar *Floebergs/floebits*
✳	Nyis *New ice*	t_E	Uppmätt istjocklek *Thickness measured in cm*
▭	Jämn is *Level ice*	2 ⌐	Vattentemperatur isoterm °C *Water temperature isoterm, °C*
ᴖᴖ	Hopskjuten is *Rafted ice*	W	Varmt maximum *Warm maximum*
		C	Kallt minimum *Cold minimum*

Figure 3.20: SMHI ice chart legend

Figure 3.21 shows the Polish coastline as ice has started forming in the sheltered regions in the inner Pomerania Bay in the west and Puck Bay and Vistula Lagoon in the east. The next ice chart in figure 3.22 of the 11th of February shows that "new ice" is marked to start forming outside most of the Polish coast.

By the 13th of Februrary shown in Figure 3.23 rafted close ice has formed in the western coastal waters. The Puck bays is marked as "fast ice". The Bay of Gdansk is marked as level ice.

By the 18th of February, shown in Figure 3.24 the entire Polish coast is marked as "Consolidated, compacted or very close ice" except the inner Puck Bay in the east marked as "fast ice" and the outer Puck Bay and outer Bay of Gdansk marked as "Very open ice". Further from shore a border region between the "close ice" and the open ocean is classified as very open ice.

By the 21st of February shown in figure 3.25 the "very close ice" starts retreating in the east. The region of "very open ice", further from shore and in the outer Puck Bay and outer Bay of Gdansk, is downgraded to "new ice".

By the 25th of February, show in Figure 3.26, the ice retreats significantly. The Puck Bay is covered in "fast ice". The northeastern most exposed section of the Polish coast is ice free. The more sheltered coast to the west is covered with "open ice" and the outer of the Bay of Pomerania is marked as "Consolidated, compacted or very close ice", the innermost sections of the Bay of Pomerania is "fast ice".

By the 28th of February, shown in Figure 3.27, the inner most Bay of Gdansk is marked as "very open ice". The outer Bay of Pomerania is downgraded to "very open ice", however region marked as "Consolidated, compacted or very close ice" in the inner most Bay of Pomerania expands eastwards along the coast as it retreats from the inner most region.

By the 7th of March, shown in Figure 3.28, the regions classified as "very open ice" in Bay of Gdansk and the Pomerania Bay expand out to sea. This is joint with the eastward retreat of the "consolidated, compacted or very close ice" in the Pomerania Bay and general retreat of the "level ice" from Kaliningrad.

By the 11th of March, shown in Figure 3.29, the regions classified as "very open ice" is only present in the inner Pomerania Bay. There is little change to the "consolidated, compacted or very close ice".

By the 18th of March, shown in Figure 3.30, the "consolidated, compacted or very close ice" expands eastwards. No regions are classified as "very open ice".

By the 21st of March, shown in Figure 3.31, the "consolidated, compacted or very close ice" moves further eastwards. Tge ice in the east retreats further into the Puck Bay.

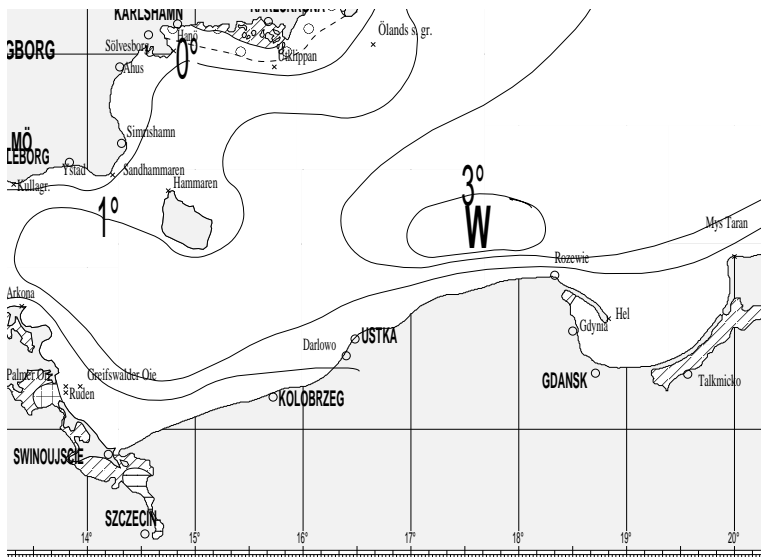By the next SMHI ice chart on the 28th of March. All sea ice is gone from the Polish coast.

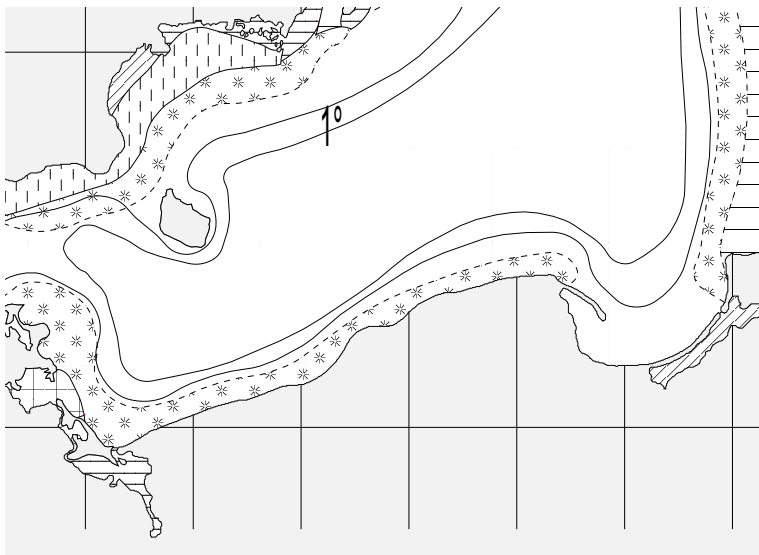**Figure 3.21:** SMHI ice chart of the Polish coast for 1985-02-07.

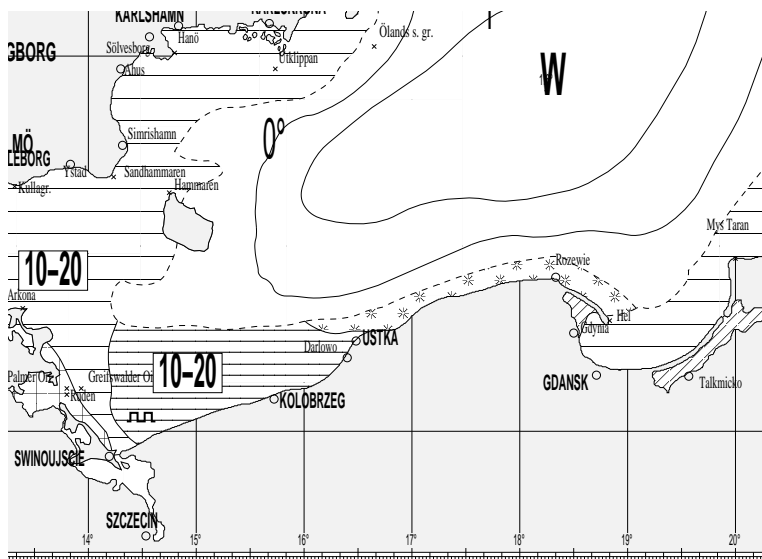**Figure 3.22:** SMHI ice chart of the Polish coast for 1985-02-11.

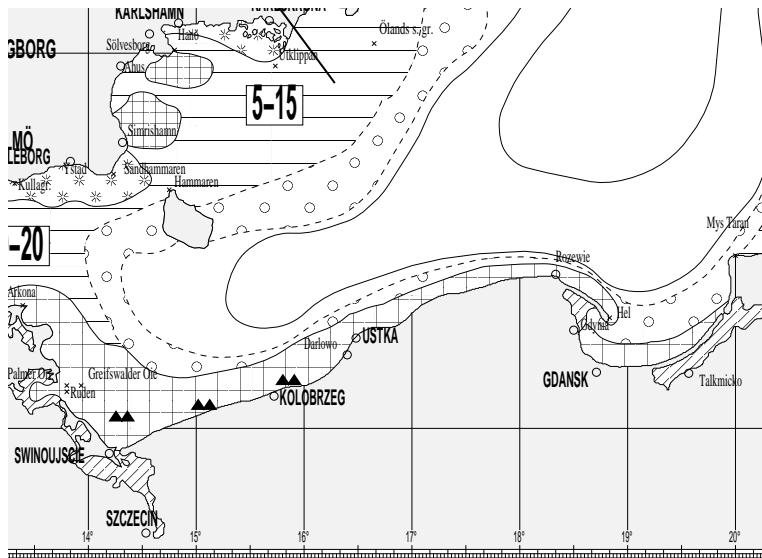**Figure 3.23:** SMHI ice chart of the Polish coast for 1985-02-13.

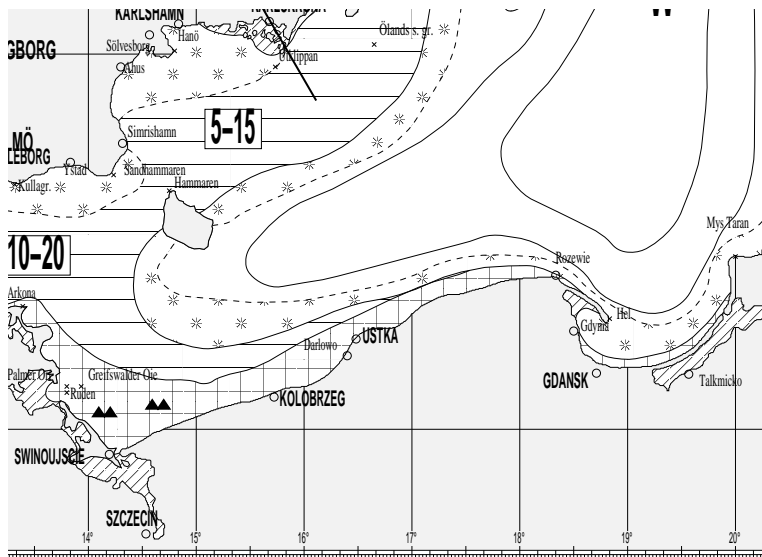**Figure 3.24:** SMHI ice chart of the Polish coast for 1985-02-18.

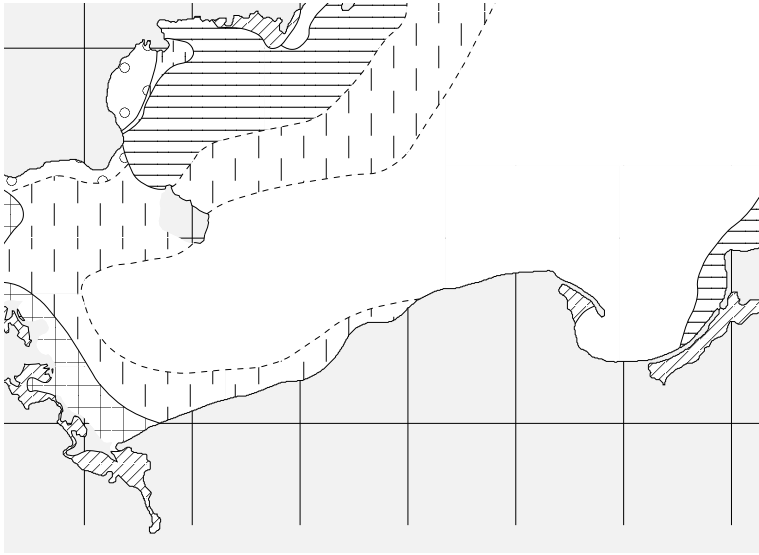**Figure 3.25:** SMHI ice chart of the Polish coast for 1985-02-21.

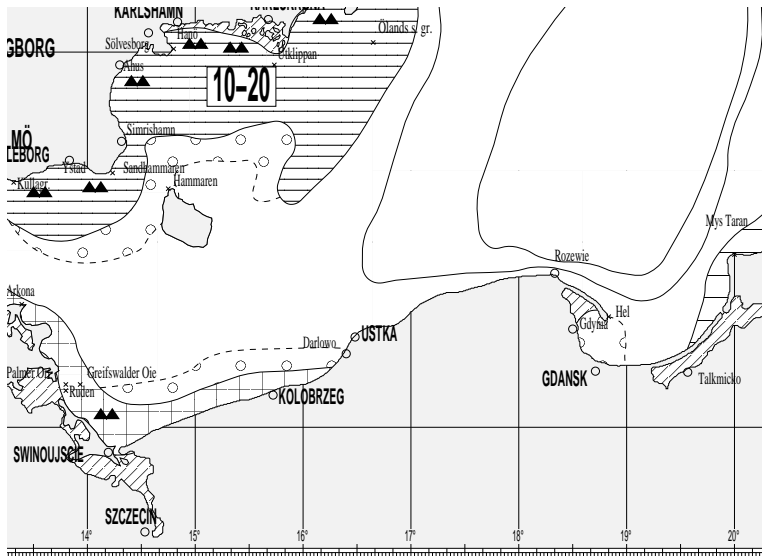**Figure 3.26:** SMHI ice chart of the Polish coast for 1985-02-25.

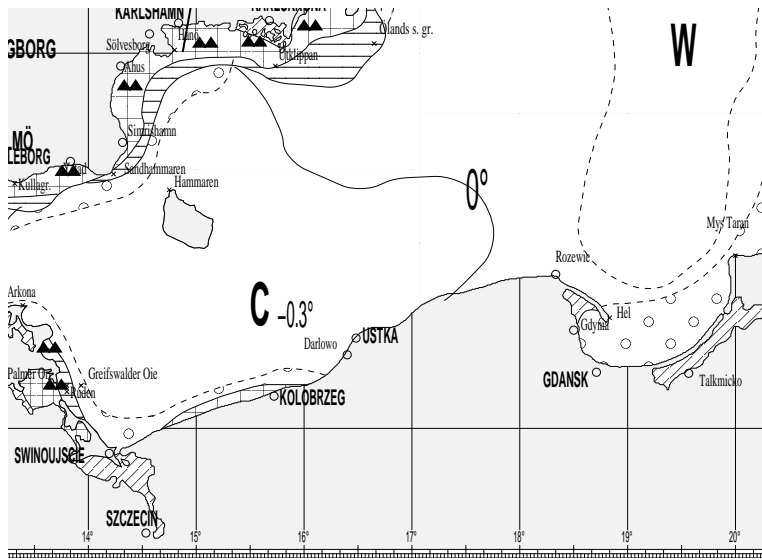**Figure 3.27:** SMHI ice chart of the Polish coast for 1985-02-28.

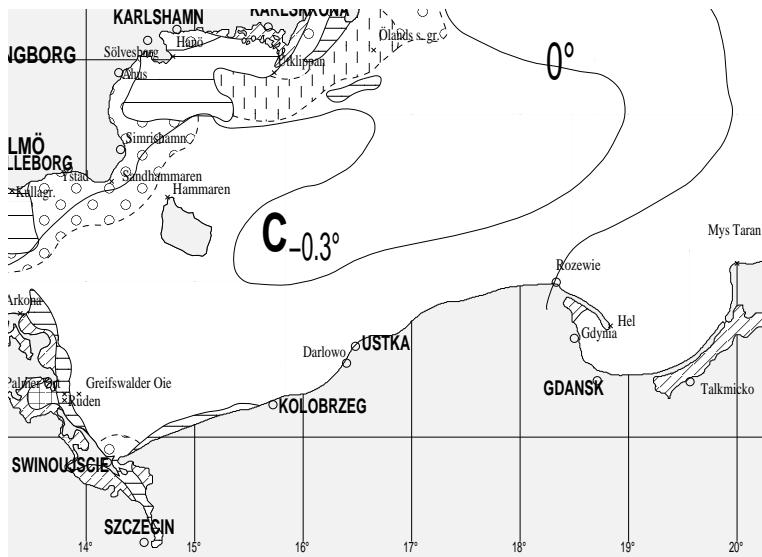**Figure 3.28:** SMHI ice chart of the Polish coast for 1985-03-07.

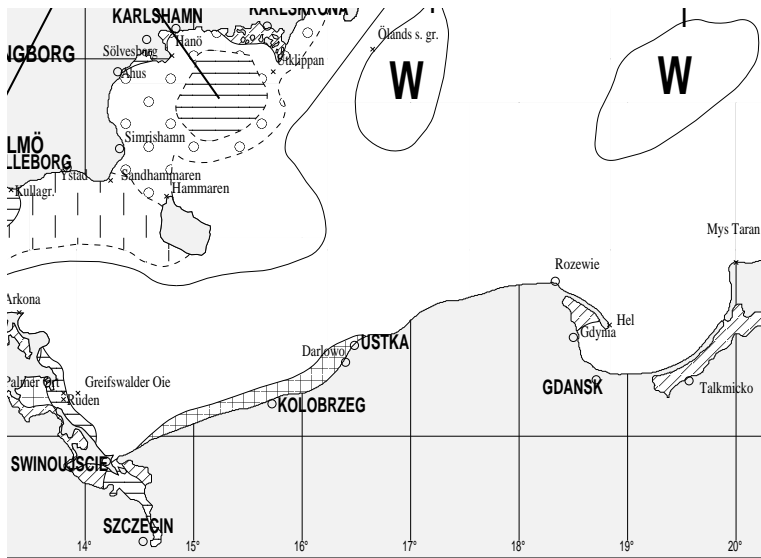**Figure 3.29:** SMHI ice chart of the Polish coast for 1985-03-11.

Figure 3.30: SMHI ice chart of the Polish coast for 1985-03-18.
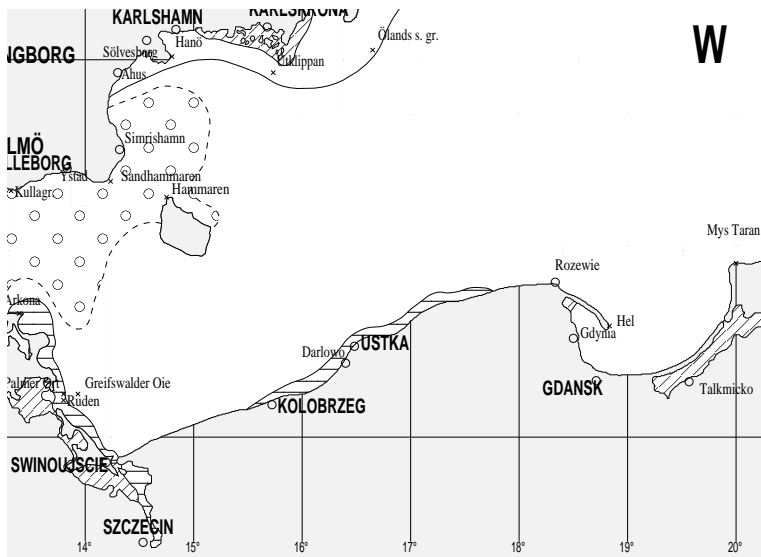

Figure 3.31: SMHI ice chart of the Polish coast for 1985-03-21.

Effect of ERA5 wind on SMHI ice

The freezing season of the 1985, 1986 and 1987 are compared to the mean daily wind speed in Figures 3.32a, 3.32b and 3.32c respectively. These years were chosen as they had significant overlapping sea ice development periods in both NSIDC and SMHI. Generally the SMHI sea ice presence overlaps with periods of relatively low daily mean wind speed. The sea ice typically starts at a low point in daily mean wind speed and ends with a significant increase in daily mean wind speed. Note that there are few datapoints. The temporal boundaries of the period with ice presence is uncertain as there is a significant period between each SMHI ice chart. The following presentation relates to these presented freezing seasons and not SMHI ice presence in general.

The 1985 figure 3.32a, has periods of consecutive days with lower daily mean speeds and periods with higher daily mean wind speeds. Two of the low periods have sea ice presence, however more periods of low wind speeds have no recorded SMHI ice.

The 1986 figure 3.32b, has one period with registered sea ice presence in SMHI ice charts. This periods does overlap with a period of low daily mean wind speed and ends with an increase in wind speeds.

The 1987 figure 3.32c, has four periods of SMHI ice charts. Three periods of SMHI ice overlap with periods of low daily mean wind speed. The last of the four periods and the longest period with consecutive SMHI ice presence in 1987 generally overlaps with low daily mean wind speeds except for a significant peak lasting less than one week after more than one week of SMHI ice in low wind speeds.

Generally SMHI ice presence is found when EAR5 daily mean wind speeds are below 8 m s^{-1}. The end of the period of ice presence is typically overlapping with an increase in daily mean wind speeds above 8 m s^{-1}.
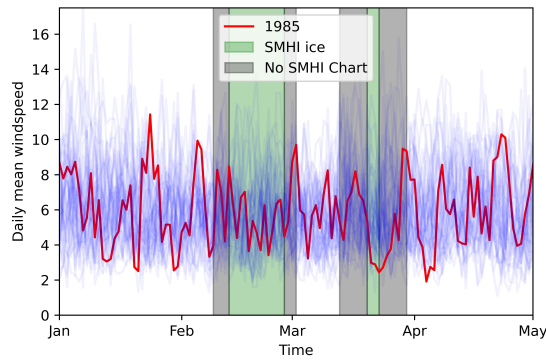
(a) The freezing season 1984-1985.
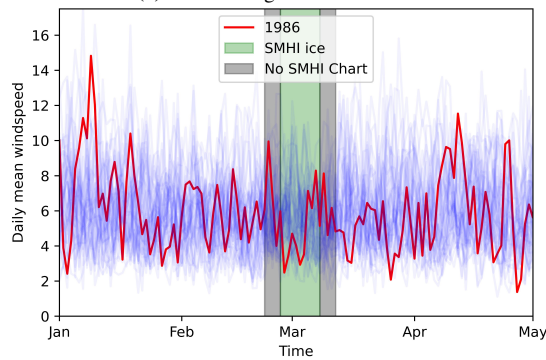
(b) The freezing season 1985-1986.
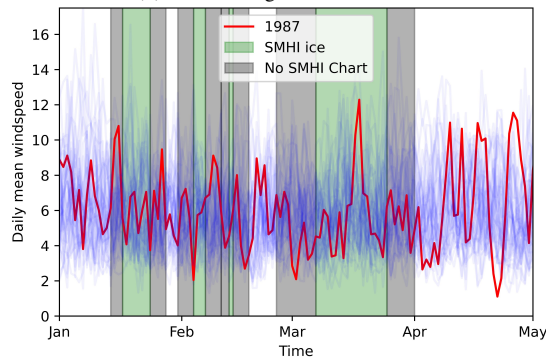
(c) The freezing season 1986-1987.

Figure 3.32: ERA5 wind speed compared with SMHI ice presence in exposed Polish coastal waters. The daily mean ERA5 wind speed off Leba Port in Polish coastal waters [m/s] is plotted as line plots. The data for the specific year is plotted in red and all other years are plotted in a transparent blue. The time period between subsequent SMHI ice charts with sea ice presence in Polish coastal waters east of Darlowo and west Wladyslawowo is marked in transparent green. The time period between the SMHI charts that record sea ice presence and the next and previous SMHI chart without sea ice presence is marked in a transparent grey.

Chapter 4

Discussion

With the goal of better understanding the sea ice conditions in the Baltic Sea the work in this project started with gathering and comparing data from various sources. Then models were applied to these sources and the resulting data was analysed and compared with other sources of this modelled data. Lastly the modelled data was used to form distributions describing the level ice thickness, ridge keel depth and frequency, conditional that ice is present.

This thesis is mainly concerned with the level ice thickness, the sea ice concentration, and the sea ice drift velocity. These parameters have value as they are and are presented, however they are also key in describing more involved sea ice conditions. The level ice thickness is further used to describe the sea ice ridging conditions. This level ice thickness is based on a Freezing Degree Day model estimating level ice thickness from surface temperature from ERA5. The freezing season is ended using sea ice concentration cutoff, thus sea ice concentration also plays a role in describing the level ice thickness. The sea ice concentration and the sea ice drift velocity are used to adjust the sea ice exposure which in turn is used estimate the sea ice strength coefficient.

Sea ice concentration, sometimes refereed to as the sea ice area fraction, is the relative fraction of the ocean surface area covered by sea ice to the total surface area considered. In newer times this statistic is readily available in the polar and sub polar regions due to the advent of satellite imaging.

Sea ice thickness is a more illusive parameter that is harder to monitor at scale. This value is typically found in complex climate models, reanalyses, analogue ice charts, thickness measurements with ice augers, measurements with EM antenna, ice draft measurements from bottom-mounted acoustic ice profilers, but also from altimetrical satellite observations.

The sea ice drift velocity can be modelled through complicated joint ocean-land-atmosphere models describing the climate as a whole in detail however these are prohibitively difficult to implement. A simpler version is assuming free drift. Knowing the local wind speed and the drag coefficients of ice in air and water describes a much simpler model.

From these parameters more complicated sea ice conditions are described. The sea ice strength coefficient is estimated through the sea ice exposure, itself estimated in a free drift model from wind speed and sea ice concentration. Furthermore sea ice ridging is described through the empirical relations with the level ice draft. These relations joint with level ice draft distribution through the freezing season and corresponding probabilities of sea ice presence are used in a Monte Carlo simulation of sea ice ridge keel draft and spatial frequency for the different sub basins in the Baltic Sea.

Despite the endeavor to provide a comprehensive understanding of Baltic Sea ice conditions, certain limitations exist regarding data availability and the inherent complexity of ice dynamics. The freezing degree day model has suggested parameters to better describe to the local sea ice conditions. The various statistical relations used to determine the sea ice ridging parameters are determined based on conditions in the Beaufort Sea with significantly more severe sea ice conditions. Furthermore, the models and simulations are constrained by available sea ice data and may not fully account for potential future changes in sea ice conditions due to factors such as climate change. The inherent complexity and variability of sea ice dynamics also pose challenges in capturing these aspect of sea ice behavior based on results from a pure thermodynamic model.

4.1 Data sources

The data sources used in this study are classified in two main categories, reanalysed and observed data. ERA5 and Copernicus Marine Service (CMS) datasets are reanalyses. They are the results of numerical models running on data assimilated from a large variety of sources to be consistent in time and space. They are generally available with higher temporal resolution and are designed to interpret the long-term trends in complex systems. On the contrary the Data Bank of Baltic Sea Ice and Surface Temperatures (BASIS) archive, the National Snow and Ice Data Center (NSIDC), The Finnish Meteorological Institute (FMI) digital ice charts and the Swedish Meteorological and Hydrological Institute analogue ice charts are observed datasets. These observed sources are of lower temporal frequency. The older observed sources are more directly reporting from human observed data instead of the more modern satellite based data. This limits old observed data to places with human presence. Naturally more data and work will be used to monitor shipping corridors and coastlines close to settlements than isolated open ocean space far from any particular point of interest. It should be noted that in the process of acquiring and processing data the quality of the observations must be assessed. The data may be indirectly observed and the observations might be of low precision. The data sources used in this study are listed in Table 2.1, and will be discussed in further detail.

Of the inspected data sources, two were disregarded. Landy et al. (2022); Dawson et al. (2022) published a dataset of altimetric data from CryoSat-2 interpreted as ice thickness. The goal of the publication was to extend the sea ice thickness data availability into the melting season. The melting season is problematic for microwave response signals, often used to estimate sea ice thickness, due to the formation of melt ponds on top of the ice. This publication uses a machine learning approach on the response data with simulated responses to interpret the melting season responses as sea ice thickness. The dataset provided is of very low spatial resolution and the reported uncertainty is at times larger than

what the other data sources report as maximum sea ice thickness. This data is presented in appendix 5.17 and will not be discussed or used any further.

The second data source disregarded in this study was the CMS_B dataset. This dataset has been discontinued by CMS, and its successor, CMS_G, is being used instead. The decision to disregard CMS_B was primarily due to the presence of unphysical sea ice thickness values exceeding 2 meters outside the Polish coast, which strongly contradicts the typical sea ice thickness observed in the region. Historical monitoring of sea ice thickness in Polish ports from 1950 to 1990 recorded maximum thicknesses of 70 cm in sheltered ports (Girjatowicz, 2011). These reasons led to the disqualification of the CMS_B dataset as a reliable data source in this study.

In Nordic regions there are two natural choices for general climate data. The NORA10 and ERA5 products are similar, however whilst the NORA10 data is tailored for the local climate the ERA5 product is available globally. The choice of ERA5 over NORA10 was simply facilitating the application of these procedures in other regions around the world without needing to change data source.

To ensure the sea ice strength calculations in this study are based on reasonably reliable data with a long time horizon, information on sea ice thickness and sea ice concentration is obtained from BASIS for the period 1960-1978 and from FMI for the years 2018-2022. However, there is a gap between 1978 and 2018 that needs to be filled. While sea ice concentration is well-documented globally by NSIDC, there is a lack of publicly available sea ice thickness charts in easily computable formats to bridge the gap between the BASIS and FMI datasets. It is worth noting that the Swedish Meteorological and Hydrological Institute (SMHI) and the Finnish Meteorological Institute (FMI) provide drawn sea ice charts, but they are not available in a gridded and georeferenced format. As an alternative, hindcasting the data is considered. One possibility is to utilize the CMS_G reanalysis, however since the CMS_G reported sea ice thickness and sea ice concentration differs significantly from other sources in the southern Baltic Sea, and as it does not cover the entire 1978-2018 time window, a search for a new sea ice thickness model was necessary.

Ice charts typically have a temporal resolution that is generally daily or less frequent, as indicated in Table 2.1. The limited temporal resolution of these charts results in reduced accuracy when determining sea ice statistics.

4.1.1   Data Bank of Baltic Sea Ice and Surface Temperatures

Figure 3.9a and Figure 3.9b present the BASIS-based MSIC (Maximum Sea Ice Concentration) and SIC_{60} (days with Sea Ice Concentration above 60%) statistics, respectively, covering the freezing seasons from 1960-61 to 1978-79. The MSIC indicates a 100% concentration in most of the Baltic Sea, with the exception of an open patch of sea in the southern Baltic Sea. While this information provides limited insight into the severity of sea ice, it does indicate its presence in most parts of the Baltic Sea. On the other hand, the SIC_{60} statistic reveals a clear decreasing trend in sea ice concentration with distance from the coast, latitude, and the Baltic Sea opening. These observations align with the understanding that colder water with less motion provides favorable conditions for sea ice formation and persistence.

Similarly, Figure 3.8a and Figure 3.8b display the BASIS-based MSIT (Maximum Sea Ice Thickness) and SIT_{10} (days with Sea Ice Thickness above 10 cm) statistics, respec-

tively, for the same freezing seasons. The SIT_{10} plot highlights the areas most exposed to thick sea ice, including the Bothnian Bay, the inner Gulf of Finland, the Archipelago Sea between Åland and Finland, and the Gulf of Riga, where the average number of SIT_{10} days exceeds 50. The northern coast of the Bothnian Bay exhibits the highest average with over 150 SIT_{10} days per year. In contrast, the MSIT values show slight variations, with the Bothnian Bay having an MSIT of 76 cm. Waters north of the Stockholm-Tallin line, as well as most of the Gulf of Riga, experienced MSIT values above 50 cm during these years. Interestingly, the Danish straits in the far southwest of the Baltic Sea display MSIT values as high as those in the northern Baltic Sea and significantly higher than other regions in the southern Baltic Sea. This can be attributed to the shallow waters and narrow straits, which facilitate easier formation and persistence of sea ice compared to open waters. Both the MSIT and SIT_{10} statistics generally decrease with distance from the coast, although this trend is more pronounced for SIT_{10}. This distinction is likely because MSIT represents a single observation, capturing the largest thickness at a given location, while SIT_{10} is based on a larger sample of sea ice records above the 10 cm threshold.

All four statistics (MSIT, MSIC, SIT_{10}, and SIC_{60}) exhibit minima in the open ocean of the Southern Baltic Sea, located north of Poland and west of Malmö. This region, situated in the southernmost part of the Baltic Sea, is characterized by a large expanse of open water where BASIS records very little sea ice presence.

4.1.2 Copernicus Marine Service

The Copernicus Marine Service (CMS_G) dataset provides information on sea ice concentration, thickness, and drift velocity, enabling the calculation of exposure and sea ice strength coefficients in conjunction with other data sources. The CMS data covers the period from 1993 to 2022.

Figure 3.13a and 3.13b illustrate the sea ice concentration derived from CMS. In the hindcast, CMS suggests that the southern Baltic Sea exhibits few observations of high sea ice concentrations, except in proximity to the Swedish, Lithuanian, and southern-most Latvian coasts. Conversely, all regions north of this area show maximum sea ice concentration (MSIC) observations of 100%. Along the Polish coast, sea ice observations are absent, except for a small region in the far east where sea ice is observed to be less than 40%. Analysis of the SIC_{60} data reveals that the entire southern Baltic Sea experiences nearly zero SIC_{60} days, indicating that sea ice events are infrequent in the hindcast. Comparatively, CMS generally exhibits fewer SIC_{60} days than BASIS, with the highest values reaching 120 in CMS compared to 190 in BASIS. It should be noted that the CMS reanalysis and BASIS archive unfortunately do not overlap in time.

Sea ice thickness data from CMS, as depicted in figures 3.12a and 3.12b, is somewhat challenging to interpret due to outliers near the Finnish coast in the Northern Gulf of Bothnia. In these outliers, sea ice thickness is hindcasted to exceed 2.7 meters, primarily near the Quark, the border region between the Bothnian Sea and the Bothnian Bay. This area does exhibit mechanical growth in contrast to the pure thermal growth assumption made for the freezing degree day (FDD) modeling approach. Ignoring the extreme MSIT outliers in the Bay of Bothnia, the highest maximum sea ice thickness (MSIT) values remain around 140 cm, significantly exceeding observations from FMI and FDD estimates based on ERA5 data. Notably, sea ice thickness observations above 10 cm are present in

most of the Baltic Sea, with some exceptions in certain patches of the southern Baltic Sea north of Poland and east of Malmö. Similar to the BASIS observations, the northern coast of the Bothnian Bay exhibits around 150 days per year with sea ice thickness exceeding 10 cm (SIT_{10}). However, the CMS hindcast displays a slight eastward skew, with relatively higher SIT_{10} values in the inner Gulf of Finland. In the Archipelago Sea significantly more SIT_{10} days are observed compared to the Åland Sea, indicating that the hindcast captures the higher likelihood of sea ice growth in an archipelago compared to the more open Strait west of the Åland Islands. Both BASIS and CMS agree that the freezing season is longer, in terms of SIT_{10} and to a lesser extent SIC_{60}, in the Archipelago Sea than the Åland Sea. Interestingly, the CMS MSIT values are similar on both sides of the Åland islands, suggesting that while sea ice formation are hindcasted to occur less frequently, the ice reaches a similar thickness of about 1 meter on both sides of the Åland islands. Note that this is considerably higher than the BASIS observations ranging from 50 cm to 76 cm in the region.

Sea ice exposure, calculated from the sea ice drift velocity and concentration, is depicted in figures 3.15b and 3.15a. These figures reveal an intriguing decrease in exposure near the shore in the Bothnian Bay, indicating that the CMS hindcast successfully captures the land-fastening of sea ice in this area. The maximum sea ice exposure occurs in the southeastern region of the Bothnian Bay, coinciding with the location of the maximum MSIT. This region, near the Quark, is known for significant mechanical growth of sea ice, which is more prominent compared to other areas in the Baltic Sea. Analyzing the number of days with sea ice exposure exceeding 1 km, the central parts of the Bothnian Bay exhibit the highest exposure to sea ice. Consistent with previous indications, the southern Baltic Sea experiences minimal sea ice in this hindcast.

The Copernicus Marine Service (CMS) dataset, which includes sea ice concentration, thickness, and drift velocity, exhibits a distinctive characteristic in the southern Baltic Sea compared to other sources. Unlike ERA5, which predicts the presence of ice in the southern Baltic Sea based on its purely thermodynamic nature, CMS suggests that this region is almost ice-free. This significant difference between CMS and other sources, such as BASIS, raises a hypothesis regarding the underlying factors.

One possible explanation for the deviation of CMS from other sources in the southern Baltic Sea is the influence of data assimilation in the model representation. CMS utilizes a complex numerical model and data assimilation techniques to incorporate various observations between ocean, land and atmosphere into a consistent framework. It is plausible that the assimilation process and model assumptions employed in CMS may introduce biases or uncertainties specifically in the representation of sea ice in the southern Baltic Sea.

Additionally, CMS may have different quality control procedures or bias correction methods that lead to a representation of sea ice conditions that is significantly different from other sources, such as BASIS.

It should be noted that a reason for the differences in observed sea ice conditions between sources could be the lack of overlap in time.

Further research and analysis are required to thoroughly investigate the reasons behind the significant difference between CMS and other sources in the southern Baltic Sea. Examining the specific data assimilation methods, boundary conditions, model parameterizations, and quality control procedures employed by CMS in this region could provide

valuable insights into the contrasting outcomes and improve the understanding of sea ice dynamics in the area, making the data more consistent with the observed sources and improving the hindcast.

4.1.3 ERA5

The ERA5 climate data, covering the period from 1959 to 2022, served as the foundation for the Freezing Degree Day (FDD) model presented previously. The sea ice thickness estimates derived from this model are depicted in Figure 3.5. The contours of maximum sea ice thickness (MSIT) are comparable to both CMS and BASIS, albeit with varying amplitudes. BASIS observations generally indicate MSIT values around 30% lower than the FDD estimates, while CMS observations tend to be 30% to 50% higher than the FDD estimates, atleast north of Gotland. South of Gotland, the FDD model produces higher MSIT estimates compared to both previous sea ice thickness sources. This disparity is stronger further away from the coast and becomes hard to classify in coastal regions. The disparity between FDD and the other sources is likely attributable to the FDD model's reliance solely on air temperature as a predictor. In regions with infrequent and mild sea ice seasons, other factors such as ocean heat flux, wind, solar radiation, and sea motion become more influential in inhibiting ice formation and reducing ice persistence.

It is important to note that the FDD model is designed to be conservative (ISO 19906:2019), which speaks to the approximately 30% overestimation when compared to BASIS.

While not directly related to the Baltic Sea, it is worth mentioning that the FDD model without using NSIDC sea ice concentration cutoffs predicts sea ice outside the Norwegian coast. The Norwegian coast as far south as Brønnøysund, does not typically experience sea ice except in sheltered fjords with more brackish surface water. This serves as an example of how the FDD model can encounter limitations due to its simplistic reliance on air temperature. The adjustment of using a NSIDC sea ice concentration cutoff both ends freezing seasons when there is no ice and removes FDD estimates of sea ice when NSIDC says there was none. Thus the expanded FDD model using the adjusted freezing season boundary conditions results in no ice off the Norwegian coast. This effect is to a lesser degree present in the Baltic Sea when there is no NSIDC ice observations at a given grid point in a given freezing season.

The FDD model seems to well describe the sea ice conditions in regions with little ice mobility, such as in archipelagos. As discussed earlier, the Finnish Archipelago on the east side exhibits significantly more ice than the more open waters to the west in the other data sources. This effect is present in FDD results as well. Further research could look into the degree to which FDD models describe sea ice conditions in sheltered waters compared to more open oceans.

4.1.4 National Snow and Ice Data Center

The sea ice concentrations globally recorded by the National Snow and Ice Data Center (NSIDC) span from 1978 to the present time. For the purpose of this study, the data was limited up to the 2021-2022 freezing season.

Figures 3.1a and 3.1b illustrate the sea ice concentration MSIT and SIC_{60} statistics. The MSIT distributions closely resemble the BASIS observations, showing 100% MSIT

in most of the Baltic Sea, except for a patch of open waters north of Poland and east of Malmö. This patch appears slightly larger in the NSIDC data compared to BASIS. This discrepancy may suggest a lower ice formation in the more recent years covered by NSIDC, as opposed to the earlier years (1960-1978) covered by BASIS. However, caution must be exercised in drawing conclusions too hastily, as this difference could also be attributed to the higher spatial resolution and increased likelihood of precise observations in NSIDC data.

The NSIDC documentation highlights a potential source of error in sea ice concentration observations known as the "land-sea spillover effect." This effect occurs when the returned microwave signal used to estimate sea ice concentration behaves differently in areas near land or inland waters compared to large open oceanic areas. Gridpoints in the NSIDC dataset displayed clear evidence of land-sea spillover, with some points exhibiting double the SIC_{60} values of neighboring points. To mitigate the impact of this spillover on the calculations involving NSIDC sea ice concentration, two data points in the northern Gulf of Bothnia and two data points in the inner Gulf of Finland were disregarded.

4.1.5   Finnish Meteorological Institute

The sea ice thickness and sea ice concentration observations provided by the Finnish Meteorological Institute (FMI) cover a relatively short time window from 2018 to 2022. Consequently, there are fewer data points available for each grid point in the Baltic Sea, resulting in less smooth contours in Figure 3.10. The maximum values of SIC_{60} and SIT_{10} in FMI data are approximately one fourth to one third of those observed by NSIDC and CMS, and roughly one sixth to one fifth of the values recorded by BASIS. This discrepancy is likely due to the limited sample size and relatively milder winters experienced since 2018 in comparison to the average conditions during the time periods covered by other data sources. Further research could look into the overlap between CMS and FMI as part of an evaluation of the CMS_G reanalysis.

According to the FMI ice charts, no sea ice is observed in the southern Baltic Sea, except for some exceptions along the German coast and in the lagoon shared by Kaliningrad and Lithuania.

4.2   Freezing Degree Day models for sea ice growth

The FDD models used in this study are simple solutions to Stefan's Equation 2.8, utilizing the cumulative freezing degree days (CFDD) as a measure of the duration and intensity of cold periods. These models serve as valuable tools for estimating sea ice thickness assuming a purely thermodynamic growth mode.

Two classes of FDD models are described in this study: those that account for the insulating effect of snow buildup and those that do not. Each class has its own set of parameters presented in the introduction 2.5.2.

To determine the start of the freezing season, it is essential to consider factors beyond the first occurrence of freezing degree days. Fluctuations in surface temperature and short periods of freezing prior to the main freezing season can lead to subsequent snow and ice melt if followed by a significant period of positive degree days. As per the international

standard for the construction of arctic structures (ISO 19906:2019), the condition that the 30-day running average air temperature was implemented as the starting boundary condition for the freezing season.

Regarding the end of the freezing season, it is logical to conclude it when no local sea ice concentration above zero is observed. Reliable sea ice concentration data from NSIDC allows for the use of a sea ice concentration threshold as a suitable indication for ending the freezing season. This method was implemented with a 10% sea ice concentration threshold given the little sensitivity of the mean end of the freezing season to the threshold. It was important to keep the threshold as low as possible to not have a bias against shorter freezing seasons especially in the south. This selection bias was presented earlier. As a result, statistics related to the duration of a freezing season, such as the SIT_{10} (number of days with sea ice thickness above 10 cm) is technically defined and well behaved however the international standard recommends the use of FDD models to estimate the end of the freezing season level ice thickness and not necessarily the instantaneous development of the level ice thickness throughout the freezing seasons. For these reasons the SIT_{10} statistics for the ERA5 based FDD model were not included in the data table 3.2.

Due to the square root nature of sea ice thickness modelled as a function of freezing degree days the model becomes partially self correcting. Too few FDD in the early freezing season leads to higher growth rate for later FDD and inversely for too many FDD early on in the freezing season (Leppäranta, 1993).

The insulating FDD model relies on solutions to a slightly modified Stefan's equation (2.13). However, this equation lacks an analytic solution without assuming a relationship between sea ice thickness and snowfall height as derived by Leppäranta and described in appendix B (Leppäranta, 1993, 1983). Consequently, a numerical solution was implemented in this study, and a delay before snowfall accumulation was incorporated due to the large timesteps used. Meaning the insulating FDD model assumes behavior similar to the non-insulating model until the sea ice thickness reaches a minimum threshold, H0 (set to 2 cm in this study). Below this threshold, the insulation effect is neglected. The choice of this threshold parameter is less significant compared to other ambiguous parameters in the model and the sensitivity of the end of the season level ice thickness is typically increased by less than 0.1 cm by this assumption.

The sea ice density, heat conduction of snow, heat conduction of ice, and the latent heat of ice are all parameters that significantly influence the resulting sea ice thickness in the model. Two alternatives for assigning values to these parameters are presented in this thesis. Starting with the international standard when deriving the non insulating FDD model, suggests an empirical constant $a = 2.6 \times 10^{-2}$ in Stefan's Law (2.5.2). The insulating model can then be accordingly given values for the physical parameters named above as either their experimentally given lab values or effective values as if $a = \sqrt{\frac{2\kappa_i}{\rho_i L_f}} = 2.6 \times 10^{-2}$. The method using the lab values for the physical parameters yielded similar results to a study by Tikanmäki and Heinonen (2022). The level ice thickness was typically reduced by less than 25% when compared to the non insulating FDD results. The insulating approach used to generate figure 3.7 used these lab values of the physical constants. The model presented in the Norströmsgrund benchmark in figure 3.6 uses the effective values for the physical parameters. This yields a much more significant effective level ice thickness reduction when compared to the non insulating FDD results.

Leppäranta (1993) shows that this effective reduction should be less than 50% of the non insulating level ice thickness assuming the snowfall is proportional to the level ice thickness. The proof for this is added in appendix B. Additionally it is assumed in this thesis that the level ice will remain a two phase system with the snow. This requires that the level ice does not submerge or suffer splash from waves. Leppäranta shows that as long as the depth of the snowfall is under a given value the ice can be assumed to not submerge. The snowdepth regularly surpasses this threshold in the models derived herein. Especially for the insulating model using effective physical parameters which yield especially low level ice thicknesses. Furthermore the introduction of insulation due to snowfall introduces a new random variable to the model and yields significantly lower level ice thicknesses when compared to the non insulating model. As will be discussed in later sections the amount of data points is a vital shortcoming of models to be discussed. For these reasons the insulating FDD model will not be used in the derivation of sea ice ridge distributions in later sections. For a more correct assessment of the questions regarding the effects of snow on the development of the level ice thickness more research is needed.

It should be noted that while the empirical values for the physical parameters named above have been extensively tested for laboratory ice and snow, actual ice and snow in the field may exhibit different properties due to various factors such as local temperature, water mixing, salt concentrations, and impurities. However, these effects were not considered in this study, and the sea ice properties were assumed to align with those described by Tikanmäki and Heinonen (2022).

The sea ice thickness derived from the non-insulating model generally exceeded the ground truth FMI values, while the insulating model yielded lower sea ice thicknesses. Therefore, the non-insulating model was chosen as the conservative approach for sea ice thickness calculations based on FDD models in this study, see Figure 3.6. In the subsequent discussion, the term "FDD model" will specifically refer to the non-insulating FDD model that utilizes the coefficient recommended by the international standard for arctic offshore constructions (ISO 19906:2019).

Notably, the CMS_G hindcasts produced considerably thicker sea ice thicknesses than the measurements from BASIS and FMI, as well as the sea ice thickness estimates generated by the ERA5 based FDD model. This discrepancy is particularly concerning in locations north of the Quark, where the sea ice is known to grow both thermally and mechanically. While the higher sea ice thicknesses in these locations could be attributed to the sensitivity of the MSIT statistic to outliers, this argument does not justify the generally higher sea ice thicknesses across the entire CMS_G dataset.

Ice growth is shown to be sensitive to the properties of snowfall for all model versions presented by Leppäranta (1983).

4.2.1 Freezing season duration

The freezing season start and end dates, and consequently the freezing season duration, by basin are shown in table 3.2.1. Additionally the SIT_{10} and SIC_{60} statistics are shown in the table 3.2. A comparison between these tables show that the SIT_{10} and SIC_{60} statistics correlate poorly with the freezing season duration defined by the running average temperature start condition and the sea ice concentration end threshold. SIT_{10} and SIC_{60} are likely too strict measures as sea ice conditions are under these thresholds for a significant part of

the freezing season and disproportionately so when the freezing season is not severe. This speaks to the stronger correlation in the northern basins than in the southern basins.

The freezing season boundary conditions yield believable durations for the freezing seasons. According to the FDD boundary conditions the freezing season typically starts in late January in the southern basins and increasingly earlier the further north. The end of the freezing season as defined by the sea ice concentration cutoff shows distinct modes for each basins in contrast to the start of the freezing season which is largely similar between basins. The more sheltered offshoots from the Baltic Proper, i.e. the Bay of Bothnia, the Gulf of Finland and the Gulf of Riga have significantly later ends to their freezing season as is expected due to the retreat of the ice edge towards the coast and into these sheltered regions as the freezing season ends.

The freezing season in the south-western Baltic Sea is well documented by the Eisatlas (Sztobryn and Holfort, 2012). The Eisatlas is a German ice atlas documenting and analysing the sea ice conditions in the south-western Baltic Sea in the period 1961-2010. The FDD model defined in this thesis has an average start of the freezing season on the 24th of Januray in Danish Waters and the Arkona Basin. The Eisatlas reports median beginning of ice occurrence in Danish waters to be mostly in the interval 15th-25th of January. In Arkona Basin the Eisatlas reports, in non-coastal waters, a mean start date between the 15th of January and as late as the 15th of February closest to Bornholm Basin. For the Bornholm, and the eastern Gotland Basin the Eisatlas shows bimodal start of the freezing season. An extended zone close to shore with freezing season start mostly between 25th of December and the 25th of January, and an open water zone marked as later than 25th of January. The FDD temporal boundary conditions report a median start of the freezing season to be 28th and 22nd of January in the Bornholm and Eastern Gotland Basin respectively. The Bornholm data is consistent, the Eastern Gotland Basin is not completely covered in the Eisatlas, however the sections shown seem to imply a mean freezing season start later than the FDD freezing season start. This is hard to say for sure as the eastern coast of basin is not covered in the Eisatlas.

The median end of the freezing season according to the NSIDC 10% sea ice concentration cutoff is on the 11th of March in Danish Waters and on the 6th of March in Arkona Basin. The Eisatlast report median end of ice occurrence typically between the 1st of March and the 20th of March in both basins with a slight skew towards later end of the freezing season in the parts of the Arkona Basin closer to the Bornholm Basin. The Bornolm Basin is reported by the Eisatlas to have a median end of ice occurrence between the 1st of March and the 30th of March. The FDD boundary condition has a mean end of the freezing season in the Borholm Basin at the 13th of March. As the Eastern Gotland Basin is not fully covered in the Eisatlas it is again difficult to assess the concordance between these sources there, however the parts of the Eastern Gotland Basin that is covered in the Eisatlas are between the 1st of March and the 30th of March, with a large portion between the 20th and the 30th of March. This is in agreement with the median end of the freezing season as per the FDD boundary condition which is the 28th of March. Overall, the freezing season start and end in the FDD model are within the reported ranges by the Eisatlas in the south-western Baltic Sea.

The sensitivity of the mean date for end of the freezing season to the NSIDC sea ice concentration cutoff threshold is shown in figure 3.3. The graph shows that the mean end

of the freezing season changes by only a couple of days as the cutoff concentration goes from 0% to 100%. Note that two different effects draw the average end of the freezing season in different directions as the NSIDC cutoff is changed in the sensitivity analysis. Removing sea ice concentration below a certain value will first remove data points for areas with less ice which are more likely to be areas with shorter freezing season thus also removing the shorter freezing seasons from the seasons being averaged over. This effect removes earlier ends of the freezing season which should make the average end later as these regions are more likely to never have sea ice concentration above the given threshold. However, cutting from the end of the freezing season also makes the freezing season shorter. Another dominant effect is a selection bias, most data points recording sea ice in the Baltic Sea are in the northern Bay of Bothnia. This is where the first ice forms and this is where the last ice retreats. All these data points have a similar freezing end mode and the average of the Baltic Sea as a whole will be quite similar to the average over just the northern Bay of Bothnia. The mean end of the freezing season in the Bay of Bothnia is the 6th of May, as shown in table 3.1, and the sensitivity ranges from the 19th of May to the 8th of May.

As will be discussed further in later sections the end of the freezing season as per the NSIDC cutoff is very late in the northern basins. It should be noted that there is not always ice everywhere in the Baltic Sea and these averages are over the start and end of the freezing season when there is a freezing season meaning that a 9th of April mean end of the freezing season in the Northern Gotland Basin should not be interpreted as, for any given year the expected end of the freezing season is the 9th of April. Rather, the interpretation should be that the mean date for the end of the freezing season at a grid point in the Northern Gotland Basin is the 9th of April conditional of a freezing season severe enough to produce ice in the Gotland Basin.

4.3 Sea ice strength coefficients C_R

In this study, a free drift ice model, as described by Hornnes et al. (2022), was utilized. This model assumes that sea ice floes drift with a fraction of the local wind speed. The rationale behind using this method lies in the availability of longer-term wind velocity data with higher spatial and temporal resolution compared to the recorded sea ice drift velocity as in the CMS$_G$, see the data source parameter table 2.1.

The free drift velocity of sea ice is commonly characterized by a Nansen number, see Equation (2.27), which represents the relative velocity of the sea ice compared to the 10 m wind. Previous studies have reported Nansen numbers in the range of 2.0% - 3.0% (Hornnes et al., 2022; Leppäranta and Omstedt, 1990). In line with these findings, a Nansen number of 0.025 was employed in this research, consistent with previous works (Hornnes et al., 2022; Popko, 2020).

While the free ice drift velocity model effectively describes the motion of drift ice (Leppäranta and Omstedt, 1990), it inherently fails to account for the stationary nature of land-fast ice. In the Baltic Sea, land-fast ice is commonly observed in archipelagos and shallow straits along the coast, where the ice is anchored towards the coast. Consequently, the free drift model tends to estimate higher sea ice drift velocities in areas with strong winds and frequent sea ice formation. This effect does not reduce in shallower waters as

shown in the combined ERA5 and NSIDC sea ice exposure model presented in Figure 2.25. Conversely, the CMS_G reanalysis, which is not based on a free drift model, exhibits very low sea ice drift velocities along the coasts (see Figure 3.15b). Given an appropriate choice of the Nansen number for drift ice, this discrepancy leads to the free drift model overestimating the actual sea ice drift velocity in regions where the sea ice remains land fast for a significant portion of the year.

The sea ice strength coefficient is calibrated based on this sea ice exposure, which represents the drift length of sea ice at a given location adjusted for the local sea ice concentration, as shown in Equation (2.25). However, considering that the free drift model used for sea ice velocity is likely to overestimate velocities coastal regions, such as the northern Bay of Bothnia. The sea ice exposure calculated using this model, shown in Figure 3.14d will also be overestimated.

To determine the sea ice strength coefficient, an empirically defined distribution, Equation (2.28) was applied to two groups of data sources: the CMS_G reanalysis and a combination of NSIDC sea ice concentration observations and sea ice drift velocity estimates based on a free drift model using ERA5 ten-meter wind velocities.

The constant shift in C_R coefficient through return period should be noted. The origin of this constant shift is the nature of the equation (2.28). The difference between the C_R coefficient for two different return periods is only depending upon the difference in return period. A similar tendency was assumed, and shown to apply, for the distribution of the extreme values of local and global pressures used to obtain the C_R exposure calibration as shown by Kärnä et al. (2006); Kärnä and Masterson (2011).

The free drift exposure model based on ERA5 and NSIDC generally yields higher sea exposure values than the CMS_G reanalysis product. This combined with the overestimated coastal exposures in the free drift model yields higher sea ice strength coefficients especially in coastal regions using the free drift model. The difference at Norströmsgrund lighthouse is 378 km year^{-1} in the free drift model yielding a 50 year sea ice strength coefficient of 1.83 MPa to 92 km year^{-1} in the CMS_G reanalysis product yielding a 50 year sea ice strength coefficient of 1.68 MPa.

The sea ice strength coefficient varies significantly between basins and between the two sources mentioned. The free drift model estimates the mean sea ice exposures as above 1 km year^{-1} for all basins, this yields relatively well behaved coefficients when compared to the CMS_G exposures which for the southern basins is significantly below 1 km year^{-1} . The strength coefficient distribution Equation (2.28), when the coefficient is expressed as a function of the cumulative probability threshold and the sea ice exposure is not behaving proportionally and as expected of the sea ice strength coefficient for very low sea ice exposures. Due to the double logarithmic nature of this expression, the sea ice strength coefficient becomes negative as the exposure goes to zero. One can imagine an ocean region where the sea ice only returns briefly for one day every 10000 years. The sea ice strength coefficient at this location would be negative. This extreme example highlights an issue with this method of calculating the sea ice strength coefficient and using it for very low sea ice exposures becomes non-physical.

4.4 Sea ice ridge statistics

The level ice thicknesses were grouped for each grid point for each week in the year. Statistical distributions of the level ice thickness in each group was calculated. These distributions were not well behaved as the basis for each location-week distribution, especially in locations with short freezing seasons, were very few data points. Due to the low temporal resolution and the time frame of the level ice thickness, the data from the FDD model as basis for the distributions had to be expanded. First experiments with location-month distributions were tested. These yielded better results but still far too many location-months were still poorly behaved. The final product groups all grid points in the same sub basin of the Baltic Sea together forming the month-basin distributions presented in 3.4 for the Bornholm Basin in the southern Baltic Sea, and the Bay of Bothnia in the Northern Baltic Sea. The remaining basins recognised in figure 1.1 are shown in appendix C. These month-basins were more well defined following the logarithmic-normal distribution used for level ice draft distributions in the Beaufort Sea by Samardžija and Høyland (2023).

From these level ice thickness distributions a transformation to level ice draft distributions were made using the relative densities of ice and water to find the ratio of submerged ice to total ice thickness. From the level ice draft distributions, the month-basin distributions for weekly deepest keel and spatial frequency of sea ice ridges were derived according to equations (2.32), (2.33) and (2.30) (Samardžija and Høyland, 2023).

The probability of ice in a given month-basin group was defined as the relative number of data points with ice to the total population of data points in the given month-basin.

From the sea ice ridge and level ice thickness distributions a Monte Carlo simulation of the Samardžija and Høyland (2023) empirical relations was applied in conjunction with the appropriate probability of sea ice as defined above to define the distributions of the level ice thickness, the weekly deepest ridge keel and the ridge spatial frequency for a given month-basin.

The Bothnian Sea and the Arkona Basin show a notable multimodal nature in the level ice draft distributions resulting in multimodal distributions for the simulated parameters. Among the simulated parameters, this multimodality is most notable in the sea ice ridge spatial frequency distribution due to the exponential nature of its transformation from the level ice draft distributions. The bimodal nature of the final distributions comes from the difference in mean of the level ice draft distributions for the months November and December, and the later months. The early freezing season months have significantly lower means at around 20 cm, whilst the later months typically peak around 40 cm. This effect is not as clear in the southern basins for two reasons. Firstly the end of the freezing season is not dominated by significantly higher sea ice thicknesses than the earlier months, and secondly, the probability of ice occurrence in the earlier months are much lower in the earlier months for the southern basins than the northern basins.

It should be noted that the statistical relations between level ice draft and the other parameters discussed above are defined for ice conditions in the Beaufort Sea, experiencing much more ice days and much thicker ice than in the Baltic Sea. The Samardžija and Høyland (2023) distributions disregard ridges under 5 m thickness. The ridges observed in the Baltic Sea are more likely to be in this range than the ridges in the Beaufort Sea. It is easy to accept that the conditions are very different between the two regions and a location specific relation for the Baltic Sea, and preferably for each Basin or location being

analysed should be determined.

More data points for each basin would allow for shorter time limit on each distribution. This would allow to go from month-basin to week-basin which could decrease the effect of the bimodal nature of the resulting distributions. For future research the FDD model could be expanded to take in data from an ERA5(FDD)-BASIS(SIC) dataset as well as the currently considered ERA5(FDD)-NSIDC(SIC). This would increase the time frame of the data by almost 20 years.

Some of the distributions are scewed to the right from a well behaved logarithmic normal distribution, implying that if the log-normal distribution is expected to describe the distributions the freezing seasons are likely overestimated. Another reason could be that the FDD models does not account for the melting of ice.

The weekly deepest keels in the Bornholm Basin are distributed with 90% between 8.88 m and 9.96 m. The mean weekly deepest keel is at 9.34 m. The weekly deepest keel in the Bay of Bothnia is distributed with 90% between 9.04 m and 11.81 m with a mean at 10.55 m. The spatial frequency is distributed in the Bay of Bothnia is distributed with 90% between 0.07 ridges km^{-1} and 1.01 ridges km^{-1} with a mean at 0.52 ridges km^{-1}. In situ sea ice ridge measurements where carried out in the Bay of Bothnia in 2017 finding the deepest ice ridge keels between 5.4 m and 10.9 m with spatial frequency between 0.2 ridges km^{-1} and 16 ridges km^{-1} (Teigen et al., 2018). It is clear that whilst the keel draft is comparable, the ridge frequencies are simulated to be with lower frequency than observed. This is at least due to the significantly lower level ice in the Baltic Sea compared to the Beaufort Sea, the culling of ridges under 5 m for the determination of the statistical distributions in the Beaufort Sea, and potentially differences in ice ridge frequency between the two regions.

4.5 Sea ice conditions in Polish coastal waters

The effort to describe sea ice conditions suffer from the fault that all the different data sources disagree on when there was sea ice and how much sea ice there was when there were sea ice. The remote sensing technologies like the NSIDC sea ice concentration product has known errors in coastal regions due to land-sea spillover (DiGirolamo et al., 2022). Remote sensing in general is unpredictable in the melting season due to the formation of melting ponds on top of the ice (DiGirolamo et al., 2022; Landy et al., 2022). The problem with analogue charts from the earlier periods is that they require human observers on location. This results in more data in areas with more people and more interest to understand sea ice conditions for trade etc. This may leave regions uncharted and introduce more human bias.

To exemplify how sea ice can develop in Polish coastal waters an analysis of SMHI ice charts was made. A comparison between between NSIDC sea ice concentration observations and SMHI ice charts was carried out. The dates of NSIDC observed sea ice at the Baltyk I, II and III locations were compared to the closest SMHI ice charts. In the following "exposed Polish coastal waters" refers to the exposed section of the Polish coast west of Darlowo and east of Wladyslawowo. The comparison yielded that 62% of the 16 NSIDC recorded sea ice occurrences as Baltyk I pointed to an SMHI ice chart with sea ice recorded in exposed Polish coastal waters. Furthermore 30% of NSIDC recorded sea

ice occurrences at Baltyk II corresponded with an SMHI ice chart with sea ice in exposed Polish coastal waters, and 20% of NSIDC recorded sea ice occurrences at Baltyk III corresponded with an SMHI chart with sea ice in exposed Polish coastal waters. These ratios were calculated without duplication such that when multiple NSIDC ice occurences refer to the same SMHI chart, the SMHI chart is only counted once.

Baltyk I is further from shore than Baltyk II which in turn is slightly further from shore than Baltyk III. When NSIDC records sea ice at a location further from shore it is more likely that the ice event is also marked in the SMHI ice charts.

Most of the NSIDC observed ice occurrences are in the period before the the freezing season 1987-1988. There is a stark drop in NSIDC ice occurrences after this season.

The three freezing season with the most overlap in sea ice recordings between NSIDC and SMHI at the Baltyk III location were the seasons 1984-85, 1985-86 and 1986-87. The sea ice season of 1985 followed clear development stages, starting in ports and inner most in large bays expanding outwards and generally eastwards before retreating. As the ice develops, as it grows and retreats, ice floes form and sections of land fast ice can break and drift away. Ocean currents and the wind direction at the time of break off and in the following days affect where the ice drifts. This can lead to level ice and rafted and ridged ice drifting further from shore and into regions where the ice usually is not present.

A comparison between the SMHI ice charts and the ERA5 wind speed was carried out in the freezing seasons referred to above. It should be noted that these are few samples and the SMHI charts are distributed every couple of days in the freezing season and sometimes with more than a week between charts. This makes it hard to determine exactly when sea ice forms and disappears. The figures 3.32a-3.32c show the daily mean wind speed at Baltyk III compared to periods between SMHI with charts with ice in exposed Polish coastal waters in green and the uncertain boundary period between ice charts with ice and those without ice marked in grey. With the exception of late March 1987, the SMHI ice charts generally overlap with periods of daily mean ERA5 10 meter wind speeds below 8 m s^{-1}. The SMHI ice charts generally have an increase in daily mean wind speeds above 8 m s^{-1} in the end of ice period or in the uncharted time period before the next ice chart without ice presence. Wind can cause ice drift. Drift leads to more rapid melting if the ice drifts over warmer water which can make the ice disappear. This can also cause more uncertainty as ice can enter new regions where it is not typically present.

Chapter 5

Conclusion and outlook

5.1 Data evaluation

The data sources analysed in this research describe the details of freezing season development and severity with significant differences, however they agree on the following general tendencies for sea ice development. The sea ice first starts in sheltered coastal waters and expands from the shore. The further into the Baltic Sea the higher the probability of ice presence in a given year. The further north-east in the Baltic Sea the more severe the freezing season. Parts of sub basins of the Baltic Sea like the Danish Waters, the Archipelago Sea and the opening of the Gulf of Riga are more prone to experience significant sea ice presence than neighbouring regions due to the sheltering effect of their high ratio of coastline to open ocean surface area. The northern Bay of Bothnia and the inner Gulf of Finland are the most prone regions of the Baltic Sea to sea ice presence due to their position furthest to the north and east, and farthest from the opening of, the Baltic Sea.

The Finnish Meteorological Institute dataset suffers from being based on too few, too similar freezing seasons. This leads to the statistics of the sea ice conditions too a little extent being representative of the full spectrum of possible local conditions. This flaw is apparent for the southern basins in the Copernicus Marine Service Global dataset, and likely also affects all the other datasets presented just in less obvious ways than for these two cases that lack sea ice in large parts of the Baltic Sea where other sources show ice presence.

5.2 Freezing Degree Day applicability

The running temperature average threshold defining the start of the freezing season removes early freezing degree days that do not contribute to the lasting sea ice development. The sea ice concentration cutoff defining the end of the freezing season removes some of the naive and purely thermodynamic bias from the nature of the model. Without sea ice

71

concentration presence there will be no sea ice development. Thus areas like parts of the Norwegian coast where the naive freezing degree day model predicts ice development are correctly classified as free of ice.

The FDD model employed is meant as a conservative approach of estimating sea ice thickness. Employing an insulating FDD model reduces the estimated sea ice thickness and thus also the conservative nature. The insulating model also introduces a new random variable, precipitation, upon which the resulting sea ice thickness depends. This increases the variability of results.

The start of the freezing season as defined by a 30 day running average temperature below 0°C is in agreement with carefully analysed freezing seasons in the south-western Baltic Sea.

The end of the freezing season as defined by a sea ice concentration cutoff might overestimate the duration of the freezing season, especially in the northern basins, however this should be investigated further.

5.3 Sea ice strength coefficient

The more complicated CMS_G ice drift model is more likely to be more accurate than the naive free drift model in the northern Baltic Sea due to significant sea ice fastening. The NSIDC and ERA5 based model has more value in the southern Baltic Sea where the free drift model is more applicable, furthermore the sea ice parameters of the CMS_G product break down in the southern Baltic Sea as the reanalysis is not based on seasons with significant ice in these basins. Since the better sea ice drift model in CMS_G breaks down in the southern Baltic Sea, the NSIDC and ERA5 based model is proposed to give an idea of which basins are more prone to sea ice compared to the others in both the north and the south.

5.4 Simulated freezing season development

The simulation of the level ice thickness, sea ice ridge draft thickness and sea ice ridge spatial frequency were based on empirical relations determined for sea ice conditions in the Beaufort Sea which are significantly more severe than the conditions in the Baltic Sea.

More data would allow for more sub divisions of the Baltic Sea whilst still having well behaved level ice draft distributions. More sub-basins and more shorter time bounds for each distribution could reduce the multimodal nature of distributions for the Arkona Basin and the Bothnian Sea. These and other sub-basins are composed of areas with different sea ice condition modes such as the stark differences observed between the western Bothnian Sea, eastern Bothnian Sea, and the Archipelago Sea.

The mean of the modelled sea ice thicknesses is typically 20 cm in the southern basins and 50 cm, is similar to the data for sea ice thickness found in other sources discussed herein. The mean of the modelled weekly deepest sea ice ridge keel draft is typically 9.5 m in the southern basins and 10.5 m in the northern basins. These values are comparable to published observations of sea ice ridges in studies carried out in the Bay of Bothnia. The mean modelled sea ice ridge spatial frequencies are typically 0.15 ridges km^{-1} in the

southern basins and 0.5 ridges km^{-1} in the northern basins. These values are significantly lower than published observations of ridge frequencies in the Bay of Bothnia.

5.5 Freezing season development

The various sources of sea ice data does not always agree on the duration, severity or presence of sea ice. Despite disagreement of details pertaining to the sea ice conditions, the general tendencies in sea ice development are often similar. Sea ice develops from the most sheltered regions and expands. During the freezing season and especially during the melting season, floes can break up or break off from land fast ice causing ice events that are hard to predict with certainty far in advance.

High winds might have a significant effect on the presence of sea ice, especially further away from shore. The effect of wind on the melting of ice floes in the Baltic Sea should be investigated further.

5.6 Outlook

To improve upon the analysis made herein an effort should be made to collect more data. Specifically an effort to expand the FDD model with sea ice concentration data from the BASIS archive is possible. This would increase the time horizon of the FDD model by almost 20 more years.

Further works with aims of understanding the sea ice conditions in the southern Baltic Sea should aim to evaluate different sources and models of sea ice drift. The free drift model and the Copernicus Marine Service model evaluated herein disagree significantly.

5.7 Concluding remarks

The significance of understanding the local sea ice conditions throughout the Baltic Sea is of vital importance to the burgeoning offshore wind industry in complicated oceanic conditions.

This thesis has presented an analysis of the sea ice conditions in the Baltic Sea with a specific focus on the use of Freezing Degree Day (FDD) methods to estimate sea ice development. FDD models with and without thermal insulation due to snowfall are considered. The models without a snow insulation term are more conservative than the insulating models. The models are highly sensitive to physical parameters and snow fall. The sea ice strength is estimated through established relations with sea ice exposure at Norströmsgrund Lighthouse, and the 50 year C_R coefficient is found to be slightly higher than 1.8 MPa at Norströmsgrund lighthouse. The sea ice exposure is up to 2 orders of magnitude smaller in the southern Baltic Sea compared to the northern Baltic Sea resulting in significantly lower sea ice strengths. The low sea ice exposure poses questions of the applicability of the statistical relations used to determine the sea ice strength coefficients in low sea ice exposures. Sea ice ridge draft and ridge spatial frequency are estimated through statistical relations with level ice draft. The 10 year deepest ridge keel draft in the

Bay of Bothnia is estimated to be 12.69 m, with a 10 year spatial frequency of 1.4 ridges km^{-1}.

Bibliography

Braithwaite, R.J., 2017. Positive degree-day factors for ablation on the greenland ice sheet studied by energy-balance modelling. Journal of Glaciology 41, 153–160.

Com-2020-741, 2020. Communication from the commission to the european parliament, the council, the european economic and social committee and the committee of the regions, an eu strategy to harness the potential of offshore renewable energy for a climate neutral future.

Dawson, G., Landy, J., Tsamados, M., Komarov, A., Howell, S., Heorton, H., Krumpen, T., 2022. A 10-year record of arctic summer sea ice freeboard from cryosat-2. Remote Sensing of Environment 268, 112744.

DiGirolamo, N., Parkinson, C.L., Cavalieri, D.J., Gloersen, P., J., Z.H., 2022. Sea ice concentrations from nimbus-7 smmr and dmsp ssm/i-ssmis passive microwave data, version 2. URL: https://nsidc.org/data/NSIDC-0051/versions/2, doi:10.5067/MPYG15WAA4WX.

Girjatowicz, J.P., 2011. Ice conditions on the souther baltic sea coast. Journal of Cold Regions Engineering 25, 71–415.

Hammer, T.C., Willems, T., Hendrikse, H., 2023. Dynamic ice loads for offshore wind support structure design. Marine Structures 87, 103335.

Hersbach, H., Bell, B., Berrisford, P., Biavati, G., Horányi, A., Muñoz Sabater, J., Nicolas, J., Peubey, C., Radu, R., Rozum, I., Schepers, D., Simmons, A., Soci, C., Dee, D., Thépaut, J.N., 2022. Era5 hourly data on single levels from 1959 to present. copernicus climate change service (c3s) climate data store (cds) (accessed on 18-september-2022).

Holloway, R., 2023. Degree day models: Modelling glacier melt. Royal Holloway University of London .

Hornnes, V., Hammer, T.C., Høyland, K.V., Hendrikse, H., Turner, J., 2022. On the use of drift ice thickness statistics from a copernicus reanalysis product for fatigue damage calculation. International Association for Hydro-Environment Engineering and Research - International Symposium on Ice 25, 1–11.

Høyland, K.V., Nord, T.S., Hendrikse, H., Tuhkuri, J., Polojärvi, A., Polach, F.B., Heinonen, J., Eik, K.J., Teigen, S.H., Serré, N., Schümann, B., Granlund, V., Borstel, T., Reimer, N., Haase, A., Sjöblom, A., 2023. Challenges with sea ice action on structures for offshore wind. Port and Ocean Engineering under Arctic Conditions 27.

Ice Struct JIP, 2012. ICESTRUCT JIP. Ice Effects on Arctic Offshore Structures Chapter 3: Sea Ice Characteristics.

ISO 19906:2019, 2019. Petroleum and natural gas industries - Arctic offshore structures (ISO 19906:2019).

Karvonen, J., Heiler, I., Seinä, A., Hackett, B., 2022. Product user manual for baltic sea – sea ice observations seaice_bal_seaice_l4_nrt_observations_011_004/011. doi:`https://doi.org/10.48670/moi-00132`.

Kärnä, t., Masterson, D., 2011. Data for crushing formula. Proceedings of the international conference on port and ocean engineering under arctic conditions 21.

Kärnä, T., Qu, Y., Bi, X., Yue, Q., Kuehnlein, W., 2006. A spectral model for forces due to ice crushing. Journal of Offshore Mechanics and Arctic Engineering 129, 138–145.

Landy, J.C., Dawson, G.J., Tsamados, M., Bushuk, M., Stroeve, J.C., Howell, S.E.L., Krumpen, T., Babb, D.G., Komarov, A.S., Heorton, H.D.B.S., Belter, H.J., Aksenov, Y., 2022. A year-round satellite sea-ice thickness record from cryosat-2. Nature 609, 517–522.

Langham, E.J., 1981. Physics and properties of snowcover. Handbook of Snow , 275–337.

Leppäranta, M., 1983. A growth model for black ice, snow ice and snow thickness in subarctic basins. Nordic Hydrology 14, 59–70.

Leppäranta, M., 1993. A review of analytical models of sea-ice growth. Canadian Meteorological and Oceanographic Society 31, 128–138.

Leppäranta, M., 2005. The Drift of Sea Ice. Springer-Praxis Books in Geophysical sciences.

Leppäranta, M., 2015. Freezing of Lakes and the Evolution of their Ice Cover. Springer Science & Business Media.

Leppäranta, M., Myrberg, K., 2009. Physical Oceanography of the Baltic Sea. Springer-Praxis Books in Geophysical sciences.

Leppäranta, M., Omstedt, A., 1990. Dynamic coupling of sea ice and water for an ice field with free boundaries. Tellus A: Dynamic Meteorology and Oceanography 42, 482–295.

Löptien, U., Dietze, H., 2014. Sea ice in the baltic sea – revisiting basis ice, a historical data set covering the period 1960/1961–1978/1979. Earth Syst. Sci. Data 6, 367–374.

Popko, W., 2020. Impact of sea ice loads on global dynamics of offshore wind turbines .

Samardžija, I., Høyland, K.V., 2023. Analysis of the relationship between level ice draft, ridge frequency and ridge keel draft for use in probabilistic assessment of ice ridge loads on offshore structures. Ocean Engineering 270, 113593.

Samardžija, I., Høyland, K.V., Leira, B.J., A., N., 2018. Probabilistic assessment of ice environment and ridge loads for the norströmsgrund lighthouse, in: International Association for Hydro-Environment Engineering and Research (IAHR), pp. 152–166.

van der Stap, F.L., Nielsen, M.B., Owen, C.C., Male, P., Hendrikse, H., 2023. On the feasibility of monopile foundations for offshore wind in the baltic sea. Port and Ocean Engineering under Arctic Conditions 27.

Stefan, J., 1891. Über die theorie der eisbildung, insbesondere über eisbildung im polarmeere. Annalen de Physik 278, 269–286.

Sztobryn, M., Holfort, J., 2012. Climatological ice atlas for the western and southern baltic sea (1961-2010).

Teigen, S.H., Lindvall, J.K., Samardžija, I., I., H.R., 2018. Proceedings of the asme 2018 37th international conference on ocean, offshore and arctic engineering. Ocean Engineering 8, V008T07A029.

Thijssen, J., Fuglem, M., 2015. Methodology to evaluate sea ice loads for seasonal operations, in: International Conference on Offshore Mechanics and Arctic Engineering, American Society of Mechanical Engineers. p. V008T07A031.

Tikanmäki, M., Heinonen, J., 2022. Estimating extreme level ice and ridge thickness for offshore wind turbine design: Case study kriegers flak. Wind Energy Open Access 25, 639–659.

Vihma, T., Haapala, J., 2009. Geophysics of sea ice in the baltic sea: A review. Progress in Oceanography 80, 129–148.

Wadhams, P., 2000. Ice in the ocean. Gordon and Breach Science Publishers.

WindEurope, 2019. Boosting offshore wind energy in the baltic sea.

Appendix

A   No submerging ice assumption

This thesis assumes that the upper surface of the level ice remains above sea level and that a combined snow-ice layer does not form from water splash, submersion or liquid rain. This assumption was presented by Leppäranta in his derivation of methodologies for thermodynamic ice growth based on Stefan's law (Leppäranta, 1993, 1983).

The argument for the upper ice boundary being above the water level starts with Archimedes' principle. According to Archimedes' principle the mass of the submerged section of an object equals the mass of the displaced fluid in which the object is partially or wholly submerged. This allows the formulation of a limiting case for the ratio of the thickness of the level ice to the thickness of the snow layer.

Considering a horizontally isotropic infinite ice sheet, the areas of the snow and ice volumes cancel such that

$$h_s \rho_s = (\rho_w - \rho_i)h_i, \tag{5.1}$$

where h_s is the thickness of the snow layer, h_i is the thickness of the ice layer, ρ_s, ρ_w and ρ_i are the mass densities of snow, water and ice respectively.

The flooding criterion becomes

$$\frac{h_s}{h_i} > \frac{\rho_w - \rho_i}{\rho_s}, \tag{5.2}$$

which for the least conservative brine freezing values; $\rho_s = 0.4 \, \frac{g}{cm^3}$, $\rho_w = 1 \, \frac{g}{cm^3}$ and $\rho_i = 0.9 \, \frac{g}{cm^3}$ allows for floating ice as long as snow thickness is less than 25 % of the ice thickness.

This does occur in the modeled FDD data considered in this thesis, however the complications of considering ice-snow layering in the numerical modelling yields very little (Leppäranta, 1993, 1983). Additionally, the FDD model using insulation of snow is only considered and not part of the final product FDD model used due to the less conservative and more fluctuating nature of the results.

B Snow reduction factor

Assuming the thickness of the snow layer is proportional with the sea ice thickness Leppäranta shows that a thermodynamic model considering the insulation effects of snow with typical values for thermal conductivity in snow and ice results in between $1/2$ and 1 times the sea ice thickness of a non snow insulating model (Leppäranta, 1993, 1983)

The thermodynamic problem defining the sea ice growth model without considering the insulating effects of snow (2.2) is solved in (2.10). Repeated here,

$$h(t) = \sqrt{h_0 + a^2 FDD(t)}, \tag{5.3}$$

with

$$FDD(t) = \int_0^t dt \max[0, T_f - T_i(t)], \tag{5.4}$$

$$a = \frac{\sqrt{2}k_i}{\rho_i L_f}, \tag{5.5}$$

and $h_0 = 0\ m$ is the sea ice thickness at the start of the freezing season.

The similar thermodynamic sea ice growth problem with the consideration of the insulating effects of a snow layer is no longer solvable analytically without two assumptions.

1. The freezing season starts with no sea ice, $h_0 = 0$.

2. The thermal conductivity of snow κ_s is constant.

3. h_s is correlated with the thickness of the level ice h_i,

$$h_s = \lambda h_i \tag{5.6}$$

with a correlation constant λ.

Under these assumptions the thermodynamic problem (2.14), repeated here:

$$\rho_i L \frac{d}{dt} h_i = \frac{\kappa(T_f - T_s)}{h_i + (\kappa_i/\kappa_s)h_s}, \tag{5.7}$$

solves analytically as

$$h_i|_{snow}(t) = (1 + \lambda \kappa_i/\kappa_s)^{-1/2} h_i|_{no-snow}(t). \tag{5.8}$$

Assuming typical values $\lambda \leq (\rho_w - \rho_i)/\rho_s \approx 0.3$ and $\kappa_i \approx 10\kappa_s$ the factor relating the ice thickness of the two models (5.8) falls between $1/2$ and 1.

C   Sea ice distributions and ridging statistics by basin

Arkona Basin
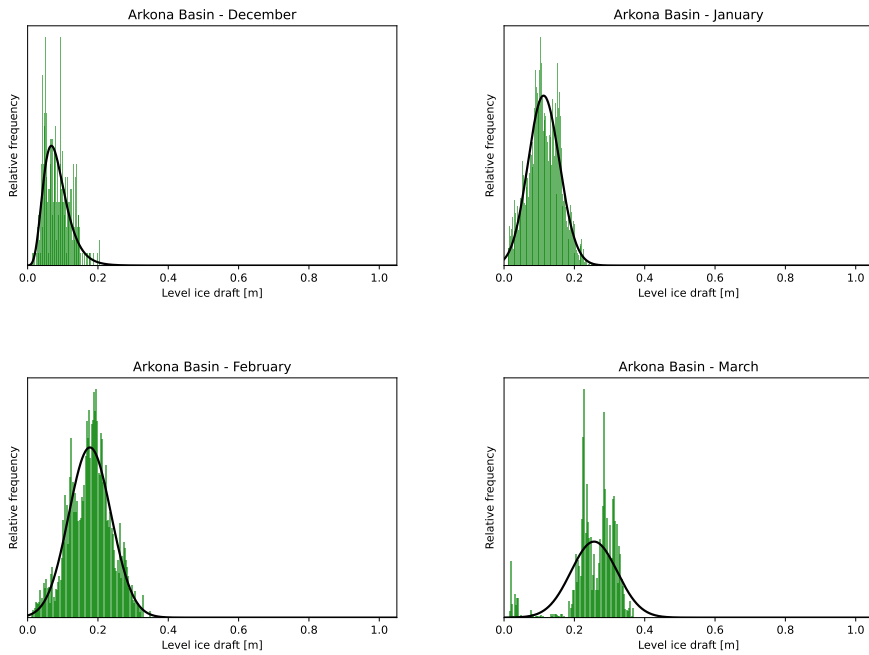
Figure 5.1: Level ice draft distributions for the months December to March from the season adjusted freezing degree day model without snow insulation.
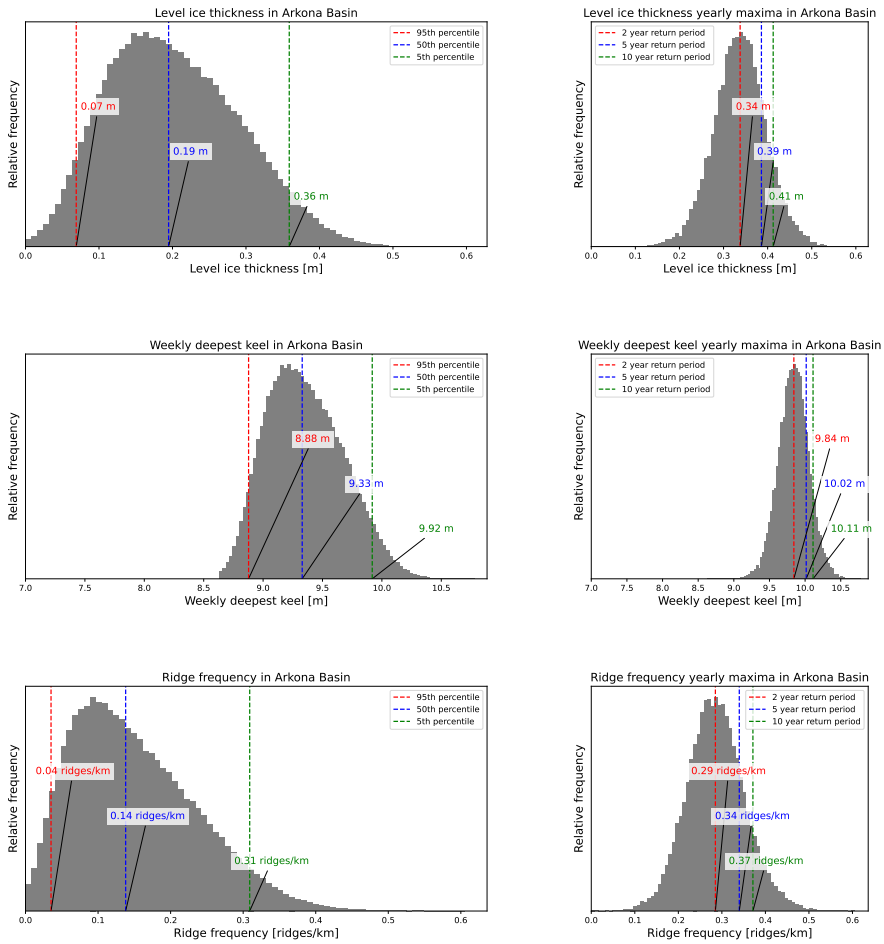
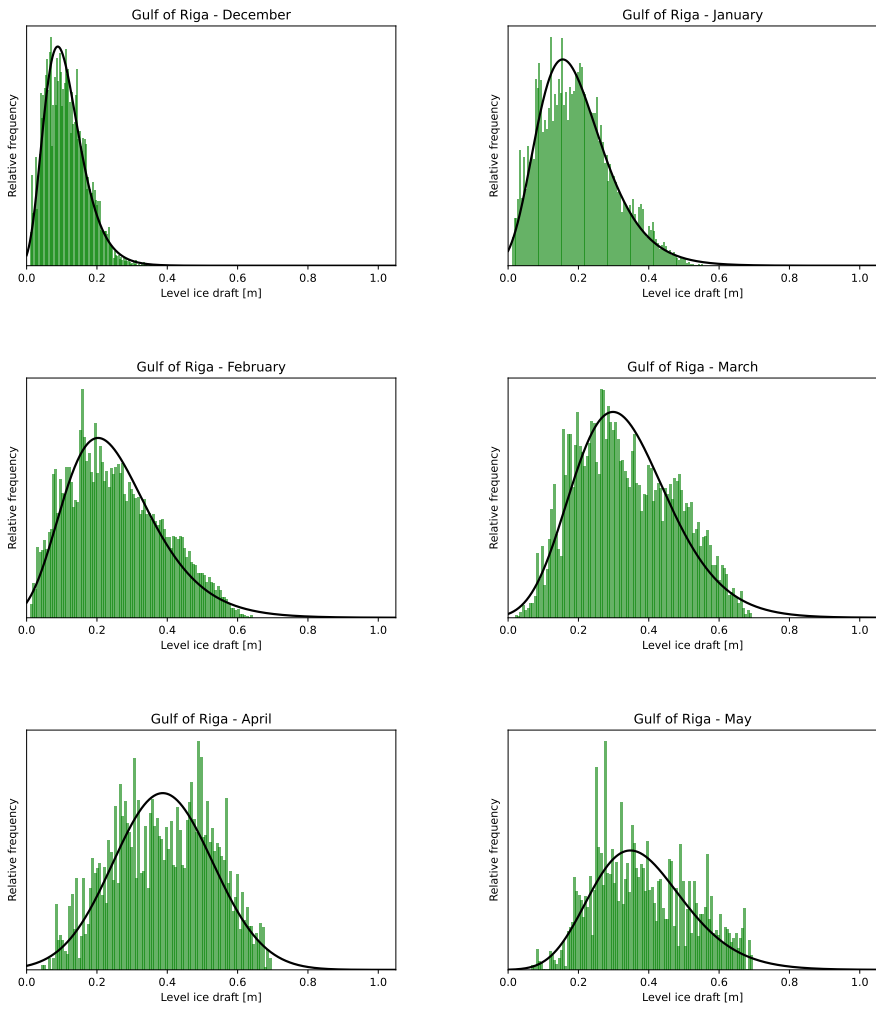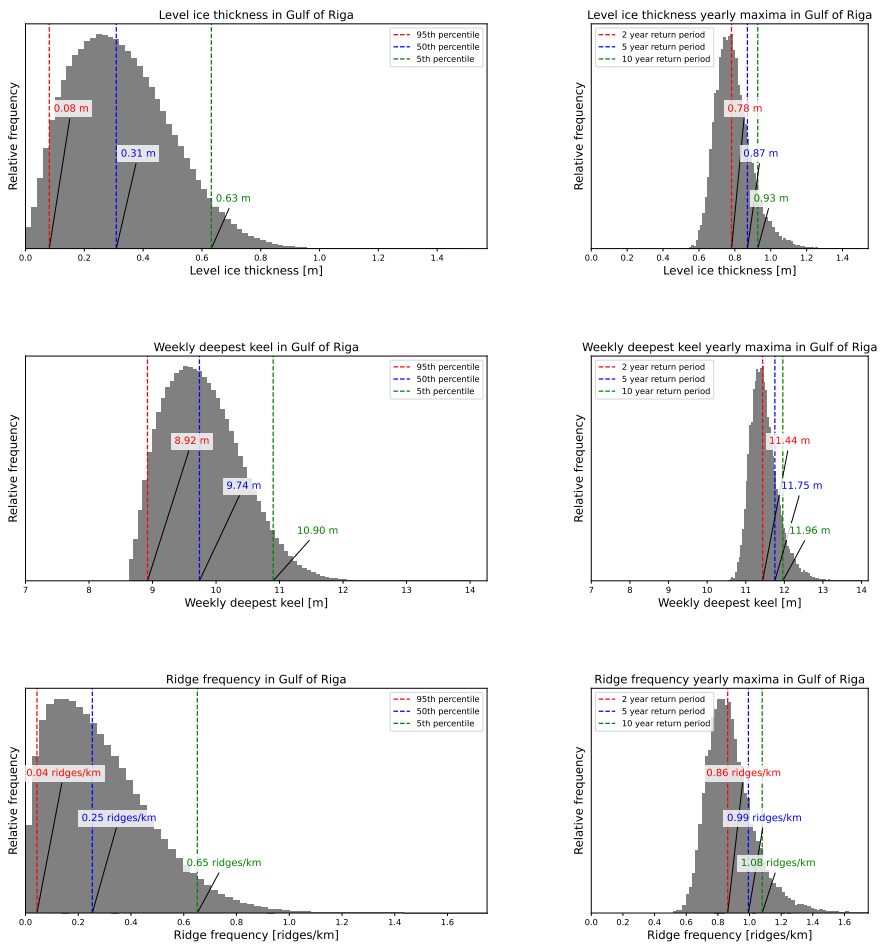**Figure 5.2:** Simulated level ice thickness, sea ice ridge keel and sea ice ridge spatial frequency distributions in the Arkona Basin.
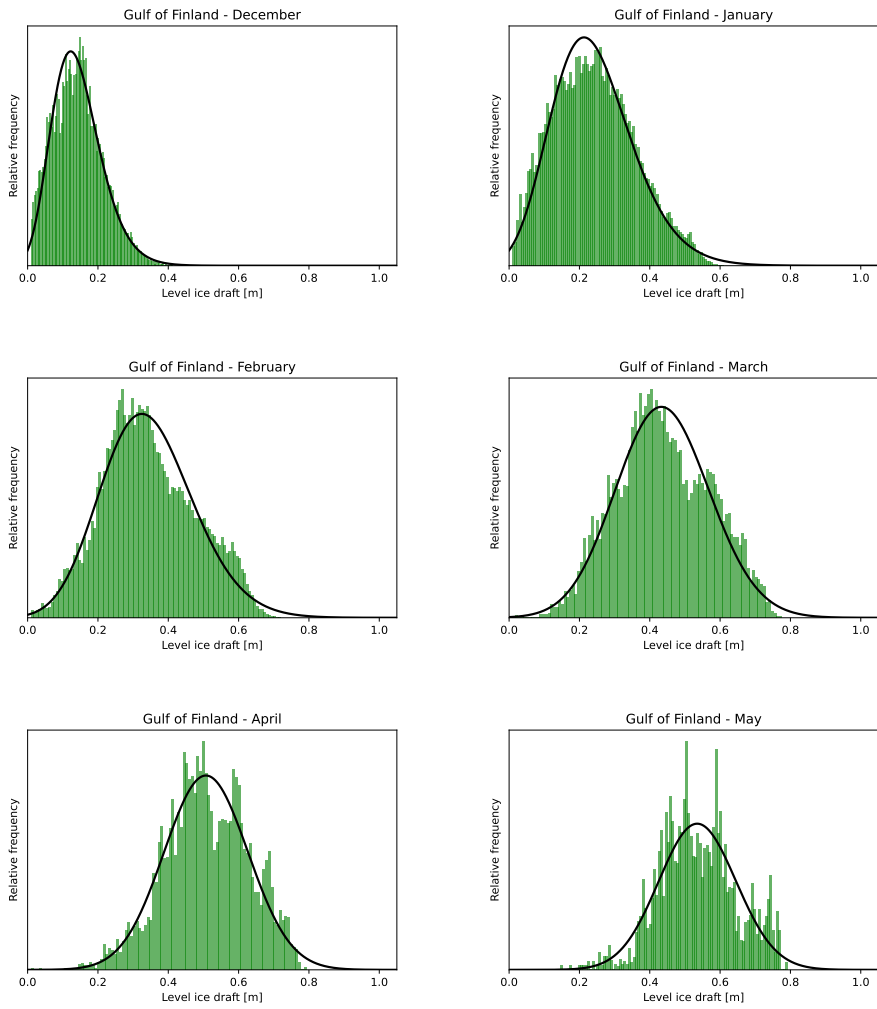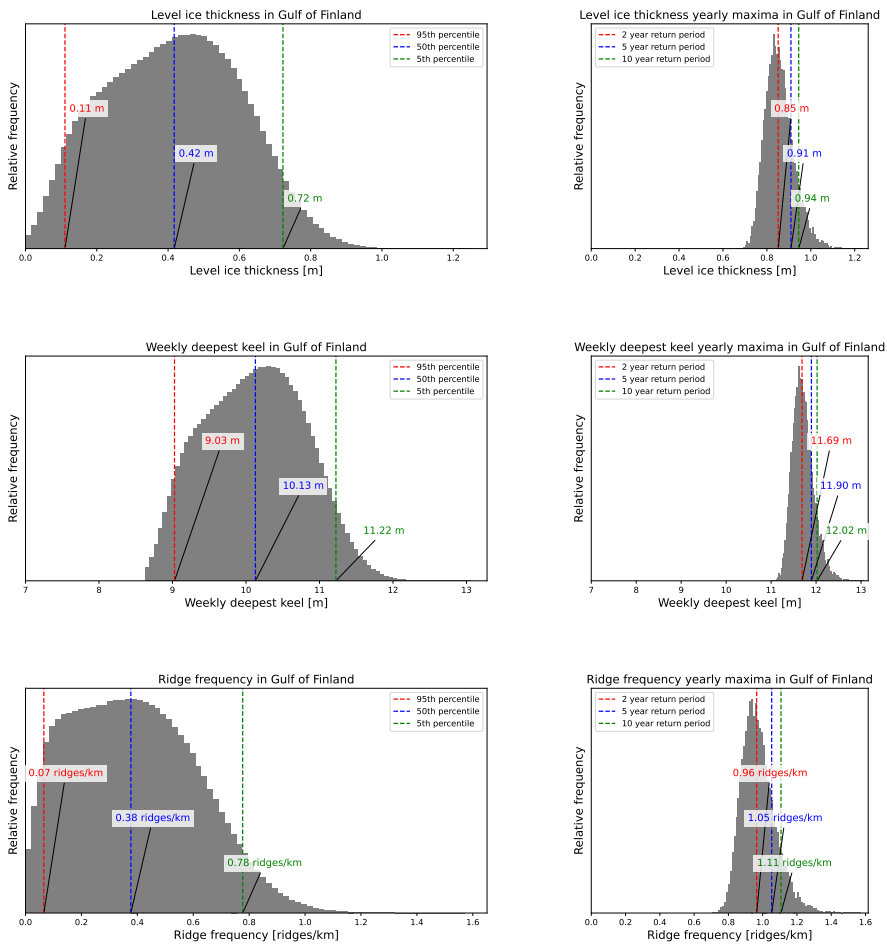
Bothnian Sea
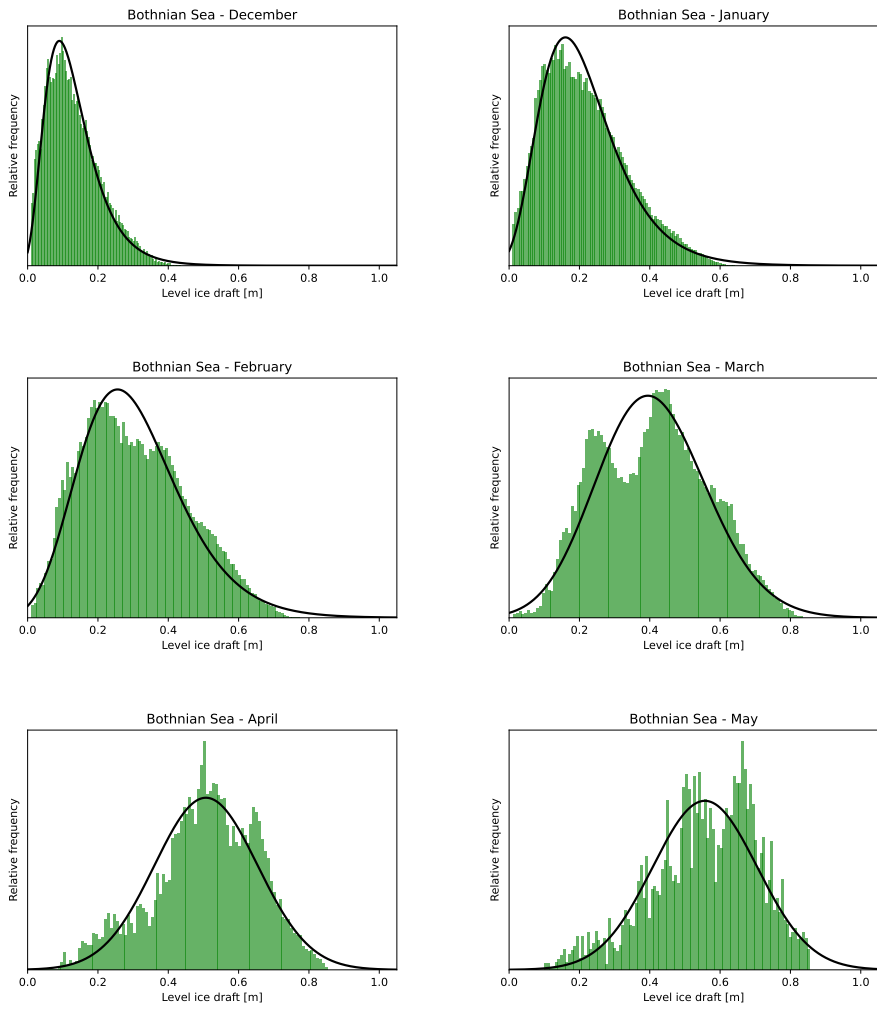
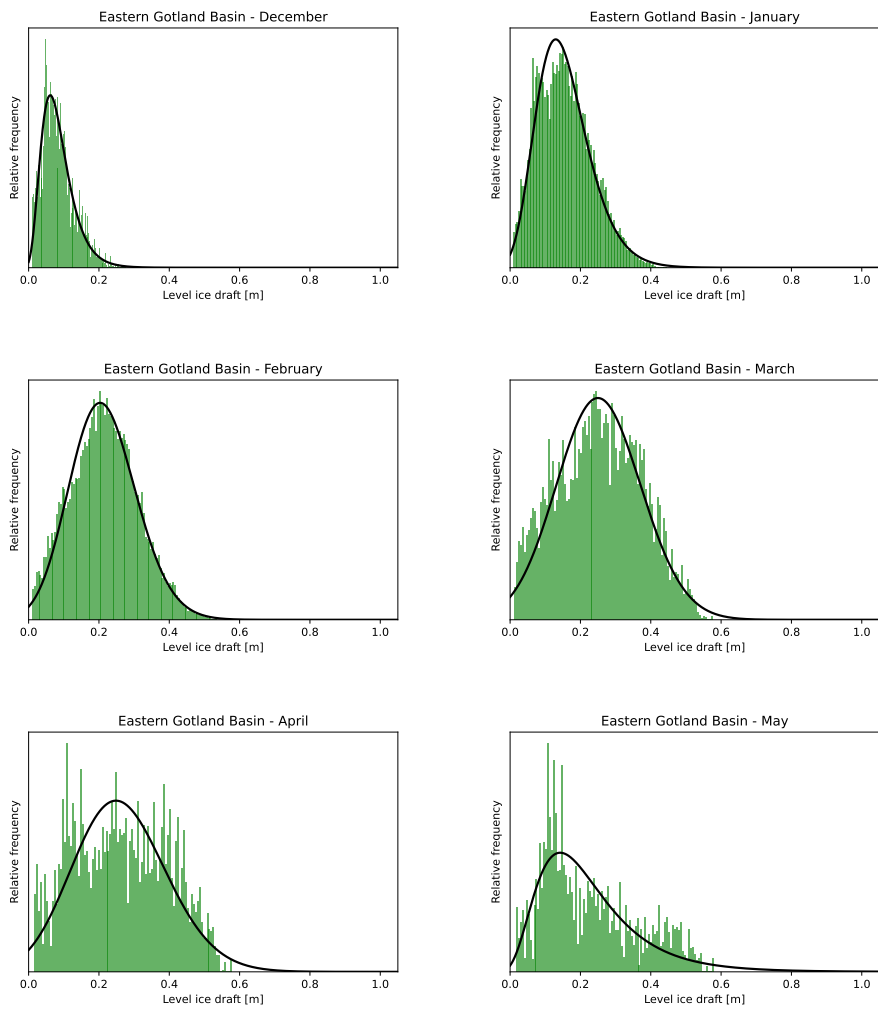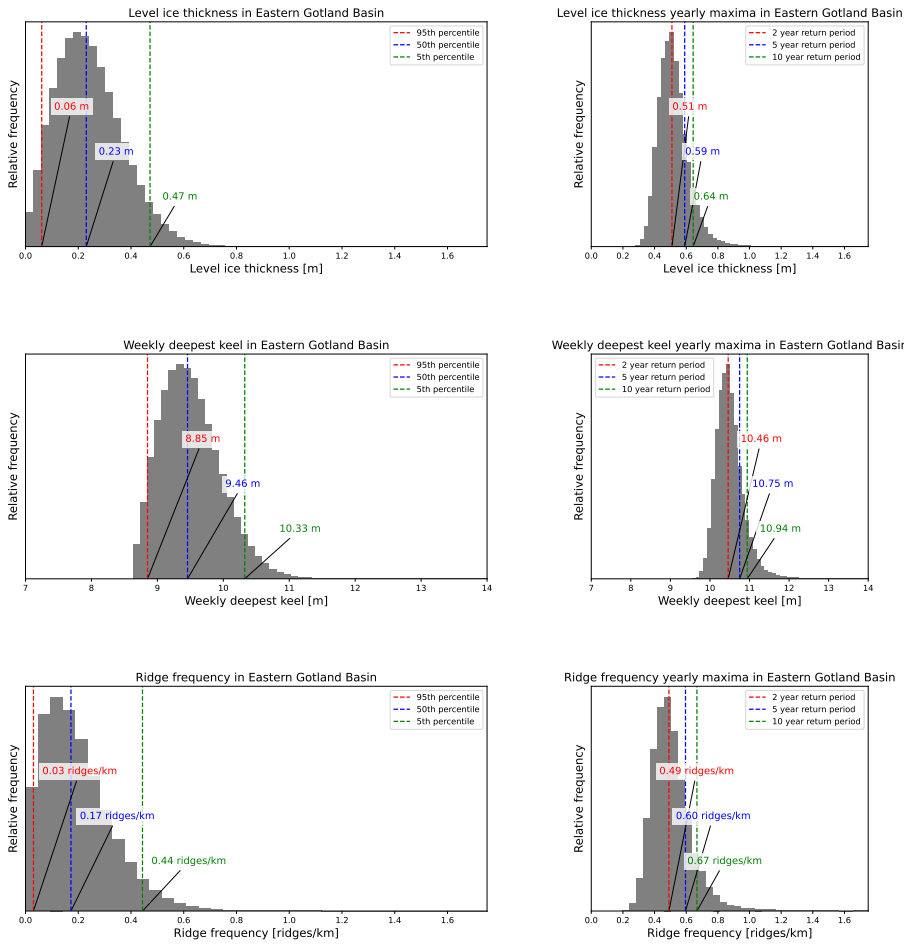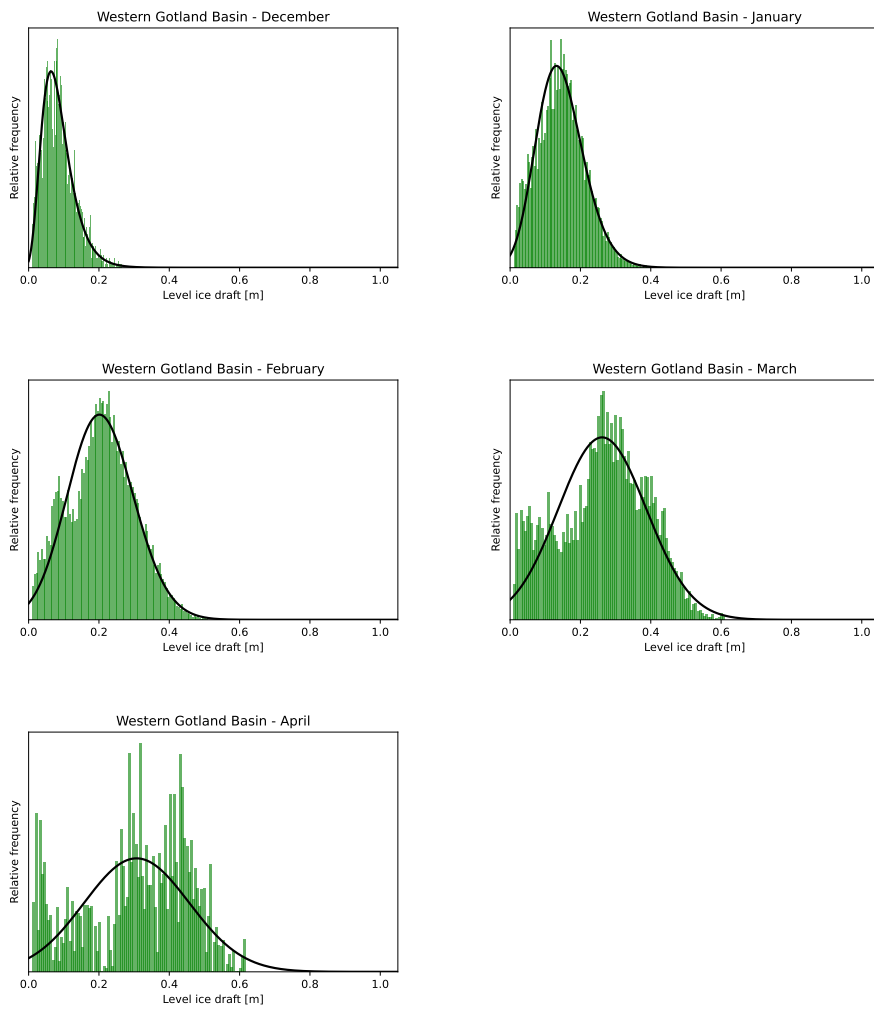**Figure 5.3:** Bothnian Sea monthly level ice distributions.
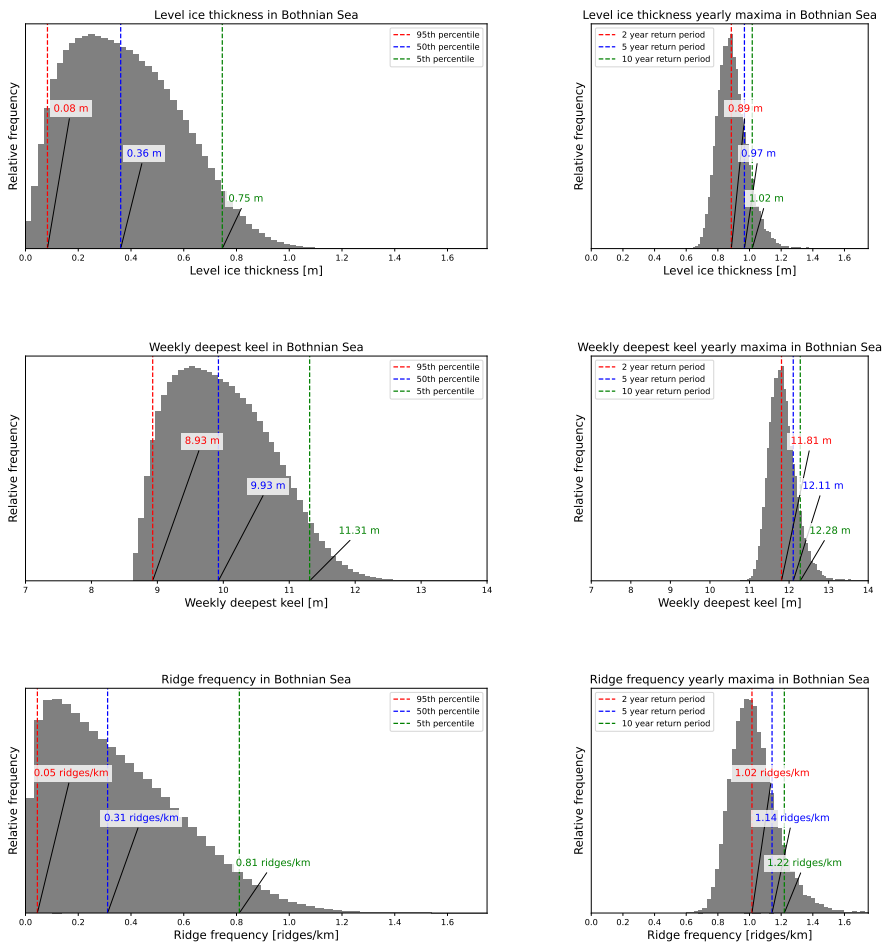
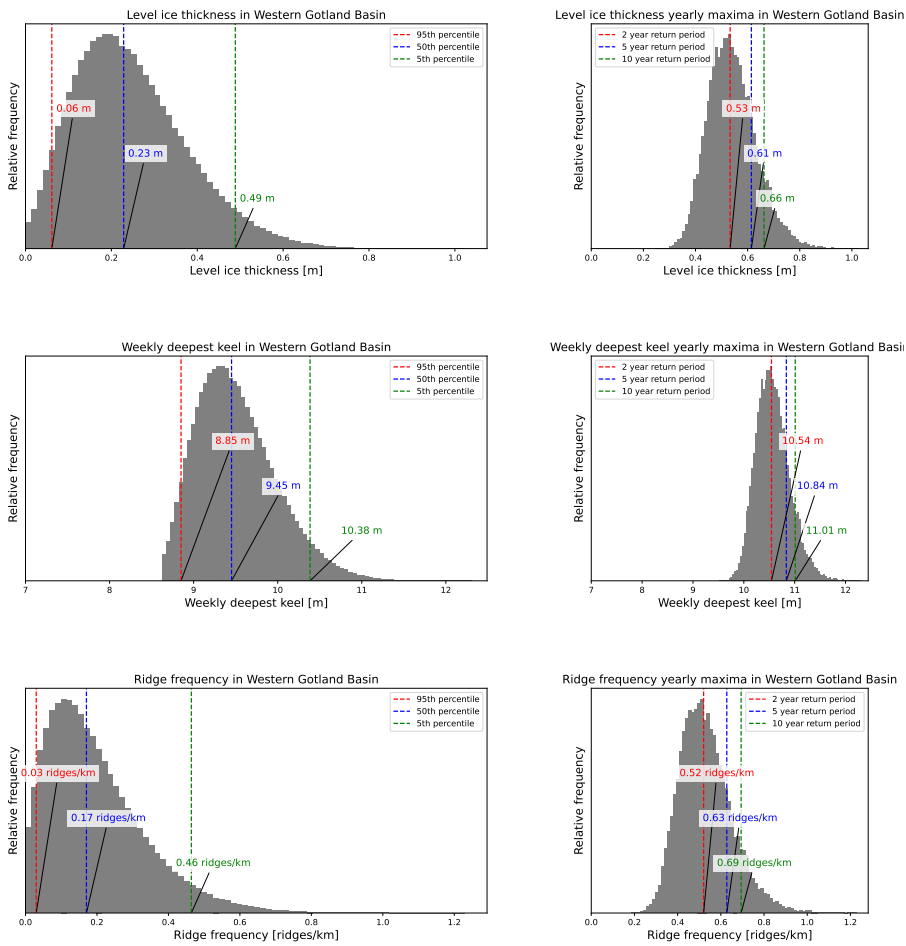**Figure 5.4:** Simulated level ice thickness, sea ice ridge keel and sea ice ridge spatial frequency distributions in the Bothnian Sea.

Gulf of Riga

Figure 5.5: Gulf of Riga monthly level ice distributions.

Figure 5.6: Simulated level ice thickness, sea ice ridge keel and sea ice ridge spatial frequency distributions in the Gulf of Riga.

Gulf of Finland

Figure 5.7: Gulf of Finland monthly level ice distributions.

Figure 5.8: Simulated level ice thickness, sea ice ridge keel and sea ice ridge spatial frequency distributions in the Gulf of Finland.
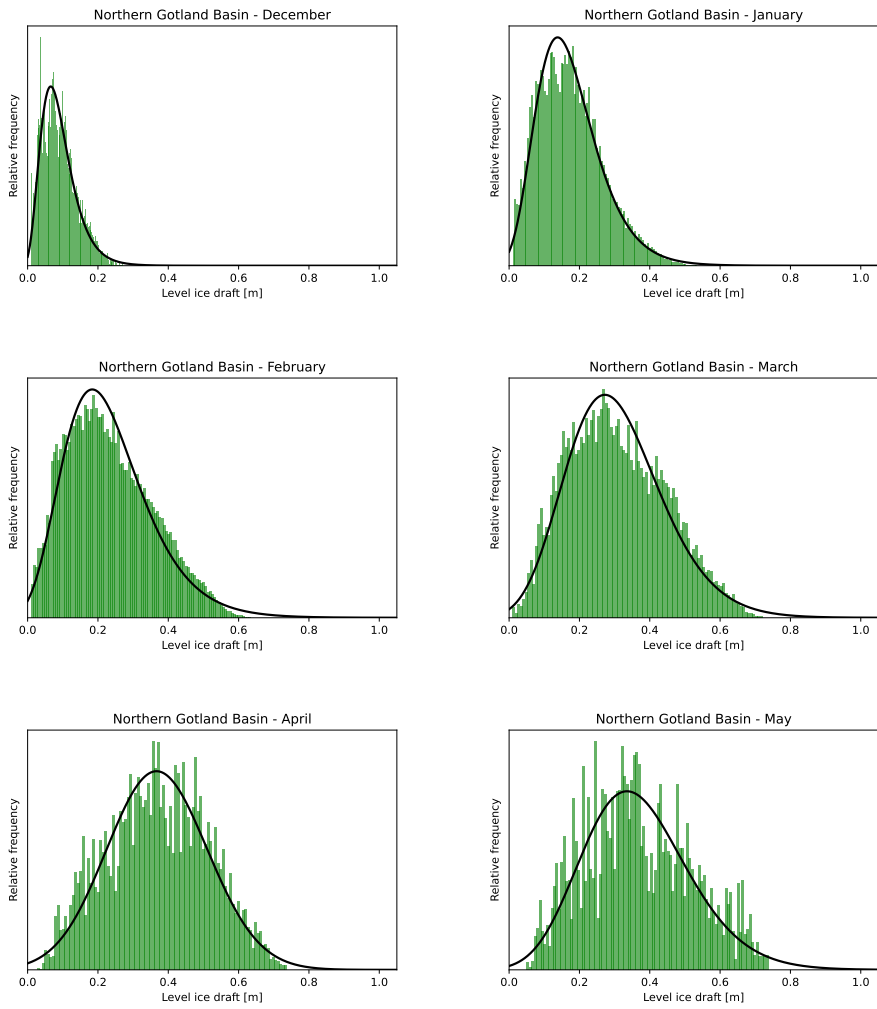
Eastern Gotland Basin

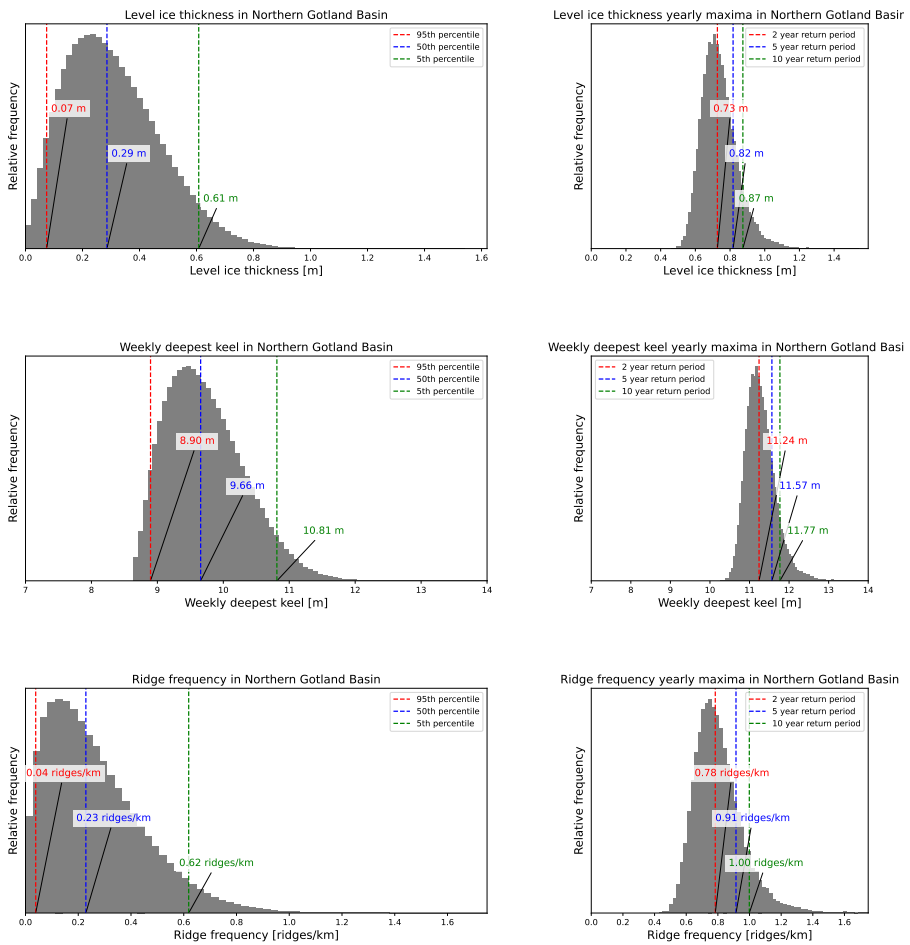**Figure 5.9:** Eastern Gotland Basin monthly level ice distributions.

Figure 5.10: Simulated level ice thickness, sea ice ridge keel and sea ice ridge spatial frequency distributions in the Eastern Gotland Basin.

Western Gotland Basin

Figure 5.11: Western Gotland Basin monthly level ice distributions.

Figure 5.12: Simulated level ice thickness, sea ice ridge keel and sea ice ridge spatial frequency distributions in the Western Gotland Basin.

Northern Gotland Basin

Figure 5.13: Northern Gotland Basin monthly level ice distributions.

Figure 5.14: Simulated level ice thickness, sea ice ridge keel and sea ice ridge spatial frequency distributions in the Northern Gotland Basin.
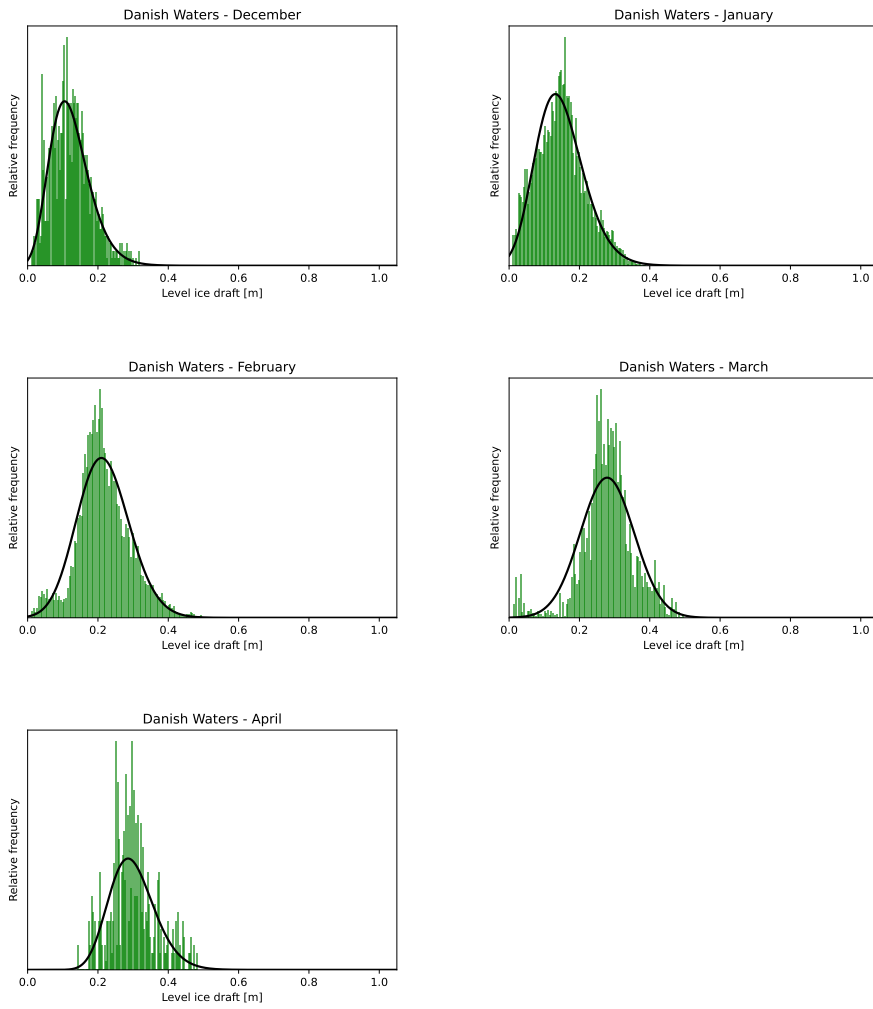
Danish Waters

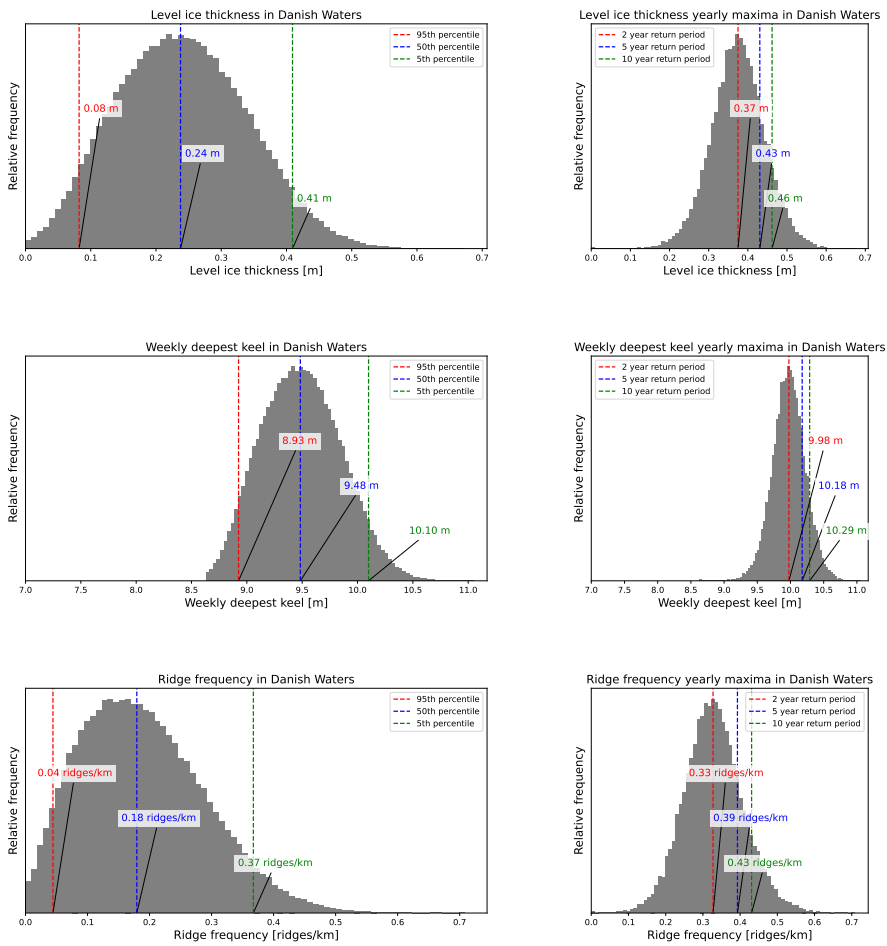**Figure 5.15:** Danish Waters monthly level ice distributions.

Figure 5.16: Simulated level ice thickness, sea ice ridge keel and sea ice ridge spatial frequency distributions in the Danish Waters.
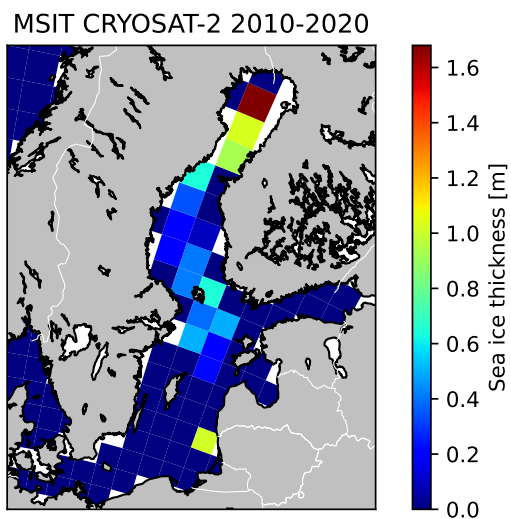
D Disregarded CryoSat-2 dataset

Figure 5.17: Sea ice thickness from CryoSat-2 interpreted sea ice thickness (Landy et al., 2022; Dawson et al., 2022).